Democratic and Popular Republic of Algeria
Ministry of Higher Education and Scientific Research
University Mohamed Khider of Biskra

Faculty of Exact Sciences and Science of Nature and
Department of Material Sciences

Ref : ……..

Thesis Presented to obtain the degree of

Doctorate in Physics

Option: Condensed Matter Physics

Entitled:

Enhancement of superconducting properties of MgNiS by using oxygen annealing atmosphere

Presented by:

Ms. SBAIHI Amira

Publicly defended on: .04 / 11/ 2024

In front of the Jury committee composed of :

LAKEL Said	Professor	University of Mohamed Khider of Biskra	President
BENRAMACHE Said	Professor	University of Mohamed Khider of Biskra	Supervisor
TIBERMACINE Toufik	Professor	University of Mohamed Khider of Biskra	Examiner
BOUBAKER Benhaoua	Professor	University of Echahid Hama Lakhdar of El Oued	Examiner
BELHAMRA Nadjette	MCA	University of Mohamed Khider of Biskra	Examiner

بسم الله الرحمان الرحيم

اللَّهُمَ أخْرِجْنِي مِنْ ظُلمَاتِ الوَهْمِ وأكْرِمْنِي بِنُورِ الفّهْمِ

اللَّهُمَ افْتَحْ لِي أبْوَابَ رَحْمَتِكَ وأبْشِر لِي خَزَائِنَ عُلُومِكَ

بِرَحْمَتِكَ يَا أرْحَمَ الرَّاحِمِين

إهداء

صديقي القارئ:

انه الثالث عشر من أبريل

لقد أتممت بفضل الله من كتابة رسالتي للحصول على درجة الدكتوراه، وأنا سعيدة جدًا بذلك. لقد تم هذا البحث بجهد وعمل ومبادرة، بسلسلة من خطوات صغيرة تسير في الاتجاه الصحيح، أثمرت عمل كبير ومقدر.

سأكتب في هذه الورقة عبارات ترجمة إهداء من قلبي أولاً لصاحب هذه الرسالة، لنفسي

فالحمد لله كثيراً طيباً، وثانيا الى هؤلاء:

لتلك المرأة التي اعتبرتها وتين قلبي وجنة عيني أمي "حدة براركة"، لذلك الشخص الذي أعتبره جبلي الذي يرفعني يوم سقوطي أبي "الفاتح صبايحي" حفظكم الله وجعلكم في حياتي دوما

الى أزهار حياتي أخواتي صبرين، بثينة وأميمة والى عطور حياتي اخوتي أكرم والحفيظ أسعدكم الله ولا أنسى خاشي أحمد.

الى ذلك الظل الذي كان شريكي في هذه الحكاية الرائعة وسيظل الى الأبد أعتز بهذا الإهداء لك.

الى أستاذي الفاضل البروفيسور سعيد بن رماش

الي صديقتي وزميلتي شيماء بن بريكة

الى صديقاتي الهام، أميمة، الشفاء، ط.شيماء، سهام، صورية، خديجة، بشرى، رندة، اية

الى أولئك الذين قد صادفتهم في حياتي وجعلتهم يوما من الأيام في ذاكرتي

أهدي لكم هذه الرسالة مع كامل حبي لكم

اليوم أُعيدَت صِيَاغَة اِسْمِي بِـ: الدكتورة أميرة صبايحي

DEDICATION

Friendly reader:

It's April 13th

By the grace of God, I have completed writing my thesis for the PhD degree, and I am very happy about this. This research was conducted with efforts, work, and initiative, as a series of small steps moving in the right direction, resulting in significant and appreciated work.

In this paper, I will write phrases as a translation of a dedication from my heart first to the owner of this message, to myself. Praise be to God, much and good, and secondly to these people:

To that woman whom I consider the vein of my heart and the paradise of my eye, my mother, ***My mother.Brarka Hadda****. To that person whom I consider my mountain that lifts me on the day I fall,* ***My father, Elfateh Sabaihi****, may God protect you and keep you in my life always.*

To the flowers of my life, ***My. sisters Sabrin, Bouthaina & Emeyma****, and to the fragrances of my life,* ***My. brothers Akram & Hafidh****, may God be pleased with you. and I do not forget Khashi Ahmed.*

To ***Daddy Long Legs*** *was my partner in this wonderful story and will remain forever, I cherish this dedication to you.*

To my esteemed professor, ***Prof. Said Benramache***

To my friend and colleague ***Dr. Chaima Ben Brika***

To my friends ***ilham, Oumaima, Elchifa, T. Chaima, Siham, Soraya, Khadija, Bouchra , Randa, Aya***

To those whom I have encountered in my life and made them one day in my memory

I dedicate this message to you with all my love

Today my name has been reformulated as: Dr. Amira Sbaihi

ACKNOWLEDGEMENT

The Beginning of Everything

*" **God has given you two hands, a mind, and a great world to use them in**". Here, I will thank God Almighty for giving me a mind and the strength to complete this research until I reached this level of results. Praise and thanks be to Allah.*

*Thanks to my esteemed **Prof. Said Benramache**, I am immensely grateful and send him a great deal of appreciation and goodwill for his tremendous help and continuous support. I acknowledge his efforts and am thankful to him for making this a day of honor for me*

I do not forget

*Thanks to the members of the esteemed scientific committee to discuss my thesis, the esteemed **Pr. Toufik Tibermacine** at university of biskra as a discussant, **Pr. Lakel Said** at university of biskra as the chair of the committee, and **Dr. Belhamra Nadjette** at university of biskra. We also thank **Pr. Boubaker Benhaoua** for coming from the University of El-oued to discuss this work. I hope you like this work and I am open to your criticism.*

Here

*I thank my wonderful friend **Dr.Benbrika Chaima** and the respected **Dr. smaili Lakhdar***

Also

*I would like to thank the esteemed **Professor Mohamed Toufik Soltani** & the engineer is **Sayah Rezgui** for their help us in conducting analyzes in their laboratories (LPPNM) &(LSMM)*

*I will also thank **Dr. Fouad Keramsi** from the Tulane University, New Orleans, Louisiana US for helping me.*

I will thank

*A number of professors: **Menasra Hayat, Mazri Radhia, Sana Alami. Zahani Sourya, Adaika Kalthoum**.*

I will always

*remember to express my sincere thanks to **Mr. Zidane Abderraouf***

And

I will thank everyone who has read this letter; you are a partner in spreading knowledge

GRAPHICAL ABSTARCT

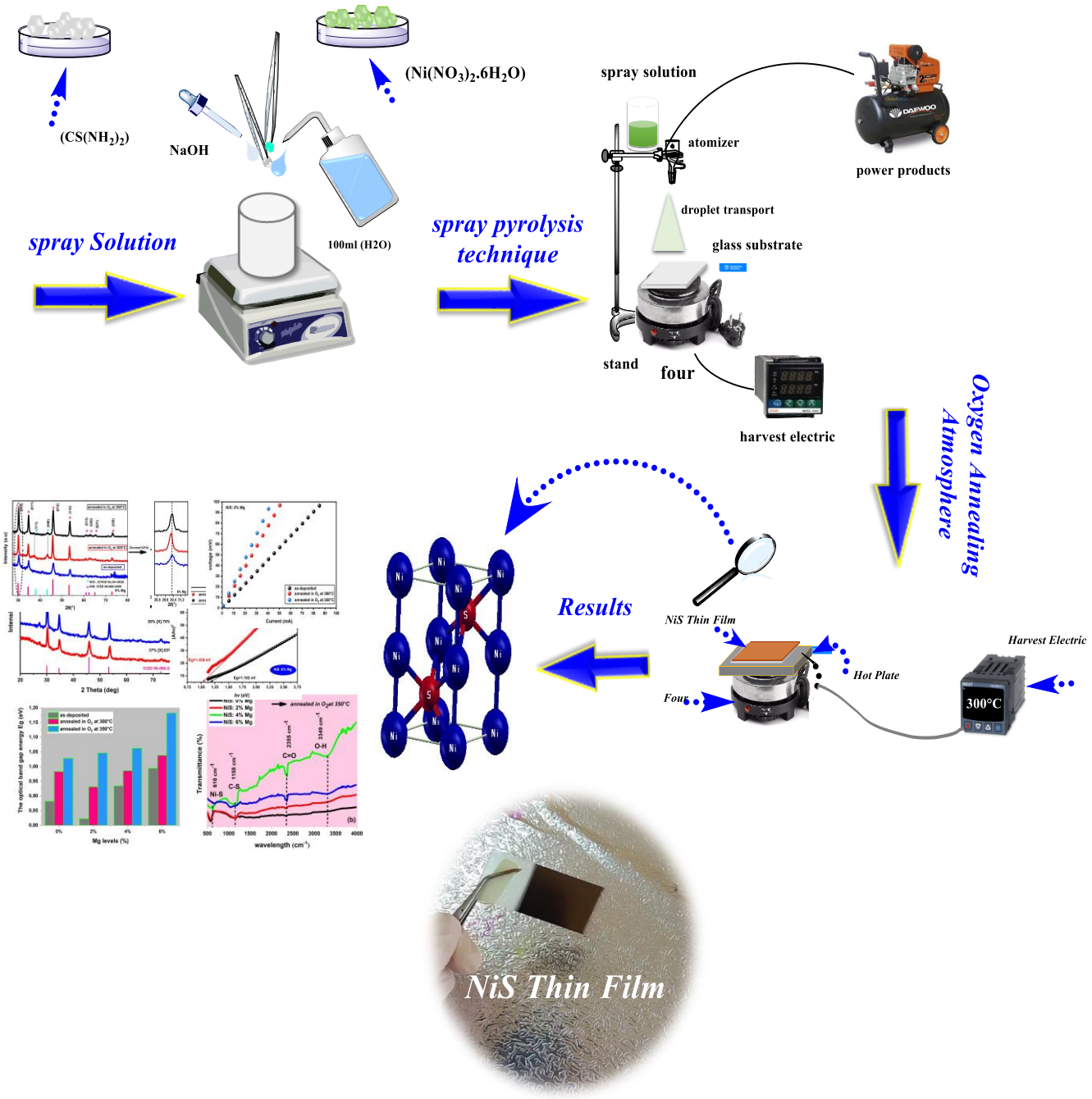

ABSTARCT

In this study, we explored the physical properties of undoped NiS films produced using spray pyrolysis. X-ray diffraction revealed that all films have a fundamental hexagonal structure with a preferred (010) orientation, and the optimal crystal size was about 22.148 nm. FTIR analysis supported these findings, highlighting the Ni-S bond at 626 cm^{-1}. Optical measurements indicated band gap energies from 0.87 to 0.92 eV. The electrical conductivity results were promising, indicating that NiS thin films are suitable for supercapacitor applications.

This study investigated magnesium (Mg) doping effects on nickel sulfide thin films at levels ranging from 2% to 8%. Key findings include a hexagonal polycrystalline structure with smaller crystallite sizes at higher Mg concentrations, notably 14.015 nm at 6%. FTIR analysis confirmed Ni-S bond at 632 cm^{-1}, and band gap energy was observed to vary between 0.882 and 0.994 eV. The lowest electrical resistance measured was 5.569 ohms, also at 6% Mg concentration.

Mg-doped NiS thin films annealed in oxygen at 300°C for 3 hours and 30 minutes, and at 350°C for 3 hours, primarily exhibited a NiS structure with a NiO phase. A significant increase in crystallite size was observed, especially at 300°C. This indicates improved crystalline structure, and the films showed good optical band gap properties and favorable sheet resistance (1.87 to 8.30 Ω/sheet). Optimal annealing for supercapacitor applications was found to be 300°C for 3 hours and 30 minutes.

Keyword: NiS Thin Films, spray pyrolysis, Electrical conductivity, Mg level, Annealing atmosphere.

RÉSUMÉ

Dans cette étude, nous avons exploré les propriétés physiques des couches non dopées de sulfure de nickel produits par pyrolyse par pulvérisation. La diffraction des rayons X a révélé que tous les couches possèdent une structure hexagonale fondamentale avec une orientation préférée (010), et la taille cristalline optimale était d'environ 22,148 nm. L'analyse par spectroscopie infrarouge transformée de Fourier (FTIR) a soutenu ces résultats, mettant en évidence la liaison Ni-S à 626 cm^{-1}. Les mesures optiques ont indiqué des énergies de bande interdite allant de 0,87 à 0,92 eV. Les résultats de conductivité électrique étaient prometteurs, indiquant que les couches minces de NiS sont adaptés pour des applications dans les supercondensateurs.

Cette étude a investigué les effets du dopage au magnésium (Mg) sur les films minces de sulfure de nickel à des niveaux allant de 2% à 8%. Les principales découvertes incluent une structure polycristalline hexagonale avec des tailles de cristallites plus petites à des concentrations plus élevées de Mg, notamment 14,015 nm à 6%. L'analyse FTIR a confirmé les liaison Ni-S à 632 cm^{-1}, et l'énergie de bande interdite a été observée varier entre 0,882 et 0,994 eV. La résistance électrique la plus basse mesurée était de 5,569 ohms, également à une concentration de 6% de Mg.

Les couches minces de NiS dopés au Mg, recuits dans l'oxygène à 300°C pendant 3 heures et 30 minutes, et à 350°C pendant 3 heures, ont principalement montré une structure NiS avec une phase de NiO. Une augmentation significative de la taille des cristallites a été observée, en particulier à 300°C. Ceci indique une amélioration de la structure cristalline, et les films ont montré de bonnes propriétés de bande interdite optique et une résistance en feuille favorable (de 1,87 à 8,30 Ω/feuille). Le recuit optimal pour des applications dans les supercondensateurs a été trouvé à 300°C pendant 3 heures et 30 minutes.

Mots clés : couches minces de NiS, Pyrolyse par pulvérisation, Conductivité électrique, Niveau de Mg (Magnésium), Atmosphère de recuit.

الملخص

في هذه الدراسة، قمنا أولا باستكشاف الخصائص الفيزيائية للأغشية NiS غير مطعمة والمحضرة باستخدام تقنية الانحلال الحراري بالرش. أظهر تحليل حيود الأشعة السينية أن جميع الأغشية لها بنية أساسية سداسية ذات اتجاه مفضل (010)، كان الحجم البلوري الأمثل حوالي 22.148 nm. قد دعم تحليلFTIR هذه النتائج، حيث سلط الضوء على رابطة Ni–S عند $626cm^{-1}$. أشارت القياسات البصرية إلى طاقات فجوة النطاق من 0.87eV إلى 0.92eV. كانت نتائج الموصلية الكهربائية جيدة، مما يشير إلى أن الأغشية الرقيقة NiS مناسبة لتطبيقات المكثفات الفائقة.

بحثت هذه الدراسة أيضا في تأثير تطعيم بالمغنيزيوم على الأغشية الرقيقة لكبريتيد النيكل بمستويات تتراوح بين 2% إلى 8%. تشمل النتائج الرئيسية بنية متعددة البلورات سداسية ذات أحجام بلورية أصغر بمستويات أعلى من المغنيزيوم، للقيمة 14.015nmعند 6٪. أكد تحليل FTIRوجود رابطة NiS عند $632cm^{-1}$، لوحظ أن طاقة فجوة النطاق تتراوح بين 0.882eV الى0.994eV. تم قياس أدنى مقاومة كهربائية ل 5.569Ω عند تركيز 6%من Mg.

أظهرت الأغشية الرقيقة NiS المطعمة بالمغنيزيوم والملدنة في الأكسجين عند 300°C لمدة 3 ساعات و30 دقيقة وعند 350°C لمدة 3 ساعات، كان الطور الاساسي للبنية NiS السداسية مع وجود مرحلة ثانوية للبنية المكعبة ل NiO وقد لوحظت زيادة في حجم البلورات، خاصة عند 300°C. يشير هذا إلى بنية بلورية محسنة، وأظهرت الأغشية خصائص جيدة لفجوة النطاق البصري ومقاومة كهربائية مناسبة تتراوح 1.87Ω إلى 8.30Ω. تم العثور على التلدين الأمثل لتطبيقات المكثفات الفائقة عند 300°C لمدة 3 ساعات و30 دقيقة.

الكلمات المفتاحية: الأغشية الرقيقة NiS، الانحلال الحراري بالرش، الموصلية الكهربائية، مستوى المغنيزيوم، جو التلدين.

TABLE OF CONTENTS

CHAPTER FOUR : The Influence of Mg Doping on Electrical, Optical and Structural Properties of NiS Thin Films Supercapacitors

CHAPTER FIVE : Effects of oxygen annealing atmosphere on Mg :NiS thin films.

FIGURE CAPTIONS

TABLES CAPTIONS

GENERAL INTRODUCTION

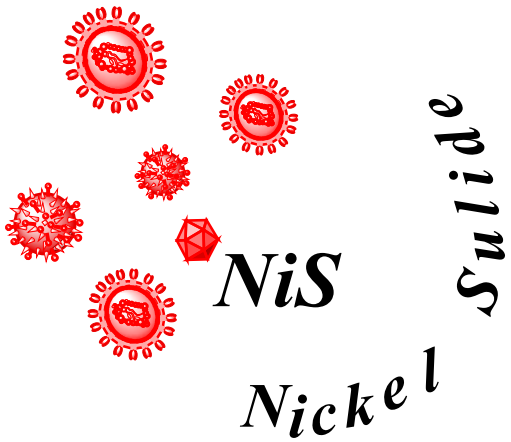

General Introduction

Advanced electrode materials in electrochemical supercapacitors have increasingly focused on nanostructured transition metal sulfides (TMSs) due to their many advantages. These include high electrical conductivity, large specific capacity, low electronegativity, distinct crystalline structures, and strong redox activity. All of these qualities have led recent studies to focus on nickel sulfide (NiS) electrode materials primarily for use in supercapacitors. This interest is due to its rich chemical composition, high specific capacity, excellent electrochemical activity, and environmental friendliness. These properties make NiS-based materials promising candidates for supercapacitors [1], [2].

Nickel sulfide (NiS) is an inorganic compound belonging to the family of metal sulfides, notable for its distinctive properties and various phases, each with unique crystal structures and properties. In nature, nickel sulfide occurs in certain types of meteorites and as a rare mineral known as millerite, characterized by its needle-like crystal form, it is synthesized through several chemical processes, including the reaction of nickel salts with hydrogen sulfide (H_2S) and high-temperature reactions between nickel and sulfur. This compound exists in two polymorphic forms: the alpha (α) phase, which features a hexagonal unit cell and is stable at high temperatures, and the beta (β) phase, which has a rhombohedral cell at lower temperatures. Studies have demonstrated that NiS structures, such as hierarchical microflowers composed of layered nanoplates, show high specific capacitance and excellent electrochemical stability. These advances indicate significant potential for NiS in the development of high-performance supercapacitors [3].

Nickel-based substances are promising in the fields of energy storage and conversion, largely due to their abundance, accessibility, and cost-effectiveness. Nickel chalcogenides, in particular, are notable for their varied valence states, which lead to the formation of distinct phases with unique electronic structures. Importantly, certain phases, such as Ni_3S_2, have shown exceptional performance in both the hydrogen evolution reaction (HER)[4],[5] and the oxygen evolution reaction (OER) [6].

A superconductor is distinct from semiconductor-based components. It relies on optical and electrical energy, which can be manifested as photocurrent, playing a crucial role in optical

transmission and measurement systems. In this thesis, we will explore the synthesis and characterization of NiS nanostructures and Mg-doped NiS heterostructures for potential use in superconductors.

To address this problem, we have deposited thin semiconducting films based on NiS thin films doped with magnesium to enhance their electrical conductivity, power, and transmission. These films are applied using a single technique: spray pyrolysis. This method offers several benefits, including straightforward and inexpensive equipment, high efficiency in choosing deposition parameters, a wide range of precursor materials, and the ability to operate in an ambient atmosphere. Additionally, it facilitates easy control over the morphology of thin film, ranging from dense to porous, or even fractal types.

The title of the thesis is represented by **" Enhancement of superconducting properties of MgNiS by using oxygen annealing atmosphere "** where it is divided into five chapters, each of which is briefly presented below: **The first chapter** offers a comprehensive overview of nickel sulfide, including a description of its thin film forms :

The second chapter describes the methods and characterization techniques used in synthesizing nickel sulfide thin films and their electrochemical testing, with a discussion on the most important principles involved.

The third chapter discusses the synthesis of nanostructured films from nickel sulfide using the spray pyrolysis deposition technique, focusing on how the sources concentration used affect the electrical conductivity of nickel sulfide.

The fourth chapter focuses on the impact of magnesium doping on the structural, optical, and electrical properties of nickel sulfide thin films.

The fifth chapter discusses the impact of the oxygen annealing process on the structural, optical, and electrical properties of nickel sulfide thin films.

Finally, a summary of the chapters is provided, outlining the results of this research work and suggesting avenues for future research.

REFERENCES

[1] Yan X, Tong X, Ma L, Tian Y, Cai Y, Gong C, et al. Synthesis of porous NiS nanoflake arrays by ion exchange reaction from NiO and their high performance supercapacitor properties. Mater Lett 2014;124:133–6.https://doi.org/10.1016/j.matlet.2014.03.067.

[2] Zhang H, Yu X, Guo D, Qu B, Zhang M, Li Q, et al. Synthesis of bacteria promoted reduced graphene oxide-nickel sulfide networks for advanced supercapacitors. ACS Appl Mater Interfaces 2013;5:7335–40. https://doi.org/10.1021/am401680m.

[3] Guan Y, Hu K, Su N, Zhang G, Han Y, An M. Review of NiS-Based Electrode Nanomaterials for Supercapacitors. Nanomaterials 2023;13:1–35. https://doi.org/10.3390/nano13060979.

[4] Qu Y, Yang M, Chai J, Tang Z, Shao M, Kwok CT, et al. Facile Synthesis of Vanadium-Doped Ni3S2 Nanowire Arrays as Active Electrocatalyst for Hydrogen Evolution Reaction. ACS Appl Mater Interfaces 2017;9:5959–67. https://doi.org/10.1021/acsami.6b13244.

[5] Kajbafvala M, Moradlou O, Moshfegh AZ. CVD growth of the nanostructured Ni3S2 thin films as efficient electrocatalyst for hydrogen evolution reaction. Vacuum 2021;188:110209. https://doi.org/10.1016/j.vacuum.2021.110209.

[6] Qin JF, Yang M, Hou S, Dong B, Chen TS, Ma X, et al. Copper and cobalt co-doped Ni3S2 grown on nickel foam for highly efficient oxygen evolution reaction. Appl Surf Sci 2020;502:144172. https://doi.org/10.1016/j.apsusc.2019.144172.

CHAPTER ONE :

A General Review of Nickel Sulfide Nanostructured

In this chapter, an overview of the literature on the various physical properties of nickel sulfide thin films is presented. Aspects such as structural, optical, and electrical properties are first discussed, followed by a brief presentation about the applications of these films.

I. 1. Introduction

The electrochemical characteristics of electrode materials are significantly influenced by their shape and structure, affecting aspects such as available surface areas, diffusion pathways of electrolyte ions, and structural stability [1]. Typically, nanostructured TMS (transition metal sulfides) systems exhibit a variety of shapes, including 0D (zero-dimensional) particles [2], 1D (one-dimensional) structures such as nanowires, nanorods [3], and nanotubes [4]. In the 2D (two-dimensional) category, there are thin films [5], nanosheets [6], and nanoplates [7]. Additionally, 3D (three-dimensional) formations like flowers and urchin-like shapes are also present[8].

Transition metal sulfides, including copper sulfide (CuS), molybdenum sulfide (MoS), nickel sulfide (NiS), and cobalt sulfide (CoS), are known for their impressive electronic, optical, and photoelectric characteristics. These materials find significant use in various advanced scientific and technological fields. Notably, nickel sulfide (NiS) stands out within this broad group due to its unique phase transition from an antiferromagnetic semiconductor at low temperatures to a paramagnetic metal at high temperatures [9].

I. 2. Presentation of Nickel sulfide

The nickel sulfide family comprises various chemical compounds with different proportions of sulfur (S) and nickel (Ni), such as Ni_3S_2, Ni_6S_5, Ni_7S_6, Ni_9S_8, NiS, Ni_3S_4, and NiS_2. This last element is characterized by its rich chemistry [10], It boasts a very considerable theoretical capacity of (1060 Fg^{-1}) [11],[7], minimal toxicity, remarkable electronic conduction, cost-effectiveness, a variety of valence states and ease of fabrication [12]. Table (I.1) provides a brief overview of the semiconducting properties of nickel sulfide, with the chemical formula NixSy, including its melting and boiling points.

Table (I.1): *Properties of Nickel sulfide.*

Parameter	*Value*
Chemical formula	NixSy
Density (Volumic mass)	5500 kg/m^3
Melting point	797°C
Boiling point	1388°C
Type of conductivity	P-type
Aspect	black solid
Designation	inorganic

Figure (I.1) displays the crystal structures of NiS, NiS_2, Ni_3S_2, and Ni_9S_8. These materials exhibit considerable stability in highly alkaline conditions due to the automatic formation of an oxide/hydroxide layer on the sulfide surfaces [13].

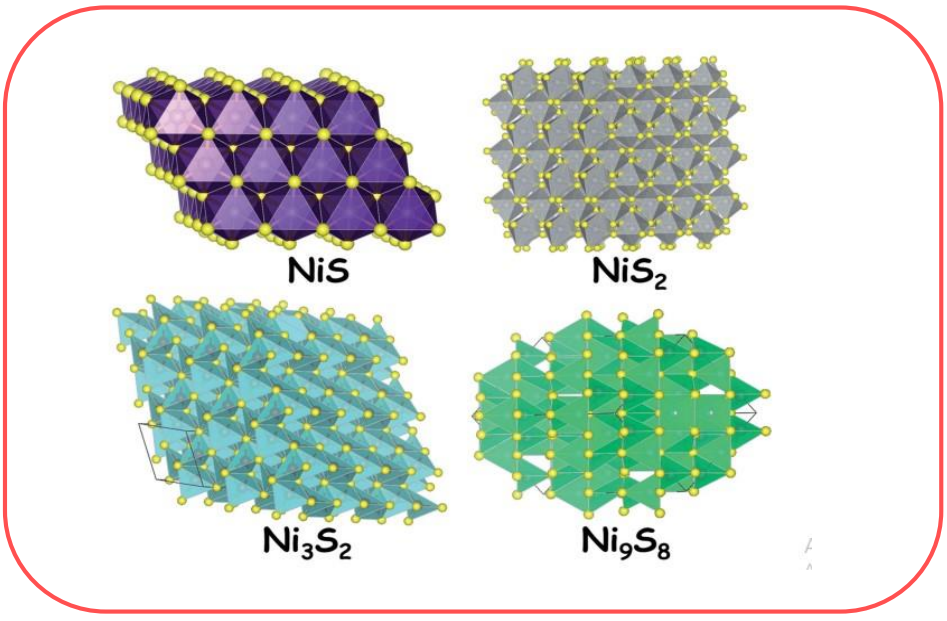

Figure (I.1): *depicts the crystal structures of different polymorphic forms of nickel sulfides.*

I. 3. Deposition Method of Nickel sulfides thin films

The schematic offers a concise classification of thin film deposition techniques as referenced in the literature. It categorizes various methods according to specific criteria and characteristics, providing a clear overview of the techniques employed in the field of thin film deposition [14].

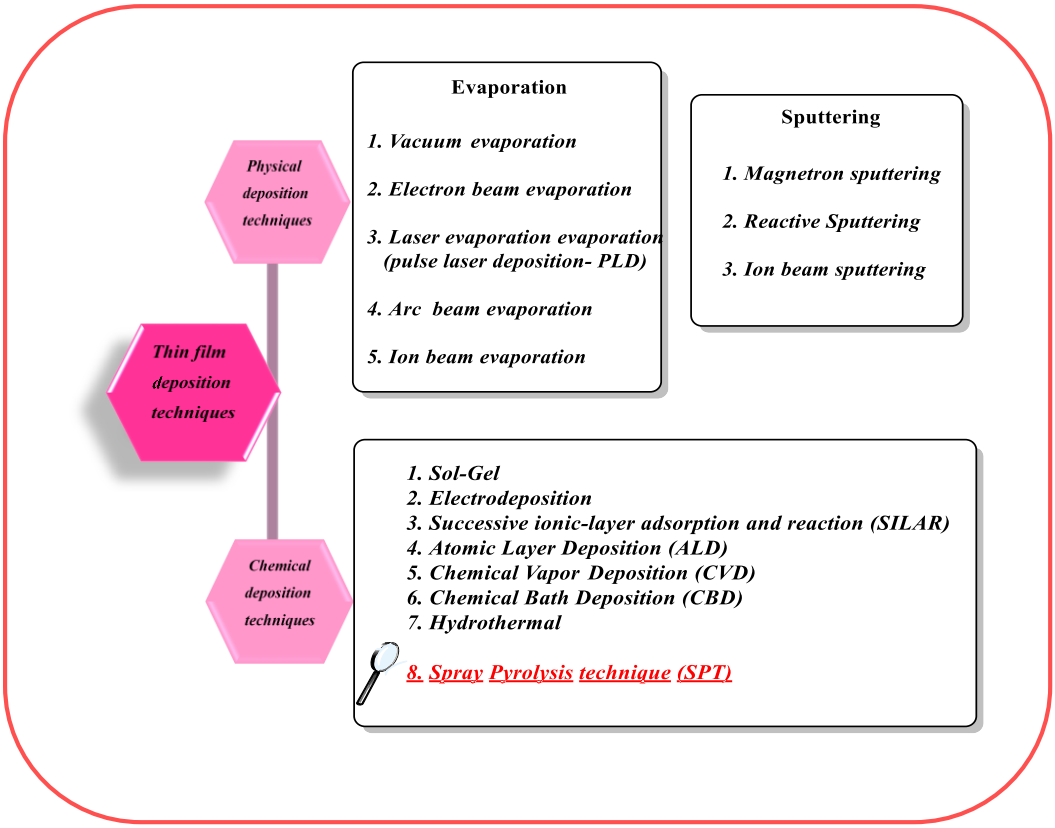

***Figure* (I.2) :** *Categorization of thin film deposition methods.*

I. 3. 1. Sol-gel method:

This technique is a straightforward and pure method for producing thin films on metal or glass substrates. The creation of a thin film via the sol-gel process encompasses three stages: (a) *creating a precursor solution*, (b) *applying the sol onto the substrate through a suitable method* and (c) *applying thermal treatment to the film that has been deposited* **[14]**,**[15]**. *Buchmaier et al.* **[16]** They prepared nickel sulfide thin films and stabilized nanocrystals using spin-coating methods. Their findings revealed that the nanoparticles comprised primarily hexagonal NiS, with cubic Ni_3S_4 forming as a secondary phase. Additionally, TEM-EDX analysis revealed that these nickel sulfide nanocrystals had a composition rich in sulfur.

I. 3. 2. Chemical Bath Deposition (CBD):

The chemical bath deposition (CBD) method is known for its low-temperature process of creating thin films, yielding semiconductors that compete with those from more advanced methods. The principle behind CBD is supersaturation, which leads to precipitation when ionic concentrations surpass the solubility threshold in solutions of sparingly soluble salts. Advantages of CBD include simultaneous multiple film deposits, suitability for complex compounds, protection against substrate damage, and enhanced crystal growth due to extended reaction times. Its effectiveness is influenced by factors such as bath temperature, pH levels, complexing agents, ion concentrations, duration of deposition, and the freshness of the stock solution **[17]**,**[18]**. *Pramanik et al.* **[19]** They conducted the chemical deposition of nickel sulphide on glass in an alkaline medium using thioacetamide. Their results showed that the films are polycrystalline, with an identified optical band gap of 0.35 eV for NiS.

I. 3. 3. Electrodeposition:

Electrodeposition is a cost-effective and efficient option compared to more costly vacuum-based methods for applying surface coatings. It is particularly useful for preventing corrosion and creating nanostructures. This technique can be performed using different modes, including potentiostatic, galvanostatic, and pulsed potential settings. By varying parameters such as time, current density, potential, pH and electrolyte composition, the thin

film's structure and properties can be finely tuned. Benefits include precision, low cost, scalability, minimal equipment expense, absence of vacuum necessity, high deposition rates, and controlled composition. The effectiveness of electrodeposition is primarily determined by the dynamics of mass transfer and the kinetics of the reactions involved [20],[21],[22]. *Arun et al.* [23] They employed an electrochemical method for precipitating nickel sulfide, aiming to assess the effectiveness of electrocatalysts in hydrogen evolution within acidic environments. This technique is distinguished for its energy efficiency and the ease with which it can be scaled up for larger substrates. A significant feature of their fabrication method is the avoidance of extra heat treatments, making use of Ni, Mo, and S as the precursors for deposition.

I. 3. 4. Atomic Layer Deposition (ALD):

Initially employed by Suntola and Antson for synthesizing compound thin films, it has found extensive use in fields such as catalysis, energy, and the environment. This method presents numerous advantages:

a) *It generates films with outstanding uniformity and precision*.
b) *The parameters of its system are customizable for consecutive thin film deposits.*
c) *It facilitates the creation of extremely thin films*.
d) *ALD provides the ability to precisely regulate film thickness and particle dimensions*.
e) *It produces films that are both dense and free of pinholes*.
f) *ALD is characterized by its rapid deposition rates*.

Variants of ALD include Plasma Enhanced ALD (PEALD) and particle ALD. On the downside, ALD can be slower in deposition and require expensive equipment and precursors, especially for large-scale operations [24],[25],[26],[27]. *Yasemin et al.* [28] Explored the growth of NiSx films on silicon using ALD technology, utilizing $Ni(amd)^2$ and H_2S as precursors. They observed self-limiting film growth across a temperature range of 125-225 °C. The team noted that the film growth rate was not affected by the reactor temperature, but it varied with the thickness of the film. Initially, over the first 50 AB cycles,

an ellipsometrically measured growth rate of 0.50 ± 0.04 Å/cycle was observed, which subsequently reduced to 0.20 ± 0.07 Å/cycle after 50 cycles.

I. 3. 5. Successive ionic-layer adsorption and reaction (SILAR):

The SILAR method, pioneered by Nicolau in 1984 for depositing CdS and ZnS thin films at room temperature, is a notable technique involving the alternate immersion of substrates in anion and cation solutions, with rinsing in between. Its advantages include simplicity and versatility, enabling direct growth and simultaneous deposition of doped and multilayer compounds. The process is quick and reproducible, reduces material waste due to a lack of precipitate formation, and is effective for depositing films on more delicate materials **[29]**,**[30]**,**[31]**,**[32]**. *Ubale et al.* **[33]** Successfully deposited high-quality (NiS_x CdS_{1-x}) composite thin films using the SILAR method. The results revealed that these deposited and annealed (NiS_x CdS_{1-x}) films exhibit a polycrystalline nature, comprising a mix of rhombic and hexagonal crystal structures attributed to NiS and CdS, respectively. The band gap values were identified as 0.92 eV for NiS and 2.3 eV for CdS.

I. 3. 6. Spray deposition method:

Synthesis methods play a crucial role in determining the structure and properties of films. To date, spray pyrolysis is one of the most important methods for preparing thin nickel sulfide films and their composites. This method has gained widespread use due to its simplicity, versatility in processing, and the ability to precisely control production. To achieve nickel sulfides with the desired morphology and manageable size, we will utilize the spray pyrolysis technique to deposit nickel sulfide thin films. This process will be elaborated upon in the subsequent chapter.

Note: In general, both nickel and sulfur sources should be carefully selected for the preparation of precursors in nickel sulfide synthesis. Common sulfur sources include thioacetamide (TAA), thiourea (TU), sodium sulfide, and carbon disulfide. These sources significantly influence the shape and size of the films. Among these sources, thiourea was particularly notable for its use in the manufacture of nickel sulfide (NiS) thin films. For nickel, key chemical compounds used in preparing the spray solutions are nickel nitrate,

nickel chloride, and nickel acetate. For further illustration, refer to figures (I.3-I.4) and table (I.2).

Table (I.2): *information of Nickel & sulfur types.*

Sample	*Synthesis Method*	*Source (Ni)*	*Source (S)*	*Condition*	*Ref*
NiS thin film	*SPT*	($NiCl_2$,5H_2O)	($SC(NH_2)_2$)	T=250°C, [$NiCl_2$, 5H_2O]=10^{-2}M +[S=C(NH2)2]=2.10^{-2} M	[34]
NiS thin film	*SPT*	($Ni(NO_3)_2.6H_2O$)	($SC(NH_2)_2$)	T= 325°C, (Ni (NO_3)2.6H_2O 10^{-1}M) + ($SC(NH_2)_2$ 2.10^{-1} M)	[35]
NiS thin film	*SPT*	($C_4H_6O_4Ni.4H_2O$)	($SC(NH_2)_2$)	T=300°C, [$C_4H_6O_4Ni.4H_2O$]= 0.07M + [$CS(NH_2)_2$]= 0.21M,	[36]

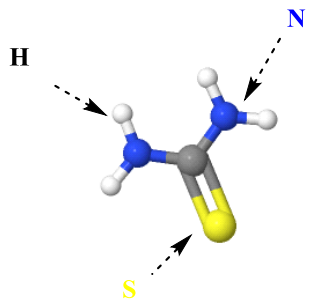

Thiourea

CH_4N_2S

Molecular Weight: 76.12 g/mol
Densit: 1.4 g/cm³
Boiling Point :150 – 160°C
Melting Point: 176 – 178°C

***Figure* (I.3):** *An image showing the source of sulfur S.*

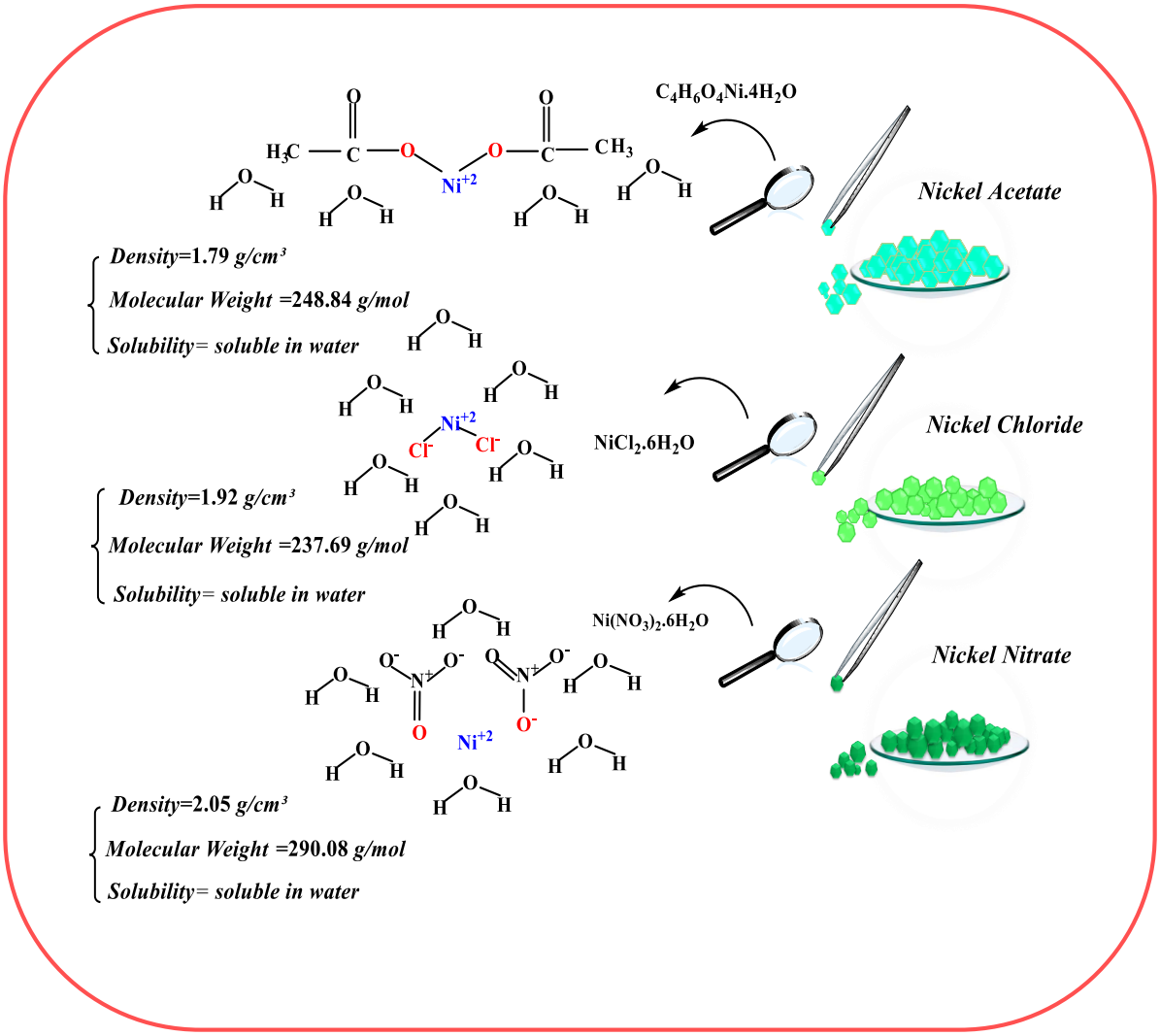

***Figure* (I.4):** *An image showing the source of Nickel Ni.*

I.4 Nickel Sulfides thin films

I. 4. 1. Structural characteristics Nickel sulfide:

Nickel sulfide undergoes crystallization in two distinct stoichiometric phases. The first, the α-NiS phase, has a hexagonal structure and is prominent at high temperatures. This phase is considered significant in the field of transition metal chemistry. The second phase, β-NiS, features a rhombohedral structure and forms at lower temperatures [37], It is known as millerite. Millerite, a naturally occurring and odorless mineral, possesses a ternary crystal

system with the R3m space group. This characteristic makes nickel sulfide a suitable and stable candidate for the electrocatalytic splitting of water, including in neutral, near-neutral, and alkaline environments . *Jeffrey et al.* **[38]** Measured the intensity of the X-ray diffraction peak in hexagonal nickel sulfide metal at high and low temperatures during the metal-semiconductor transition. Their goal was to study the atomic positions in both phases. They observed a change in the unit cell symmetry from P63/mmc to P63mc in the semiconducting phase.

The lattice parameter refers to the physical dimensions of unit cells in a crystal lattice. Typically, lattices in three dimensions have three lattice constants, known as a, b, and c. However, in hexagonal phase crystal structures, a special case arises where the a and b constants are equal, leading to only the a and c constants being referenced. Similarly, in rhombohedral phase crystal structures, all a, b, and c constants are equal, and only the a constant is referred to. Nevertheless, the full set of lattice parameters includes not only the three lattice constants but also the three angles between them. For the hexagonal crystal system, the crystallographic parameters are: a = b = 3.420 Å, c = 5.300 Å, with Alpha (°) = Beta (°) = 90°, and Gamma (°) = 120°, as recorded in the ICSD 98-060-2488 card.

According to the Chemical Vapor Deposition (CVD) method, *Boughalmi et al.* **[34]** and *Gahtar et al.* **[35]** Prepared thin films of nickel sulfide on glass substrates at various temperatures using the spray pyrolysis technique, as shown in Table I.2. Through X-ray diffraction (XRD) analysis, it was determined that the nickel sulfide thin film possesses a polycrystalline nature with a hexagonal structure.

Gahtar et al **[39]**. Deposited thin films of nickel sulfide on glass substrates at a temperature of 325°C using the spray pyrolysis technique (SPT), varying the concentrations at 0.03, 0.05, and 0.07 M. Their results from X-ray diffraction analysis revealed that all polycrystalline samples exhibited a hexagonal structure. Furthermore, they found that the most prominent peak, corresponding to the (111) plane, was higher than all other diffraction peaks, indicating it as the preferred orientation. It was concluded that the nickel sulfide thin films prepared at a concentration of 0.03 M possessed a highly crystalline structure. On the other hand, he explored the impact of substrate temperature on the physical properties of

membranes using the same technique. In his research, (NiS) thin films were deposited at various temperatures: 523, 573, and 623 K. It was discovered that the (NiS) thin films exhibited orthogonal, hexagonal, and hexagonal structures, corresponding to Ni_3S_2, $Ni_{17}S_{18}$ and NiS_2, respectively. Additionally, these films demonstrated preferential orientations along the (110), (015), and (010) planes, respectively **[40]**. *Gahtar et al.* **[36]** Also explored the effect of annealing time on the physical and chemical properties in another study. In this research, the prepared layers were heated in a conventional oven at a temperature of 300°C for different durations: 1 hour, 2 hours, and 3 hours. Noticeable changes were observed in the structural properties of the NiS films due to varying annealing times. X-ray diffraction analysis revealed that all the polycrystalline samples had a hexagonal structure. The results indicated that both partial stress and dislocation density decreased as the annealing time increased. Additionally, the grain size grew with longer annealing times, suggesting the formation of high-quality, densely structured NiS thin films.

The table (I.3) below reviews various works and research studies focusing on the crystallite size and structural phases of nickel sulfide prepared using different methods.

***Table* (I.3):** *The preferred orientation, Structure and Crystallite size of various deposited NiS thin films.*

Phase	*Condition*	*Preferred orientation*	*Structure*	*The Crystallite size*	*Method*	*Ref*
NiS	T=250°C, $[NiCl_2,2H_2O]$ =10^{-2}M [S=C(NH2)2]=2.10^{-2}M	(100)	Hexagonal	29.997 nm	(SPT)	**[34]**
NiS	$[C_4H_6O_4Ni.4H_2O]$=0.07M $[CS(NH_2)_2]$=0.21M,T=300°C, Annealing time (0h, 1h, 2h &3h at 300°C	(012)	Hexagonal	19.573 nm 16.796 nm 23.500 nm 16.795 nm	(SPT)	**[39]**
NiS	$[Ni(NO_3)2.6H_2O]$/ $[CS(NH_2)_2]$=1/3, Ionized water=150ml, [C_1=0.03M, C_2=0.05M, C_3=0.07 M], T=300°C	(010)	Hexagonal	23.903 nm 27.519 nm 42.678 nm	(SPT)	**[39]**

Ni_3S_2 **$Ni_{17}S_{18}$** **Ni_1S_2**	[NiCl2, 2H2O]=10^{-2} M, [S=C(NH2)2]=2.10^{-2}M, T=250°C, 3-00°C, 350°C	(110) (015) (010)	Hexagonal	49.8 nm 45.9 nm 84.6 nm	(SPT)	[40]
β-NiS	Ni(acac)$_2$] as nickel & H_2S gas as sulfur precursors. T=200−240 °C	(300)	Rhombo-hedral	/	(ALD)	[41]
β-NiS	bis (2.2, 6.6 tetramethylheptane-3.5 dionate) nickel(II) [Ni(thd)$_2$] & hydrogen sulfide (H_2S)	without any	Rhombo-hedral	/	(ALD)	[42]
NiS	T=80°C, 0.162 g ($NiCl_2$), 9.515 g ($Na_2S_2O_3$), The deposition time (10 60min).	(002)	Hexagonal	/	Electrod ep-osition	[43]
NiS	T= 80°C, 20ml of 0.8 M ($NiSO_4\,6H_2O$), 20 ml of 0.8 M (C_2H_5NS), Deposition Time (60, 90, 120, 150min)	(010)	Hexagonal	90min=07nm 120min=19nm 150min=11nm	(CBD)	[44]
NiS	/	/	Rhombo-hedral	30 nm	Electro-epositio n	[45]
Zn_x :N_{x-1}iS	20ml of 15 M ($NaS_2O_3.6H_2O$), 20 ml of 15 M ($Ni(NO)_3.\,6H_2O$), 20 ml of 15 M EDTA, [x(Zn^{+2})=0, 0.2, 0.4, 0.6, 0.8, 1]	/	Orthorh-ombic	8.92 nm 8.94 nm 8.99 nm 10.15 nm 9.52 nm 10.20 nm	(CBD)	[46]
NiS	25ml of (0.05M) $NiCl_2.6H_2O$ +25ml of (0.2M) CH4N2S + 30ml of NH4OH, T=60°C	/	Hexagonal	39.73 nm	(CBD)	[47]

I. 4. 2. Optical properties Nickel sulfide:

The analysis of the optical observation spectrum is one of the most effective methods for understanding and advancing knowledge of the band structure and the energy band gap (Eg). For optical characterization, a UV-Vis-NIR spectrophotometer was employed. The optical absorbance spectrum measurement of NiS was conducted over a wavelength range of 200 nm to 900 nm. This range was divided into three regions: the UV region (λ = 280–380 nm), the visible region (λ = 380–740 nm), and the near-IR region (λ = 740–900 nm).

In their study, *Yang et al.* **[48]** Analyzed the photoluminescence (PL) properties of NiS nanoparticles embedded in a silica gel matrix. Their results revealed two distinct emission peaks in the PL spectrum: the first peak appeared at 440 nm when excited at 380 nm, and the second peak occurred at 610 nm with excitation at 490 nm. This unique emission behavior is attributed to the NiS nanoparticles within the porous structure of the silica gel However, in their study, *Sartale et al.* **[49]** Investigated the synthesis of NiS thin films by employing the SILAR method for deposition on both glass and FTO-coated glass substrates. Their optical measurements revealed that the activation energy and optical band gap of the films were 0.15 eV and 0.45 eV, respectively. Based on the results summarized in Table (I.4), the optical band gap values for NiS thin films are reported to range from approximately 0.9 to 2.7 eV.

***Table* (I.4):** *The transmittance /absorbance and the optical band gap (Eg) of various deposited NiS thin films.*

Phase	*Condition*	*Transmittance /absorbance*	*The optical band gap (Eg)*	*method*	*Ref*
NiS	T=250°C, [$NiCl_2$, $2H_2O$]=10^{-2}M [S=C(NH2)2]=2.10^{-2}M	T= 20 %	0.55 eV	(SPT)	**[34]**
NiS	T= 325°C, (Ni (NO_3)$_2$.$6H_2O$ 10^{-1}M), ($SC(NH_2)_2$ 2.10^{-1} M)	T=0.62%	1.03 eV	(SPT)	**[39]**
NiS_2	T= 55°C (Annealed at temperatures of 100°C, 200°C, 300°C and 400°C) $NiCl_2$, $Na_2S_2O_3.5H_2O$, NH_3	/	1.8 eV 3.1 eV 2.0 eV 2.6 eV	(CBD)	**[50]**

NiS	/	T=0.62%	1.03 eV	(SILAR)	[51]
NiS	T= 80°C, 20ml of 0.8 M ($NiSO_4 6H_2O$), 20 ml of 0.8 M (C_2H_5NS), Deposition Time (60, 90, 120, 150min)	/	2.06 eV 1.97 eV 1.93 eV 2.03 eV	(CBD)	[44]
NiS_2	T= 40°C, ($NiSO_4.6H_2O$), ($Na_2S_2O_3.5H_2O$), Deposition Time (10, 15 ,20, 25min)	/	1.22eV 1.20 eV 1.17 eV 1.15 eV	Electrod-eposition	[52]
NiS	T=35°C, 25ml of 0.1M ($NiSO_4.6(H_2O)$), 25ml of 0.1M ($Na_2S_2O_3$), 3ml of ($C_6H_{15}NO_3$)	A~2.5	0.72 eV	(CBD)	[53]
NiS	T= room temperature ($NiSO_4.6(H_2O)$), 10ml of 0.8M (C_2H_5NS), 15ml of 7.4M($C_6H_{15}NO_3$), 35ml of 14M (NO_3)	/	2.8 eV	(CBD)	[54]
NiS	T=80°C, 0.162 g ($NiCl_2$), 9.515 g ($Na_2S_2O_3$), The deposition time (10-60min).	A~2.0	0.72 eV	Electrod-eposition	[43]
NiS	T=27°C, 0.1M ($NiSO_4.6(H_2O)$), 0.5M ($Na_2S_2O_3$).	A~2.5	2.4 eV	(CBD)	[55]
NiS	T=27°C, 0.1M ($NiSO_4.6(H_2O)$), 0.1M ($Na_2S_2O_3$).	/	0.45 eV	(SILAR)	[49]
NiS	T= room temperature, 10ml of ($NiSO_4$), 15ml of ($C_2H_{15}NO_3$)& ($C_2H_5NS_3$).	A~1.5	0.4 eV	(CBD)	[56]
Cu : Ni_3S_2	1. Metal diethyl-dithiocarbamate complex, 2.Nickel Nitrate (Ni $(NO_3)_2.6H_2O$) complex / Bis (N, N-diethyldithiocarbamate) nickel (II) complex, 3.Copper Nitrate ($CuNO_3.5H_2O$) complex or Bis (N, N-diethyl-dithiocarbamato) copper (II) complex.	A~ (1-2)	0%Cu= 2.1 eV 6% Cu= 1.89 eV 10% Cu= 1.63 eV	(PVD)	[57]
NiS	T=70°C, [$NiCl_2$, $2H_2O$]=10^{-2}M [S=C(NH2)2]=2.10^{-2}M	A~ (9-14)	1.39 eV	(CBD)	[58]

Zn_x : $N_{x-1}iS$	20ml of 15 M ($NaS_2O_3.6H_2O$), 20 ml of 15 M ($Ni(NO)_3$. $6H_2O$), 20 ml of 15 M EDTA, [$x(Zn^{+2})$=0, 0.2, 0.4, 0.6, 0.8, 1]	A~ (0-7)	2.54 eV 2.53 eV 2.52 eV 2.50 eV 2.40 eV 2.25 eV	(CBD)	[46]

I. 4. 3. Electrical properties Nickel sulfide:

The study of the electrical properties of nickel sulfide thin films is crucial due to their potential use in various electronic devices. Properties like conductivity, resistance, and dielectric behavior can vary based on the method of synthesis and the specific conditions under which the films are prepared. However, *Basha et al.* **[44]** Successfully created NiS thin films on glass substrates using chemical bath deposition at 80 °C for durations ranging from 60 minutes. Their electrical measurement findings indicated that the conductivity of these films varied from 1.35 to 48.3 S/cm. This conductivity range demonstrates their potential effectiveness in solar cell applications, showcasing their suitability for such use, in their research, *Boughalmi et al.* **[59]** Focused on the metallic behavior of nickel sulfide thin films fabricated via the spray pyrolysis technique at 250 °C. Their findings revealed that the direct current conductivity displayed metallic behavior. Additionally, Hall effect measurements at 24 °C resulted in a negative Hall coefficient, indicative of electronic conductivity, with a charge carrier density of around 3.67×10^{22} cm^{-3} and an electron mobility of approximately 0.6 cm^2/Vs. Furthermore, their theoretical framework, aligned with experimental results, showed that the structural parameters and density of states of NiS confirm the metallic behavior.

***Table* (I.5):** *The Conductivity electrical /resistivity and the Film thickness of various deposited NiS thin films.*

Sample	*Condition*	*Film thickness (e)*	*The Conductivity (σ)/resistivity(ρ)*	*Method*	*Ref*
NiS	T=250°C, [$NiCl_2$, $5H_2O$]=10^{-2}M [$S=C(NH_2)_2$]=2.10^{-2} M	/	σ= 4.4 10^2 (S/cm)	(SPT)	[34]

NiS	T= 325°C, (Ni $(NO_3)_2.6H_2O$ 10^{-1}M), $(SC(NH_2)_2$ 2.10^{-1} M)	936.253 nm	σ= 1.10 10^5 (S/cm)	(SPT)	[35]
NiS	$[C_4H_6O_4Ni.4H_2O]$= 0.07M $[CS(NH_2)_2]$= 0.21M, T=300°C, annealed 0h, 1h, 2h and 3h	/	σ= $(\Omega.cm)^{-1}$: 0h =3.56 10^4 1h =5.76 10^4 2h =7.91 10^4 3h =4.97 10^4	(SPT)	[36]
Ni_3S_2 **$Ni_{17}S_{18}$** **Ni_1S_2**	$[NiCl_2, 2H_2O]=10^{-2}$ M, $[S=C(NH_2)_2]=2.10^{-2}$ M, T=250° T=300°C T=350°C	798 nm 390 nm 681 nm	σ= $(\Omega.cm)^{-1}$: 250°C =6.24 10^4 300°C =4.29 10^4 350°C =9.47 10^4	(SPT)	[40]
NiS	T=27°C, 0.1M ($NiSO_4$.6 (H_2O)), 0.5M ($Na_2S_2O_3$).	~ 0.3µm	ρ~10Ωcm	(CBD)	[55]

I. 5. Nickel sulfide applications

The electrochemical behavior of nickel sulfide is currently classified as that of a battery-type material because it is a nearly infinite and diffusion-limited reaction process, and due to its low cost, high capacity and conductivity in electronic and environmental sustainability, nickel sulfide has been widely used in hybrid supercapacitors [60]. which is why it has been used in many technological applications, including dye-sensitized solar cells [61] IR detectors, potential cathode material for rechargeable lithium batteries [62], catalysis [63] hydrogen production [64], paramagnetic-antiferromagnetic agents [65] and electrodes of LIBs [66] and SCs [67]. Many studies have focused on electrocatalytic hydrogen generation using nickel chalcogenides, with nickel sulphides being particularly prominent. Owing to their reasonable (though not strong) stability under light and their applicability to reduction processes in both acidic and alkaline environments, they are considered some of the most attractive electrocatalysts for the hydrogen evolution reaction (HER). Serve nickel sulfide effectively as electrocatalysts for the hydrogen evolution reaction (HER) and as pre-catalysts for the oxygen evolution reaction (OER). The OER performance in alkaline environments significantly improves when these sulphides are doped with Fe and Co ions[13].

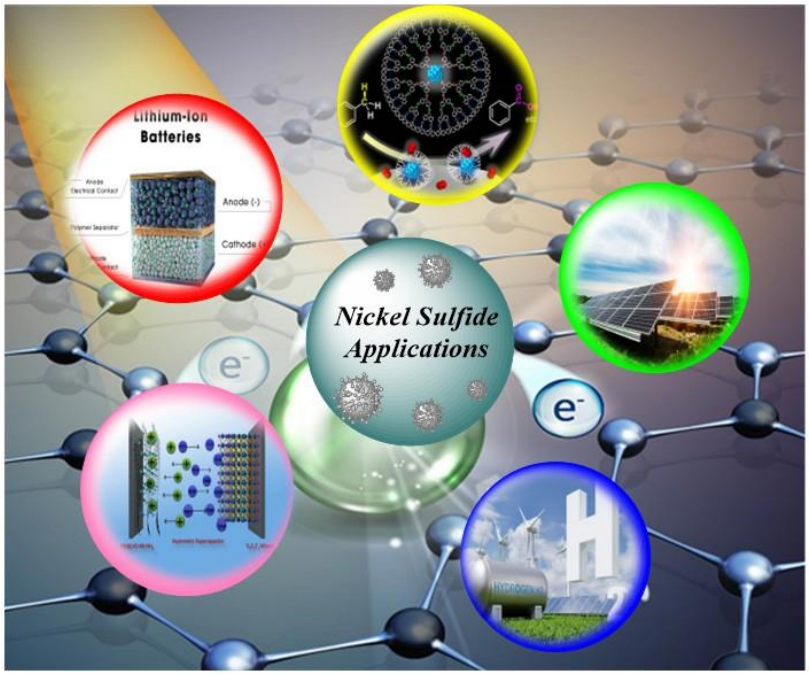

***Figure* (I.5):** *Applications of nickel sulfide.*

I. 5. 1. Electrodes of LIBs and Supercapacitors (SCs):

Conversion-reaction based metal sulfides, designated as M−S (where M = Fe, Co, Ni, etc.), demonstrate higher theoretical capacities for storing Li due to their redox reactions. A significant challenge with sulfide anodes, however, is electrode pulverization during charge and discharge cycles, leading to rapid declines in specific capacities [68]. In contrast, supercapacitors, known for their high capacitance values compared to other capacitors but with lower voltage limits, effectively bridge the gap between electrolytic capacitors and rechargeable batteries. They store energy via a dual mechanism of double-layer capacitance and pseudocapacitance, substantial energy density, and robust cycle stability. Additionally, their relatively affordable cost adds to their appeal in various applications.enabling faster charging and discharging than traditional batteries [37].

Jasinski et al. **[69]** Reported that nickel sulfides are versatile enough to serve as both cathode and anode materials in lithium-ion batteries (LIBs). Particularly under conditions of deep discharge, these compounds react with Li^+ ions to form metallic Ni and Li2S, exhibiting promising theoretical capacities. Specifically, capacities of 590, 445, and 704 mAh g^{-1} have been noted for NiS, Ni_2S_3 and Ni_3S_4, respectively. However, initial studies into nickel sulfides role in LIBs have indicated a relatively low utilization rate. *Kumar et al.* **[70]** Employed the continuous ion layer adsorption and reaction (SILAR) technique on a nickel foam base. When they created solid-state asymmetric supercapacitors, the developed NS-SnS (NTS) heterogeneous electrode materials demonstrated an impressive specific capacitance of 1653 F g^{-1} at a current density of 1 A g^{-1}. Additionally, these materials exhibited a noteworthy high energy density of 83 W h kg^{-1} at a power density of 117 W kg^{-1}. Moreover, these electrodes showed superior rate performance and maintained stability over numerous cycles.

I. 5. 2. Hydrogen Evolution Reaction (HER):

Because nickel sulfide is highly stable, superconductive, and capable of chemically reducing protons to hydrogen gas as efficiently as expensive noble metals, it can be difficult to produce using specific surface site compositions or shapes, for example, compatible thin films **[28]**, *Yasemin et al.* **[28]** Evaluated the electrocatalytic activity of NiSx prepared using the ALD technique for molecular hydrogen evolution. Films were grown on conductive glass supports. The overvoltage was recorded at a current density of 10 mA/cm^2 in both acidic aqueous reaction media and phosphate buffer of pH 7 and was found to be 440 and 576 mV, respectively, with very low NiSx loading. These results indicate promise for ALD-grown NiSx materials as water-compatible electrocatalysts.

I. 5. 3. Oxygen reduction reaction (ORR):

Falkowski et al. **[71]** Displyed prepared the heazlewoodite phase of Ni_3S_2 thin films on gold electrodes by electrodeposition of nanoparticles in heir article as highly active, toxic and corrosion-resistant catalysts for the reduction of oxygen to water at a neutral pH. In pH7 phosphate buffer. The Ni_3S_2 thin films showed high Faradaic efficiency for the electron

reduction of O_2 to water with four electrons, a Tafel slope of 109 mV/decade, and a catalytic onset at 0.8 V versus the reversible hydrogen electrode. Under these conditions, the activity and stability. A nickel-based oxygen evolution catalyst was produced by *Oluwaniyi et al.* [72] Using nickel sulfide deposited in the electrolyte. The results of this catalyst, which generates current densities of 10 mA/cm^2 at a relatively low overvoltage of 320 mV in an alkaline electrolyte (1 M KOH), are described. According to his research, he demonstrated that the sulfur anion present in nickel sulfide is depleted using the catalyst. Electroactive NiS converts to amorphous nickel oxide in the potential range when water is oxidized to oxygen. Nickel sulfide shows higher catalytic activity, which is not related to the sulfur anions present in the active catalyst but rather to its ability to act as a precursor to the highly active nickel oxide OER electrocatalyst. The nickel sulfide derivative, nickel oxide, was found to be amorphous with a fairly high specific surface area, proving the importance of two previously demonstrated factors in the electrocatalysis of oxygen evolution.

Table (I.6) presents a summary of various studies on the advancements in electrochemical performance of nickel sulfide nanostructures.

***Table* (I.6):** *comparative analysis of the electrochemical performance of nanostructured nickel sulfide electrodes of various different preparation methods.*

Sample	*nanostructured*	*Method of Preparation*	*Specific capacitance/ Energy density*	*Ref*
Ni_3S_2	thin films	Pulsereversal electrodeposition	600F/g at 1A/g 450 F/g at 8 A/g	[73]
NiS	nanoplates	hydrothermal	35.07 W h kg^{-1} at 420 W kg^{-1}	[7]
β-NiS	flower-like coral-like urchin-like flake-like	solvothermal	2425.89F g^{-1} at 1 A g^{-1} 1056.25F g^{-1} at 1 A g^{-1} 814 F g^{-1} at 1 A g^{-1} 1760 F g^{-1} at 1 A g^{-1}	[74]
Ni_3S_2	nanosheet	hydrothermal	1370.4F g^{-1} at 2 A g^{-1}	[75]
Ni_3S_2	nanorod/nanowire	hydrothermal	48.5 W h kg^{-1} at 87.4 W kg^{-1}	[76]
Ni_3S_2	nanoparticles	hydrothermal	13 400 mF cm^{-2} at 10 mA cm^{-2}	[77]

References

[1] Gao Y, Zhao L. Review on recent advances in nanostructured transition-metal-sulfide-based electrode materials for cathode materials of asymmetric supercapacitors. Chem Eng J 2022;430:132745. https://doi.org/10.1016/j.cej.2021.132745.

[2] Ameen S, Akhtar MS, Kim YS, Shin HS. Synthesis and electrochemical impedance properties of CdS nanoparticles decorated polyaniline nanorods. Chem Eng J 2012;181–182:806–12. https://doi.org/10.1016/j.cej.2011.11.111.

[3] Sun S, Nie Y, Sun M, Liang T, Sun M, Yang H. Facile synthesis of CoNi2S4 one-dimensional nanorods as anode for high performance lithium ion batteries. Mater Lett 2016;176:87–90. https://doi.org/10.1016/j.matlet.2016.04.094.

[4] Zhang Y, Ma M, Yang J, Sun C, Su H, Huang W, et al. Shape-controlled synthesis of NiCo2S4 and their charge storage characteristics in supercapacitors. Nanoscale 2014;6:9824–30. https://doi.org/10.1039/c4nr02833c.

[5] Ji F, Jiang D, Chen X, Pan X, Kuang L, Zhang Y, et al. Simple in-situ growth of layered Ni 3 S 2 thin film electrode for the development of high-performance supercapacitors. Appl Surf Sci 2017;399:432–9. https://doi.org/10.1016/j.apsusc.2016.12.106.

[6] Yang X, Zhao L, Lian J. Arrays of hierarchical nickel sulfides/MoS2 nanosheets supported on carbon nanotubes backbone as advanced anode materials for asymmetric supercapacitor. J Power Sources 2017;343:373–82. https://doi.org/10.1016/j.jpowsour.2017.01.078.

[7] Harish S, Naveen AN, Abinaya R, Archana J, Ramesh R, Navaneethan M, et al. Enhanced performance on capacity retention of hierarchical NiS hexagonal nanoplate for highly stable asymmetric supercapacitor. Electrochim Acta 2018;283:1053–62. https://doi.org/10.1016/j.electacta.2018.06.161.

[8] He Q, Wang Y, Liu XX, Blackwood DJ, Chen JS. One-pot synthesis of self-supported hierarchical urchin-like Ni3S2 with ultrahigh areal pseudocapacitance. J Mater Chem A 2018;6:22115–22. https://doi.org/10.1039/c8ta05050c.

[9] Jana S, Mukherjee N, Chakraborty B, Mitra BC, Mondal A. Electrodeposited polymer encapsulated nickel sulphide thin films: Frequency switching material. Appl Surf Sci 2014;300:154–8. https://doi.org/10.1016/j.apsusc.2014.02.026.

[10] Rui X, Tan H, Yan Q. Nanostructured metal sulfides for energy storage. Nanoscale 2014;6:9889–924. https://doi.org/10.1039/c4nr03057e.

[11] Sun C, Ma M, Yang J, Zhang Y, Chen P, Huang W, et al. Phase-controlled synthesis of α-

NiS nanoparticles confined in carbon nanorods for High Performance Supercapacitors. Sci Rep 2014;4:1–6. https://doi.org/10.1038/srep07054.

[12] Gaikar P, Pawar S P, Mane R S, Nuashad M SD V. Synthesis of nickel sulfide as a promising electrode material for pseudocapacitor application. RSC Adv 2016;6:112589–112593. https://doi.org/10.1039/c0xx00000x.

[13] Anantharaj S, Kundu S, Noda S. Progress in nickel chalcogenide electrocatalyzed hydrogen evolution reaction. J Mater Chem A 2020;8:4174–92. https://doi.org/10.1039/c9ta14037a.

[14] Pedanekar RS, Shaikh SK, Rajpure KY. Thin film photocatalysis for environmental remediation : A status review Thin fi lm photocatalysis for environmental remediation : A status review. Curr Appl Phys 2020;20:931–52. https://doi.org/10.1016/j.cap.2020.04.006.

[15] Znaidi L. Sol – gel-deposited ZnO thin films : A review. Mater Sci Eng B 2010;174:18–30. https://doi.org/10.1016/j.mseb.2010.07.001.

[16] Buchmaier C, Glänzer M, Torvisco A, Poelt P, Wewerka K, Kunert B, et al. Nickel sulfide thin films and nanocrystals synthesized from nickel xanthate precursors. J Mater Sci 2017;52:10898–914. https://doi.org/10.1007/s10853-017-1265-5.

[17] Mane RS, Lokhande CD. Chemical deposition method for metal chalcogenide thin films. Mater Chem Phys 2000;65.

[18] Hone FG, Tizaz A. Short Review of Factors Affecting Chemical Bath Deposition Method for Metal Chalcogenide Thin Films. Int J Thin Film Sci Technol 2019;8.

[19] Pramanik P, Biswas S. Deposition of nickel chalcogenide thin films by solution growth techniques. J Solid State Chem 1986;65:145–7. https://doi.org/10.1016/0022-4596(86)90098-8.

[20] Xiao F, Hangarter C, Yoo B, Rheem Y, Lee KH, Myung N V. Recent progress in electrodeposition of thermoelectric thin films and nanostructures. Electrochim Acta 2008;53:8103–17. https://doi.org/10.1016/j.electacta.2008.06.015.

[21] Saji VS. Electrodeposition in bulk metallic glasses. Materialia 2018;3:1–11. https://doi.org/10.1016/j.mtla.2018.09.021.

[22] Manivannan R, Victoria SN. Preparation of chalcogenide thin films using electrodeposition method for solar cell applications – A review. Sol Energy 2018;173:1144–57. https://doi.org/10.1016/j.solener.2018.08.057.

[23] Murthy AP, Theerthagiri J, Premnath K, Madhavan J, Murugan K. Single-Step Electrodeposited Molybdenum Incorporated Nickel Sulfide Thin Films from Low-Cost

Precursors as Highly Efficient Hydrogen Evolution Electrocatalysts in Acid Medium. J Phys Chem C 2017;121:11108–16. https://doi.org/10.1021/acs.jpcc.7b02088.

[24] Cai J, Han X, Wang X, Meng X. Atomic Layer Deposition of Two-Dimensional Layered Materials: Processes, Growth Mechanisms, and Characteristics. Matter 2020;2:587–630. https://doi.org/10.1016/j.matt.2019.12.026.

[25] CCai J, Shan B, Chen R. Surface functionalization on nanoparticles via atomic layer deposition. Sci Bull 2020;65:678–88. https://doi.org/10.1016/j.scib.2020.01.016.

[26] Muñoz-Rojas D, Maindron T, Esteve A, Piallat F, Kools JCS, Decams JM. Speeding up the unique assets of atomic layer deposition. Mater Today Chem 2019;12:96–120. https://doi.org/10.1016/j.mtchem.2018.11.013.

[27] Yang H, Chen Y, Qin Y. Application of atomic layer deposition in fabricating high-efficiency electrocatalysts. Chinese J Catal 2020;41:227–41. https://doi.org/10.1016/S1872-2067(19)63440-6.

[28] Yasemin C, Peters AW, Avila JR, Ho WL, Goswami S, Farha OK, et al. Atomic Layer Deposition of Ultrathin Nickel Sul fi de Films and Preliminary Assessment of Their Performance as Hydrogen Evolution Catalysts 2016. https://doi.org/10.1021/acs.langmuir.6b02699.

[29] Nicolau YF. Solution deposition of thin solid compound films by a successive ionic-layer adsorption and reaction process. Appl Surf Sci 1985;22–23:1061–74. https://doi.org/10.1016/0378-5963(85)90241-7.

[30] Sankapal BR, Mane RS, Lokhande CD. Successive ionic layer adsorption and reaction (SILAR) method for the deposition of large area (approximately 10 cm2) tin disulfide (SnS2) thin films. Mater Res Bull 2000;35:2027–35. https://doi.org/10.1016/S0025-5408(00)00405-0.

[31] Mohamed Mustakim NS, Ubani CA, Sepeai S, Ahmad Ludin N, Mat Teridi MA, Ibrahim MA. Quantum dots processed by SILAR for solar cell applications. Sol Energy 2018;163:256–70. https://doi.org/10.1016/j.solener.2018.02.003.

[32] Pathan HM, Lokhande CD. Deposition of metal chalcogenide thin films by successive ionic layer adsorption and reaction (SILAR) method. Bull Mater Sci 2004;27:85–111. https://doi.org/10.1007/BF02708491.

[33] Ubale AU, Bargal AN. Characterization of nanostructured photosensitive (NiS) x (CdS) (1 À x) composite thin films grown by successive ionic layer adsorption and reaction (SILAR) route. Mater Res Bull 2011;46:1000–10.

https://doi.org/10.1016/j.materresbull.2011.03.016.

[34] Boughalmi R, Rahmani R, Boukhachem A, Amrani B, Driss-Khodja K, Amlouk M. Metallic behavior of NiS thin film under the structural, optical, electrical and ab initio investigation frameworks. Mater Chem Phys 2015;163:99–106. https://doi.org/10.1016/j.matchemphys.2015.07.019.

[35] Gahtar A, Benramache S, Ammari A, Boukhachem A. Study of the Structural, Optical, Electrical and Morphological Properties of Nickel Sulfide Thin Films Used in Supercapacitors. Ann West Univ Timisoara - Phys 2021;63:1–13. https://doi.org/10.2478/awutp-2021-0001.

[36] Gahtar A, Benali A, Benramache S, Zaouche C. Effect of annealing time on the structural, morphological, optical and electrical properties of NiS thin films. Chalcogenide Lett 2022;19:103–16. https://doi.org/10.15251/CL.2022.192.103.

[37] Pothu R, Bolagam R, Wang QH, Ni W, Cai JF, Peng XX, et al. Nickel sulfide-based energy storage materials for high-performance electrochemical capacitors. Rare Met 2021;40:353–73. https://doi.org/10.1007/s12598-020-01470-w.

[38] Trahan J, Goodrich R G WSF. X-Ray Diffraction Measurements on Metallic and Semiconducting n.d. https://doi.org/10.1103/PhysRevB.2.2859.

[39] Gahtar A, Benramache S, Ammari A, Boukhachem A, Ziouche A. Effect of molar concentration on the physical properties of NiS thin film prepared by spray pyrolysis method for supercapacitors. Inorg Nano-Metal Chem 2022;52:112–21. https://doi.org/10.1080/24701556.2020.1862225.

[40] Gahtar A, Benramache S, Zaouche C, Boukacham A, Sayah A. Effect of Temperature on the Properties of Nickel Sulfide Films Performed by Spray Pyrolysis Technique. Adv Mater Sci 2020;20:36–51. https://doi.org/10.2478/adms-2020-0015.

[41] Singh R, Ayyub MM. Atomic Layer Deposition of Crystalline β -NiS for Superior Sensing in Thin- Film Non-Enzymatic Electrochemical Glucose Sensors 2021. https://doi.org/10.1021/acsaelm.1c00145.

[42] Sarkar NMK, Mahuli N. Atomic layer deposition of NiS and its application as cathode material in dye sensitized solar cell Atomic layer deposition of NiS and its application as cathode material in dye sensitized solar cell 2016;142. https://doi.org/10.1116/1.4938078.

[43] Bharathi B, Thanikaikarasan S, Chandrasekar P V., Kollu P, Mahalingam T, Ixtlilco L. Studies on electrodeposited NiS Thin Films. J New Mater Electrochem Syst 2014;17:167–71. https://doi.org/10.14447/jnmes.v17i3.417.

[44] Basha KAJ, Guddeti PR, Kotte TRR. Effect of Deposition Time on the Properties of NiS Films Prepared by. INDIAN J Sci Technol 2022:2492–9. https://doi.org/doi.org/10.17485/IJST/v15i45.1783.

[45] Press D. Reports in Electrochemistry and semiconductor studies Electrosynthesized NiS 2 thin films and their optical and semiconductor studies 2023. https://doi.org/10.2147/RIE.S47068.

[46] Younus J, Shahzad W, Ismail B, Fazal T, Shah M, Iqbal S, et al. Engineering the optical properties of nickel sulphide thin films by zinc integration for photovoltaic applications. RSC Adv 2023;13:27415–22. https://doi.org/10.1039/d3ra04011a.

[47] Pratik P, Khushalchand G, Burungale R, Sawant K, Salunkhe D, Gavade P, et al. Modified Structural , Optical and Electrochemical Properties of Nickel Sulphide for Superior Supercapacitor Electrode. Int Res J Sci Eng Spec Issue 2023. https://doi.org/10.5281/zenodo.7763091.

[48] Yang P, Lü M, Song CF, Zhou G, Xu D, Yuan DR. Photoluminescence characteristics of NiS nanocrystallites embedded in sol-gel silica xerogel. J Phys Chem Solids 2002;63:2047–51. https://doi.org/10.1016/S0022-3697(02)00192-0.

[49] Sartale SD, Lokhande CD. Preparation and characterization of nickel sulphide thin films using successive ionic layer adsorption and reaction (SILAR) method. Mater Chem Phys 2001;72:101–4. https://doi.org/10.1016/S0254-0584(01)00314-5.

[50] Osuwa JC, Uwaezi PU. EFFECTS OF ANNEALING ON OPTICAL AND SOLID STATE PROPERTIES OF NiS 2 THIN FILMS 2011;8:587–94.

[51] Sathya D. NiS THIN FILMS FOR SOLAR CELL APPLICATIONS BY SUCCESSIVE IONIC LAYER NiS THIN FILMS FOR SOLAR CELL APPLICATIONS BY SUCCESSIVE IONIC LAYER ADSORPTION AND REACTION (SILAR) METHOD 2022.

[52] Anand JS, Rajes K. M. Rajan, Mohd Zaidan Bin Abdul Aziz. Electrosynthesized NiS2 thin films and their optical and semiconductor studies. Reports Electrochem 2013:25. https://doi.org/10.2147/rie.s47068.

[53] Thangaraj M, #1 KJ, Karthigaivel K, #3 SR, Bhuvaneswari B V. Preparation and Characterization of NiS Thin film on ITO coated Glass substrate for Solar cell Applications. n.d.

[54] Sonawane MS, Patil RS. “Studies of Physical Properties of Nanocrystalline Nickel Sulphide Thin Films Grown by Simple Chemical Route.” Arch Phys Res 2014;5:32–7.

[55] Patil RS. Characterization of nickel sulphide thin films prepared by modified chemical method. vol. 53. 2015.

[56] Suresh S, Solay Anand SSR, Arul R, Isha D. Structural, morphological, optical and electrical properties of nickel sulphide thin films. Chalcogenide Lett 2016;13:291–9.

[57] Majid S, Ahmad KS. Optik Analysis of dopant concentration effect on optical and morphological properties of PVD coated Cu-doped Ni 3 S 2 thin films. Opt - Int J Light Electron Opt 2019;187:152–63. https://doi.org/10.1016/j.ijleo.2019.05.025.

[58] Sanap VB, Pawar BH. STUDY OF NANOSTRUCTURED NICKEL SULFIDE THIN FILMS FOR PHOTOVOLTAIC APPLICATIONS 2014;1:206–8.

[59] Boughalmi R, Rahmani R, Boukhachem A, Amrani B, Amlouk M. Metallic behavior of NiS thin film under the structural , optical , electrical and ab initio investigation frameworks. Mater Chem Phys 2015;163:99–106. https://doi.org/10.1016/j.matchemphys.2015.07.019.

[60] Tan Y, Xue WD, Zhang Y, He DX, Wang WJ, Zhao R. Solvothermal synthesis of hierarchical α-NiS particles as battery-type electrode materials for hybrid supercapacitors. J Alloys Compd 2019;806:1068–76. https://doi.org/10.1016/j.jallcom.2019.07.222.

[61] Sun H, Qin D, Huang S, Guo X, Li D, Luo Y, et al. Dye-sensitized solar cells with NiS counter electrodes electrodeposited by a potential reversal technique. Energy Environ Sci 2011;4:2630–7. https://doi.org/10.1039/c0ee00791a.

[62] Mgabi LP, Dladla BS, Malik MA, Garje SS, Akhtar J, Revaprasadu N. Deposition of cobalt and nickel sulfide thin films from thio- and alkylthio-urea complexes as precursors via the aerosol assisted chemical vapour deposition technique. Thin Solid Films 2014;564:51–7. https://doi.org/10.1016/j.tsf.2014.04.086.

[63] Cao F, Liu R, Zhou L, Song S, Lei Y, Shi W, et al. One-pot synthesis of flowerlike Ni7S6 and its application in selective hydrogenation of chloronitrobenzene. J Mater Chem 2010;20:1078–85. https://doi.org/10.1039/b916866d.

[64] Zhang B, Ye X, Dai W, Hou W, Xie Y. Biomolecule-assisted synthesis and electrochemical hydrogen storage of porous spongelike Ni3S2 nanostructures grown directly on nickel foils. Chem - A Eur J 2006;12:2337–42. https://doi.org/10.1002/chem.200501005.

[65] Yang SL, Yao H Bin, Gao MR, Yu SH. Monodisperse cubic pyrite NiS2 dodecahedrons and microspheres synthesized by a solvothermal process in a mixed solvent: Thermal stability and magnetic properties. CrystEngComm 2009;11:1383–90. https://doi.org/10.1039/b900444k.

[66] Han SC, Kim KW, Ahn HJ, Ahn JH, Lee JY. Charge-discharge mechanism of mechanically alloyed NiS used as a cathode in rechargeable lithium batteries. J Alloys Compd 2003;361:247–51. https://doi.org/10.1016/S0925-8388(03)00380-3.

[67] Chou S-W, Lin J-Y. Cathodic Deposition of Flaky Nickel Sulfide Nanostructure as an Electroactive Material for High-Performance Supercapacitors. J Electrochem Soc 2013;160:D178–82. https://doi.org/10.1149/2.078304jes.

[68] Shi W, Zhu J, Rui X, Cao X, Chen C, Zhang H, et al. Controlled synthesis of carbon-coated cobalt sulfide nanostructures in oil phase with enhanced li storage performances. ACS Appl Mater Interfaces 2012;4:2999–3006. https://doi.org/10.1021/am3003654.

[69] JASINSKI R, BURROWS B. Cathodic Discharge of Nickel Sulfide in Propylene Carbonate- Liclo4 Electrolyte. Electrochem Soc-J 1969;116:422–4. https://doi.org/10.1149/1.2411887.

[70] Kumar N, Mishra D, Kim SY, Jin SH. Self-assembled nis-sns heterostructure via facile successive adsorption and reaction method for high-performance solid-state asymmetric supercapacitors. Thin Solid Films 2020;709:138138. https://doi.org/10.1016/j.tsf.2020.138138.

[71] Falkowski JM, Concannon NM, Yan B, Surendranath Y. Heazlewoodite, Ni3S2: A Potent Catalyst for Oxygen Reduction to Water under Benign Conditions. J Am Chem Soc 2015;137:7978–81. https://doi.org/10.1021/jacs.5b03426.

[72] Mabayoje O, Shoola A, Wygant BR, Mullins B. The Role of Anions in Metal Chalcogenide Oxygen Evolution Catalysis: Electrodeposited Thin Films of Nickel Sulfide as "Pre-catalysts." ACS Energy Lett 2016. https://doi.org/10.1021/acsenergylett.6b00084.

[73] Dhaiveegan P, Hsu Y, Tsai Y, Hsieh C, Lin J. Pulse-reversal deposition of Ni 3 S 2 thin fi lms on carbon fi ber cloths for supercapacitors. Surf Coat Technol 2018.

[74] Zhang Y, Zhang J, Ding D, Gao Y. Controllable synthesis of three-dimensional β-NiS nanostructured assembly for hybrid-type asymmetric supercapacitors. Nanomaterials 2020;10. https://doi.org/10.3390/nano10030487.

[75] Huo H, Zhao Y, Xu C. 3D Ni3S2 nanosheet arrays supported on Ni foam for high-performance supercapacitor and non-enzymatic glucose detection. J Mater Chem A 2014;2:15111–7. https://doi.org/10.1039/c4ta02857k.

[76] Li T, Zuo Y, Lei X, Li N, Liu J, Han H. Regulating the oxidation degree of nickel foam: A smart strategy to controllably synthesize active Ni3S2 nanorod/nanowire arrays for high-performance supercapacitors. J Mater Chem A 2016;4:8029–40.

https://doi.org/10.1039/c6ta01547f.

[77] Wang YF, Zhao SX, Yu L, Zheng XX, Wu QL, Cao GZ. Design of multiple electrode structures based on nano Ni3S2 and carbon nanotubes for high performance supercapacitors. J Mater Chem A 2019;7:7406–14. https://doi.org/10.1039/c9ta00517j.

CHAPTER TWO :

Part Experimental (A/B)

The second chapter is split into two key sections. The initial section provides an in-depth examination of a significant method used in creating thin films, namely the spray pyrolysis technique. The latter section delves into the essential characterization techniques and various relationships utilized in the study. These include X-ray diffraction, visible and ultraviolet ray spectroscopy, Fourier Transform Infrared Spectroscopy (FTIR), and four-point probe measurements. The focus of the study was on the preparation of nickel sulfide thin films, which was conducted in the University of Biskra's laboratory.

PART A : ELABORATION TECHNIQUES

II. 1. Introduction

The characteristics of thin films are highly sensitive and precise, making the selection of a suitable preparation technique critical and subject to meticulous investigation. Films of alloys, metals, ceramics and superconductors can be deposited onto a variety of substrate materials using a variety of techniques, each having unique advantages and disadvantages. For this particular study, we have selected one of the most significant and precise techniques, the Spray Pyrolysis Technique (SPT). Renowned for its simplicity, ease, effectiveness, and cost-efficiency, SPT stands out as a favorable choice compared to other methods [1].

II. 2. Generalities of spray pyrolysis technique

One suitable process for producing thin films is spray pyrolysis (SPT). The term "spray" in English refers to the emission of a liquid, such as perfume, deodorant, or insecticide, dispersed into fine droplets through spraying. "Pyrolysis" derives from the term "pyrolytic," signifying the heating of a substrate. In order to liberate a metal or compound, a source material must undergo thermal breakdown. The substrate's temperature supplies the required energy, known as activation energy, to initiate the chemical reaction between the compounds. Spray pyrolysis is a widely used process that has been established as a powerful tool for preparing various thin films, such as metal oxides, superconducting materials, and nanophase materials. The advantages of spray pyrolysis include its capacity to produce materials with different band gaps throughout the deposition process and its flexibility for large-area film creation [2].

SPT or Spray Pyrolysis Technique, is a widely-used solution-based method for depositing a diverse range of thin films. Key factors in the SPT process include the flow rate, temperature, distance between the substrate and nozzle, size of the droplets, concentration of the precursor, as well as the spraying solution's volume.

II. 2. 1. Advantages of spray pyrolysis Technique :

- Simply controllable reaction environment, either in air at atmospheric pressure or in a neutral gas;
- This kind of reactor is easy to manufacture;
- In the case of solar cells or flat screens, this technique can be utilized to deposit on enormous surfaces;
- The possibility of preparing many materials;
- Easy and customizable;
- This is an inexpensive and economical technology;
- Simple in implementation and fast;
- An easy way to add precursors by spraying;
- This method produces thin films that are of high quality [3],[4].

II. 2. 3. Disadvantage of spray pyrolysis Technique :

While SPT offers a number of benefits, it also has certain drawbacks [5]:

- SPT offers a reduced yield;
- It still has trouble determining the growing temperature;
- Under air environment conditions, sulfide oxidation is a possibility;

II. 2. 4. Classification & equipment of the Spray Pyrolysis Technique :

The spray pyrolysis technique is flexible and can be used to produce powders as well as deposit dense, porous films. Moreover, it can prepare multilayered films. However, the glass industry and the manufacture of solar cells have been using this technology for many years. The substrate heater, temperature controller, atomizer, and precursor solution make up the essential components of the pyrolysis apparatus [6].

Different categorizations of spray techniques exist, depending on the energy source used to initiate the precursor reaction. These include spray pyrolysis in a tubular reactor, vapor

flame spray pyrolysis, the emulsion combustion approach, and flame spray pyrolysis [7]. The precursor atomization methods can vary and are often defined by the technique employed, such as using air pressure, electrostatic forces, or ultrasonic methods in spray pyrolysis processes [8].

The type of atomizer utilized in the system is typically responsible for the other categorization of the categorization for the spray pyrolysis type. Additionally, the atomization technique often affects the aerosol's droplet size, which in turn affects the film quality. Atomizers come in three main varieties: air blast, electrostatic, and ultrasonic. Electrostatic Spray Deposition (ESD) is the name of the spray pyrolysis technique that uses an electrostatic atomizer; Pressurized Spray Deposition (PSD) is the name of the technique that uses an air blast atomizer; and Ultrasonic Spray Pyrolysis (SP) is the technique that uses an ultrasonic atomizer [9].

***Table* (II.1):** *Characteristics of atomizers popular in spray pyrolysis.*

Atomizer	*Droplet size (μm)*	*Atomization rate (cm^3 /min)*
Pressure	10-100	3-no limit
Nebulizer	0.1-2	0.5-5
Ultrasonic	1-100	<2
Electrostatic	0.1-10	[10]

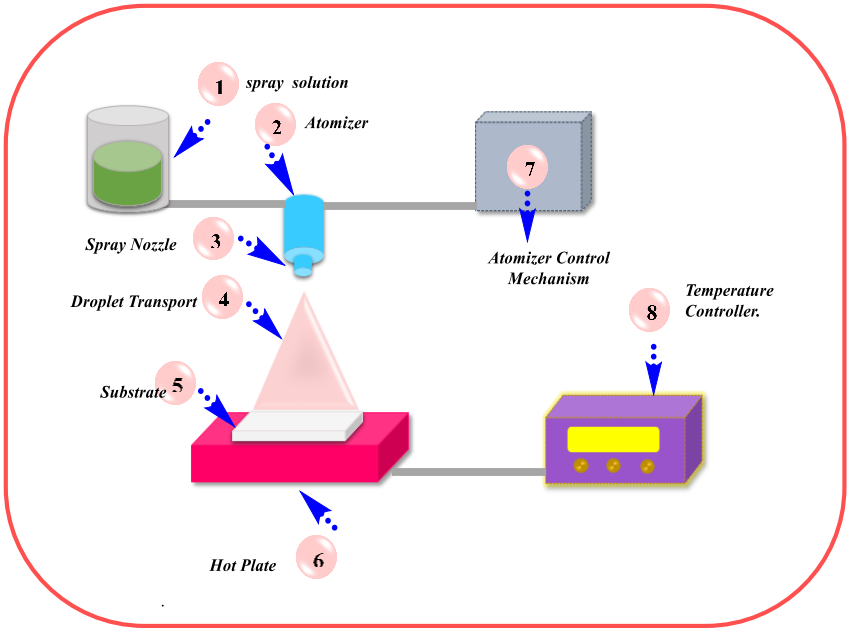

***Figure* (II.1):** *Diagrammatic representation of spray pyrolysis equipment.*

Among the atomization types, compressed air spray precipitation is the most convenient, effective and economical. The spray parameters can be controlled quite simply. figure (II.1) is a diagram illustrating the basics of spray pyrolysis.

II. 3. Principle of deposition processes in spray pyrolysis

Three phases are the foundation of the spray pyrolysis deposition process, and they can happen concurrently or sequentially during film creation; divide it into three main steps:

a) Atomization of the precursor solution.
b) Aerosol transport of the droplet.
c) Decomposition of the precursor to initiate film growth.

II. 3. 1. Atomization of the precursor solution

Atomization is the initial stage of the spray pyrolysis deposition process. The latter consists of generating droplets of a spray solution with an initial velocity that is sent towards the surface of the heated substrate. In spray pyrolysis procedures, air blast, ultrasonic and electrostatic sprays are typically utilized **[11]**.

II. 3. 2. Aerosol transport of the droplet

It is important that the largest possible number of droplets be transferred to the surface of the substrate without turning into powder or salt particles, and this is achieved by dissolving the raw material in a solvent and then turning it into fine droplets of an appropriate size and transferring these drops to the hot surface with a carrier gas. There are several factors Affected by droplet transport.

The thermophoretic forc : The thermophoretic forc work to keep most of the drops away from the surface, and their effect is greater if the distance between the substrate and the vaporizer is large, without forgetting the change in the size of the drops due to the effect of temperature.

The gravitational force : It is the force that pulls the droplet downward due to weight, and the weight depends on the mass of the the droplet; thus, it has a relationship with the droplet size and density.

The electric force : It has an effect only on methods that rely on an electric source to atomize the solution or to control the path, increasing the frequency leads to smaller droplet sizes.

Compressed air atomization not affected by electrical forces, and the effect of electrical force on droplets is much greater than the force of gravity [12].

The stokes force : It is the force of the fluid's resistance to the movement of the droplets, and it directly proportional to the coefficient of viscosity of this fluid, the diameter of the droplet and its limiting velocity. Therefore, drops of large size or high speed are subject to greater force.

II. 3. 3. Decomposition of the precursor to initiate film growth

The chemical reaction that is the basis for pyrolysis technology is the thermal decomposition of the raw material. In order to explain this process, we propose to classify the processes that occur with increasing temperature see figure (II.2).

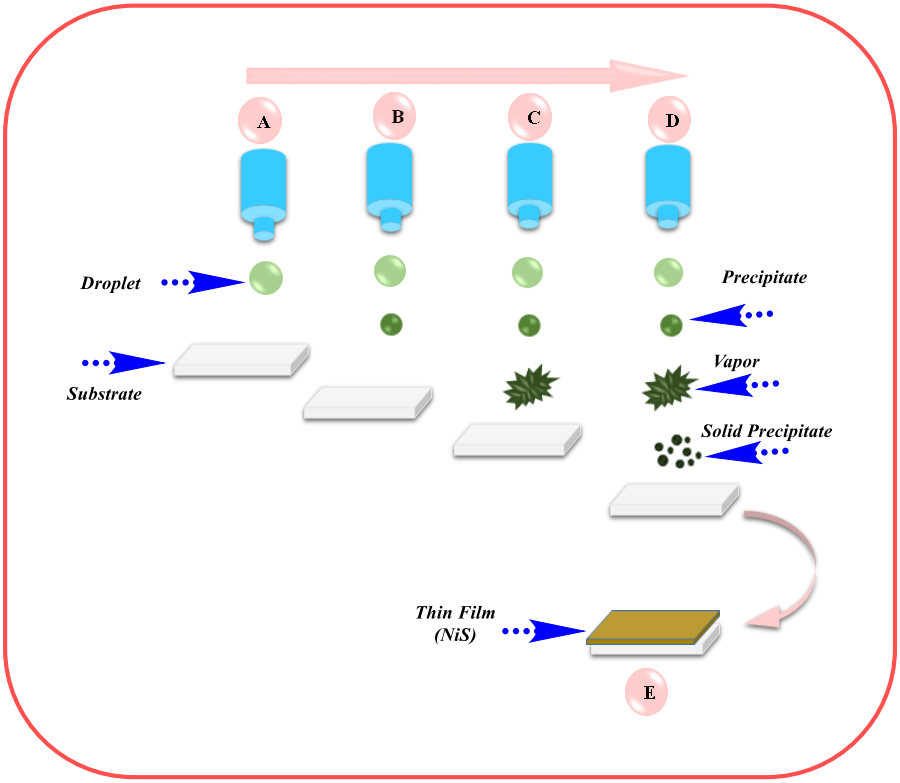

***Figure* (II.2):** *Description of the depositiùon processes.*

Process A involves the droplet landing on the substrate's surface, where the solvent evaporates entirely to leave a dry precipitate that facilitates the breakdown process.

During In process B, the precipitate reaches the surface where the decomposition occurs after the solvent evaporates before the droplet reaches the substrate surface. When the droplet gets close to the substrate.

In process C, the solvent evaporates, the solid melts and evaporates (also known as sublimating), and the vapor diffuses to the substrate to participate in a heterogeneous reaction there. It is indeed CVD**.**

In process D, the chemical reaction occurs in the vapor phase when the metallic compound vaporizes at the highest temperatures before it reaches the substrate **[13]**.

II.4 Protocol methodology

II.4.1 Preparation of spray solution :

Our work is divided into two main parts: preparing a solution that is pure with nickel sulfide and a solution that is doped with magnesium in different concentrations. To prepare the spray solution, we must first choose the chemical compounds used. In this work, we proposed using both nickel nitrate ($Ni(NO_3)_2.6H_2O$) and thiourea ($CS(NH_2)_2$) as sources of nickel and sulfur, respectively. At first, we considered the total concentration. 0.15 mole. Through the concentration value, we proposed studying the difference between a change in the concentration ratio of the source of both nickel and sulfur. The chosen ratios were as follows: {($Ni(NO_3)_2.6H_2O$)=X} and {($CS(NH_2)_2$)=Y}:{30% [X].70%[Y]}, {33%[X].67%[Y]} & {37%[X].63%[Y]}. Our investigation into nickel sulfide commenced with mass measurement according to the N° 1 formula. This was followed by dissolving it in distilled water (H_2O) and adding a few drops of sodium hydroxide (NaOH). Finally, the mixture was heated to 50°C and stirred magnetically for one hour, resulting in a clear green solution, as shown in figure (II.3).

$$\boldsymbol{m(g) = C(mol/l).V(l).M(g/mol)} \qquad \text{N° (II.1)}$$

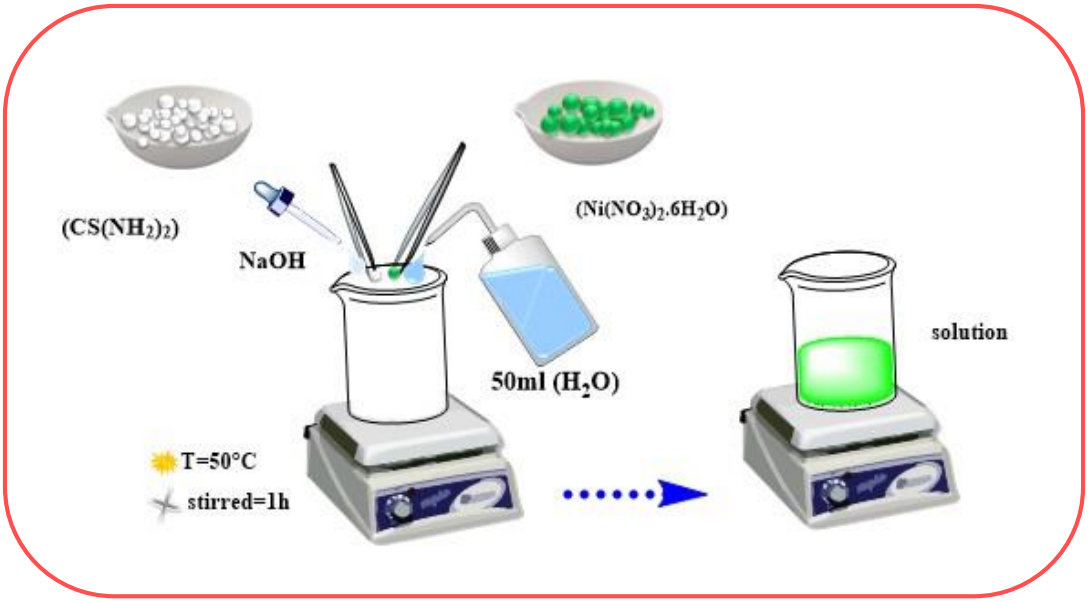

***Figure* (II.3):** *Description of the Preparation of the spray solution pure.*

On the other hand, we follow the same steps as the previous experimental work, only here we choose the following concentration value (30% [X].70%[Y]), to prepare a solution of nickel sulfide activated with magnesium Mg, and we used magnesium nitrate hexahydrate ($Mg(NO_3)_2.6H_2O$) as a source of magnesium. $x=[Mg^{+2}]/[Ni^{+2}]$, where the molar percentage varies from 2% to 4%, 6%, and 8%.(see figuer II.4).

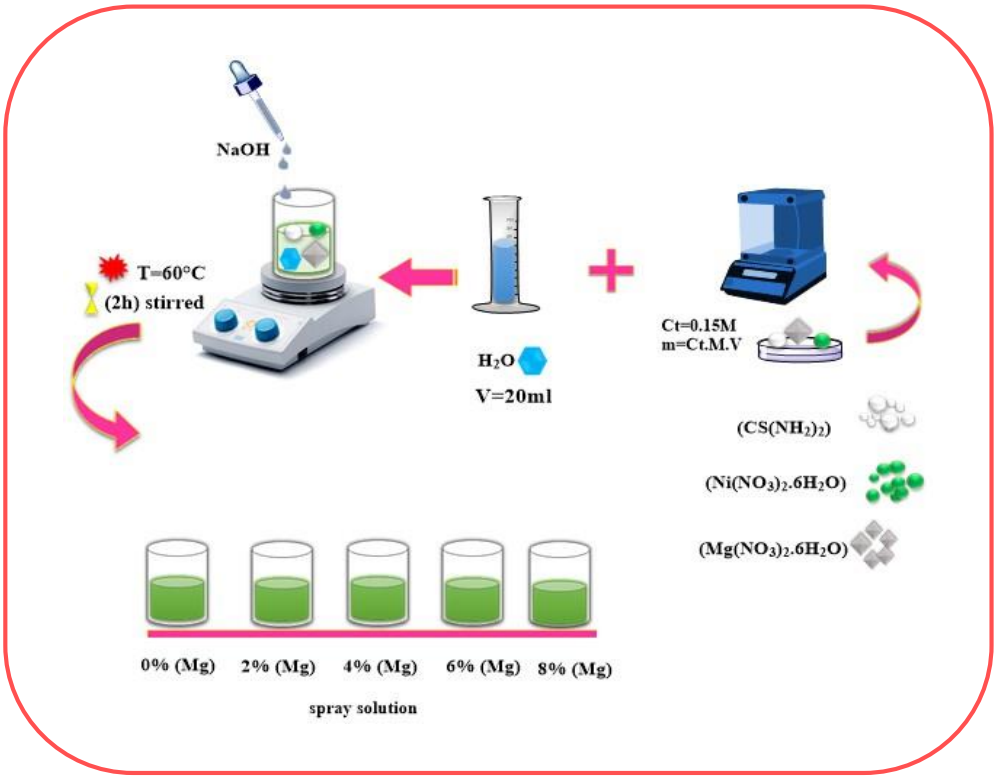

***Figure* (II.4):** *Description of the Preparation of the spray solution doped with Mg.*

II. 4. 2. Preparation of the Films :

At the start of the deposition of the films, the type of substrate must be chosen. In our work, we used the glass substrate *CAT.NO.7101 microscope glass slide* , see figure (III.5). Rinsing with the water distilled and we washed them well with acetone and ethanol for 5 minutes respectively. The substrate was heated on a plate using a Four at a temperature of 250 °C. Using the experimental protocol for the spray pyrolysis method shown in (figure II.6), thin films pure and doped of nickel sulfide with magnesium were deposited.

***Figure* (II.5):** *CAT.NO.7101 microscope glass slide.*

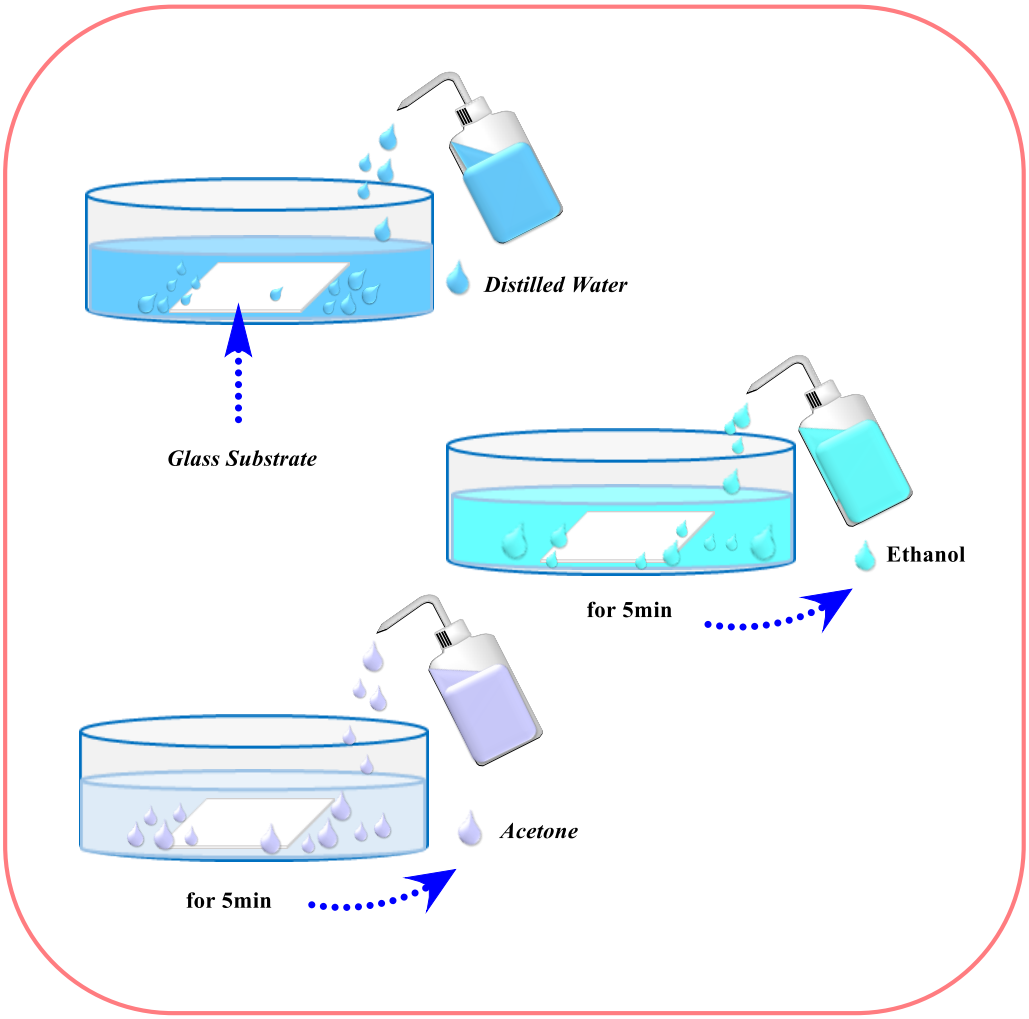

***Figure* (II.6):** *Preparation of glass substrates.*

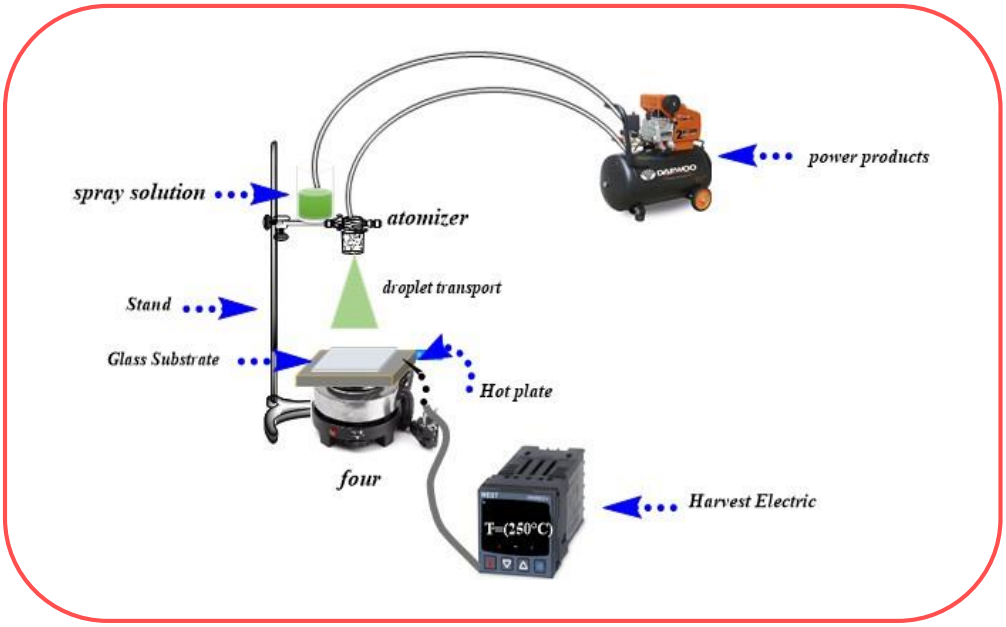

***Figure* (II.7):** *Description of the Preparation of thin films by (SPT).*

II. 4. 3. Oxygen Annealing Atmosphere :

The last annealing was done for 3h 30 minutes for 300 °C and 3h for 350 °C in a furnace with an oxygen atmosphere see figure (II.8 & II.9).

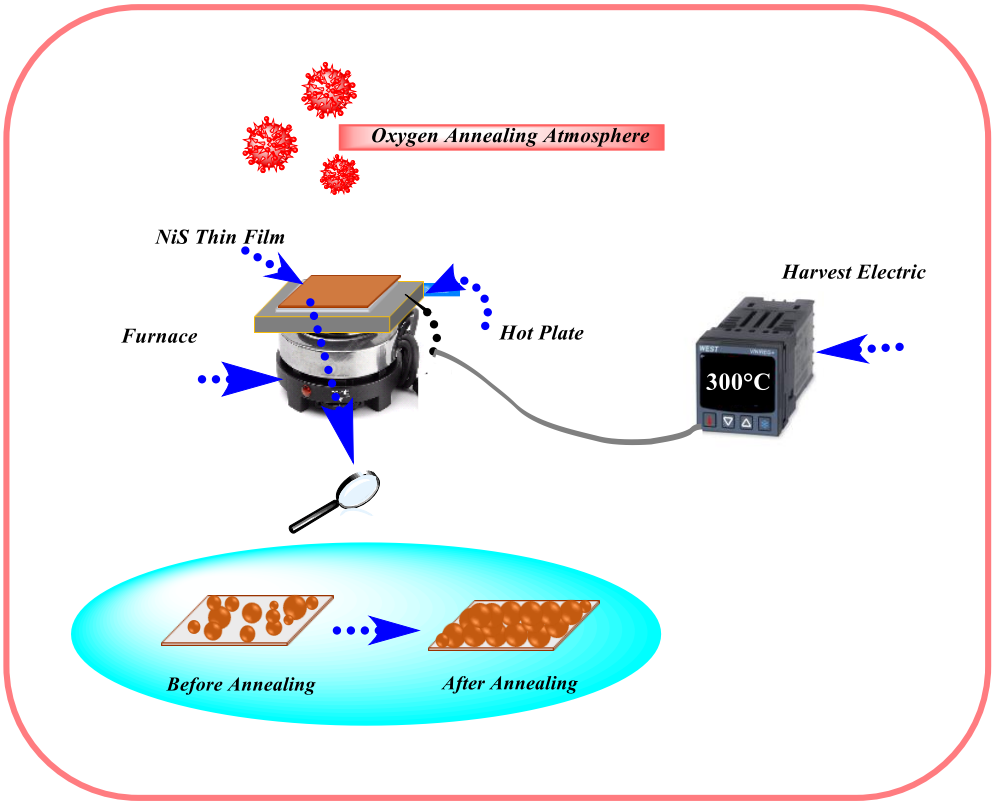

***Figure* (II.8):** *Description of the Oxygen Annealing Atmosphere method.*

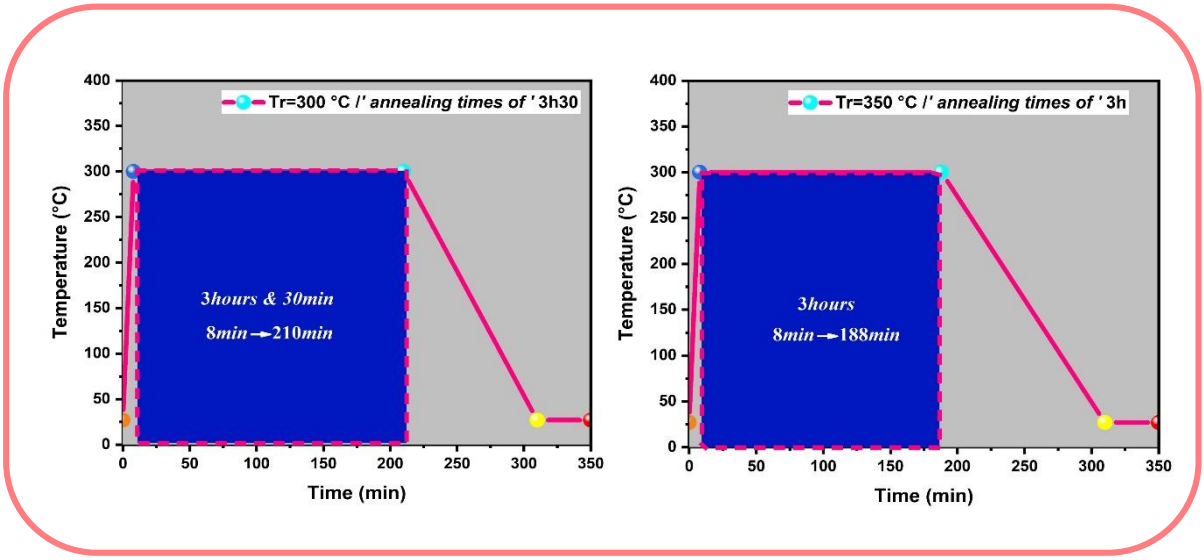

***Figure* (II.9):** *Description of the Oxygen Annealing Atmosphere.*

PART B : CHARACTIRIZATION TECHNIQUES

II.1. Introduction

Several characterisation techniques were applied to the thin films that we created in order to examine and investigate various properties, including:

- X-ray diffraction technique (XRD).
- Weight difference method.
- Ultraviolet-visible spectroscopy (UV-Vis).
- Four-probe method.
- Fourier transform infrared spectroscopy (FTIR).

II.2. X-Ray diffraction technique

This technique is a structural characterization method based on the phenomenon of X-ray diffraction on a crystalline material, and it is fundamental and very important when evaluating thin films and to know the crystal structure of materials, as well as the arrangement of atoms with in the crystals, the crystalline dimensions, and to determine certain parameters, such as the degree of crystallinity, and the preferential orientation of the grains constituting the sample, It is a simple and non-destructive sample analysis technique.

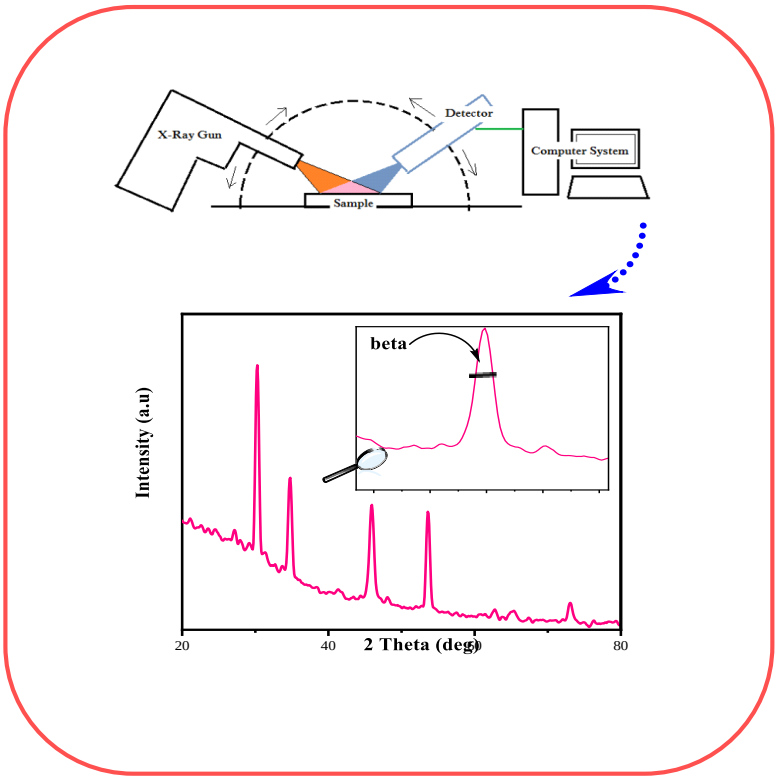

***Figure* (II.10):** *Schematic diagram of X-ray diffractometer & The exraction of the full width at half maximum (β beta) from X-ray diffraction peak.*

Thin films were characterized using various analytical techniques. The XRD diffractrogram was obtained by a *DRX Malvern Pnm analytical Empyrean system* with a Cu-Ka radiation source of λ =0.15406 nm in the range of 30°–80°. objective is to investigate nickel sulfide thin film structural characteristics. (*The characterization of the samples was performed at the crapc platform in Laghouat Province*).

- ***Analysis conditions***

Scanning area in (°) 2 Θ_i:10, 2 Θ_f:90

Step in (°) : 0.002°

Quantity of sample to analyze: 2 g minimum.

***Figure* (II.11):** *Empyrean the Intelligent X-ray Diffractometer.*

Nickel sulfide thin film crystalline quality is investigated by X-ray diffraction. It in turn provides us with the tools to assess the sample's texture, average crystallite size, and other characteristics, as well as the various phases and their distribution within it.

II. 2 .1 The Lattice parameters :

Equations provided by *Bragg's law* are used to calculate the lattice parameters for the unit cell of the phase that is present. The lack of reflection peaks suggests that the material is amorphous [14].

$$2d_{hkl} \sin\theta = n\lambda \qquad \text{N° (II.2)}$$

- d_{hkl} the spacing between the planes in the atomic lattice.
- θ is the angel between the incident ray and the scattering planes.
- n is an integer.

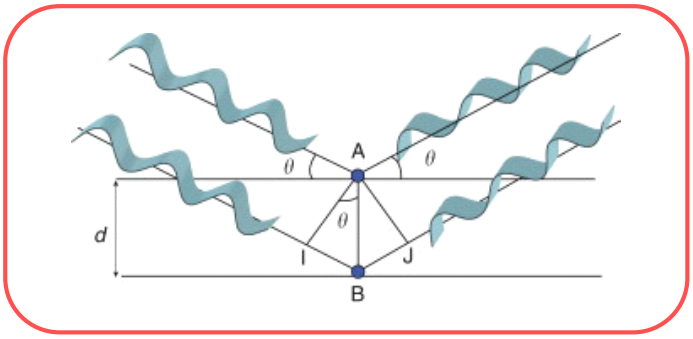

***Figure* (II.12):** *Schematic of X-ray diffraction.*

The lattice parameters designate the dimension of an elementary mesh. In the case of a hexagonal structure such as in our study for NiS, we are interested in two parameters α & c , see figure (II.12).

The following formula (II.3) is used to find the hexagonal lattice parameters (a=b & c) of nickel sulfide thin film [15]:

$$\frac{1}{d^2{}_{hkl}} = \frac{4}{3}\left(\frac{h^2+k^2+hk}{a^2}\right) + \frac{l^2}{c^2} \qquad \text{N° (II.3)}$$

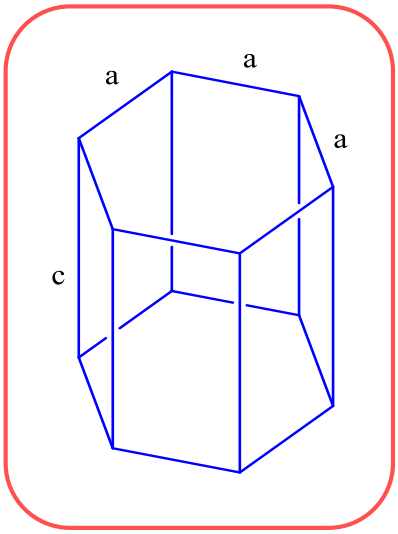

***Figure* (II.13):** *Diagram of the hexagonal structure of NiS.*

II. 2. 2. The Crystallites size (D) :

In this technique, the detector scans across the range of reflection angles to capture the diffracted X-rays. The data, including intensity levels, are recorded by a computer and can be viewed in figure (II.12). This information is then compiled in a table and matched against standards from the Joint Committee on Powder Diffraction Standards (ICSD) to ascertain the identity of the material under investigation. Whether using a powder, a single crystal, or a thin film as the sample, the Scherrer equation is applied to deduce the crystallite size from the broadening of the most intense peak, known as the full width at half maximum (FWHM) **[6]**.

The *Debye–Scherrer's* equation was used to calculate the crystallite size **[16]**:

$$D_{hkl} = \frac{k\lambda}{\beta \cos\theta} \qquad \text{N° (II.4)}$$

Where:

- $\boldsymbol{\beta}$ (rad) is full width at half-maximum FWHM (see figure II.10).
- $\boldsymbol{\theta}$ is the half diffraction angle of the centroid of the peak.
- $\boldsymbol{\lambda}$ is the wavelength of X-ray (λ = 1.5406 A°).
- $\boldsymbol{k}$ is a constant (k =0.89).

II. 2. 3. The dislocations density :

A flaw in the crystal caused by the misregistry of the lattice in one area and that in another is called a dislocation. Dislocations are not equilibrium flaws, in contrast to vacancies and interstitial atoms; therefore, thermodynamic principles are unable to explain the significance of involving dislocation [17].

$\delta_{(hkl)}$ represents the dislocation density, it is calculated using the following relation [18]:

$$\delta_{(hkl)} = \frac{1}{D^2} \qquad \text{N° (II.4)}$$

II. 3. Weight Difference Method

The thickness of the membrane is a very important parameter for the thin films, and this is due to our need for it in studying many of the physical properties of the films. There are several different ways to measure the thickness of the film, including the weight difference method, which we will use in this work because it is simple and available. The latter depends on the difference between the mass of the substrate before the thin film deposition process and its mass after deposition, see figure (II.14).

To use this process, conditions must be met:

- There is no chemical interaction of the substrates with the solvent or with the secondary elements of the process sedimentation.
- No-penetration of materials into the substrates.

The calculation is done according to the following relation [19]:

$$t = \frac{m}{\rho \times s} \qquad \text{N° (II.5)}$$

Where:

- ***t*** is the film thickness of the film.
- ***m*** the mass deposited onto a substrate.
- ***S*** the area of the film.
- ***ρ*** is the density of NiS in bulk state.

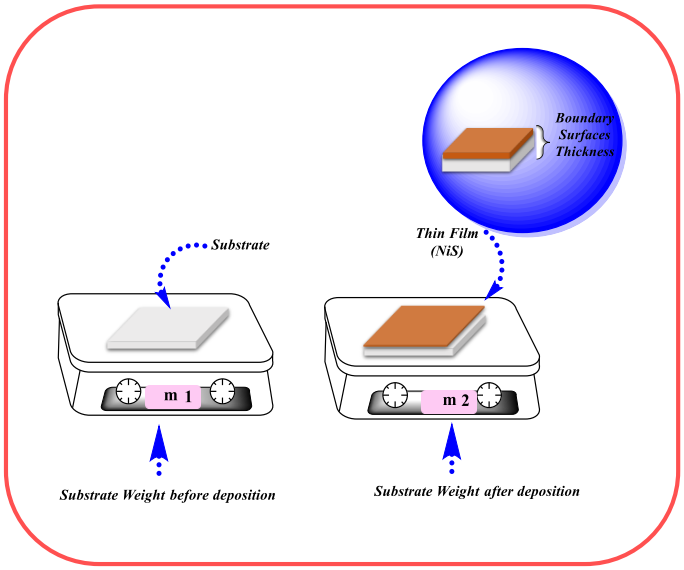

***Figure* (II.14):** *Schematic of Weight difference.*

II. 4. Spectroscopy UV-VISIBLE

The optical properties of NiS thin films were measured by a UV-visible spectrophotometer (*PERKINELMER Lambda 35*) at room temperature in a wavelength range of 200–1200 nm. (The characterization of the samples was performed at the laboratory, Biskra.) as shows in figure (II.15).

***Figure* (II.15) :** *PERKINELMER Lambda 35 spectrophotomet.*

II. 4. 1. Principle :

UV-VIS spectroscopy operates on the principle that, when a monochromatic light beam passes through a homogeneous medium made of an absorbing substance, the rate at which the intensity of radiation decreases with respect to the thickness of the absorbing medium is directly proportional to both the concentration of the medium and the intensity of incident radiation [20] :

$$I = I_0 \exp(-at) \qquad \text{N° (II.6)}$$

Where :

- **α** is the absorption coefficient.
- ***t*** is the thickness of the film.
- I_0 and I are the intensity of the incident and transmitted beams, respectively.

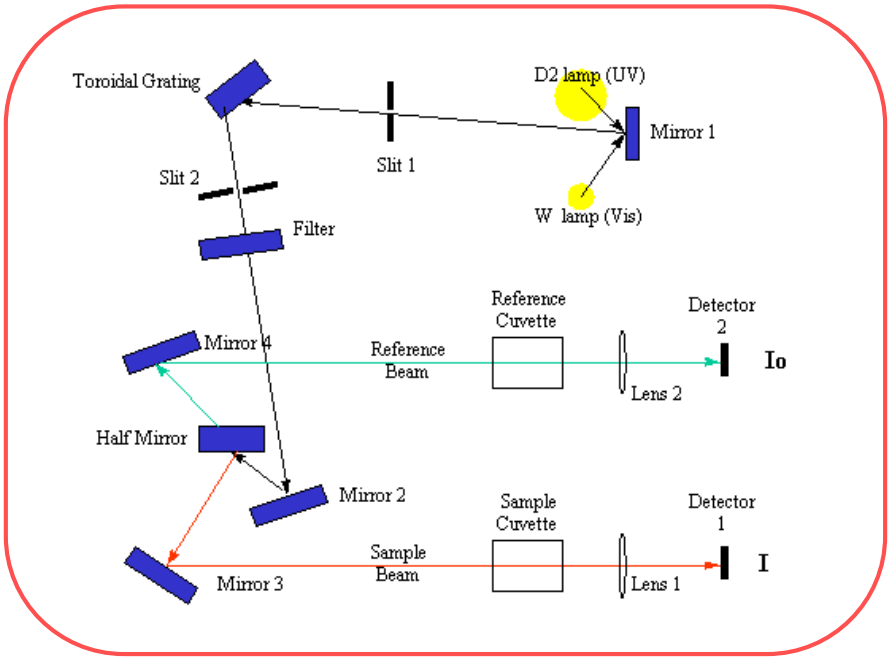

***Figure* (II.16):** *The principal operation of UV–Visible spectrophotometer.*

The absorption coefficient (**α**) can be calculated using the following expression :

$$a = \frac{1}{t}\ln\left(\frac{100}{T(\%)}\right) \qquad \text{N° (II.7)}$$

Where :

- ***T*(%)** is the transmittance (quantity of the transmitted light), and can be directly measured by :

$$T(\%) = \frac{I}{I_0}.100 \qquad \text{N° (II.8)}$$

The optical band gap energy (***Eg***) of NiS thin films was derived from the transmission spectra through the utilization of the following relations [21]

$$A = \alpha t = -\ln(T) \qquad \text{N° (II.9)}$$

$$(Ahv)^2 = B(hv - Eg)/A = \alpha t \qquad \text{N°(II.10)}$$

Where:

- ***A*** is the absorbance.
- ***B*** is a constant.
- (***hv***) is the photon energy $\frac{1240}{\lambda(\mathrm{nm})}$. (ev)
- (***Eg***) is the band gap energy.

On the other hand, we can determine the urbach energy through the following equation [22]:

$$A = A_0 exp\left(\frac{hv}{Eu}\right) \qquad \text{N° (II.11)}$$

Where:

- A_0 is a constant
- *Eu* is the Urbach Energy, by plotting *Ln*(*A*) in terms of *hv*,

we can ascertain the value of Eu as the reciprocal of the linear tangent that intersects the photon energy at x=0.

II. 5. Four-probe method

Figure (II.17) illustrates a diagram of the four-point method, featuring four equidistant probes made from a material that can withstand high temperatures. These probes are mounted on a motorized mechanical stage that can adjust vertically, thereby guaranteeing consistent contact with the film for accurate measurements.

The electrical conductivity of the resistivity of a material with a fixed known thickness t can be determined using a four point measurement technique. This method involves forcing a fixed DC current I through two ports in the material, then measuring the DC voltage V at the remaining two ports. Four high temperature points, evenly spaced apart, make up the

configuration. After that, the thin film's sheet resistivity is calculated using the following formula [9] :

$$R_{Sh} = \frac{\pi}{Ln(2)} \times \frac{V}{I} \& \sigma = \frac{1}{\rho} = \frac{1}{t \times R_{Sh}} \qquad \text{N° (II.12)}$$

Where:

- R_{Sh} sheet resistivity.
- **σ** electrical conductivity.
- ρ is the electrical resistivity.
- t is the film thickness.
- I is the applied current.
- V is the measurement voltage.

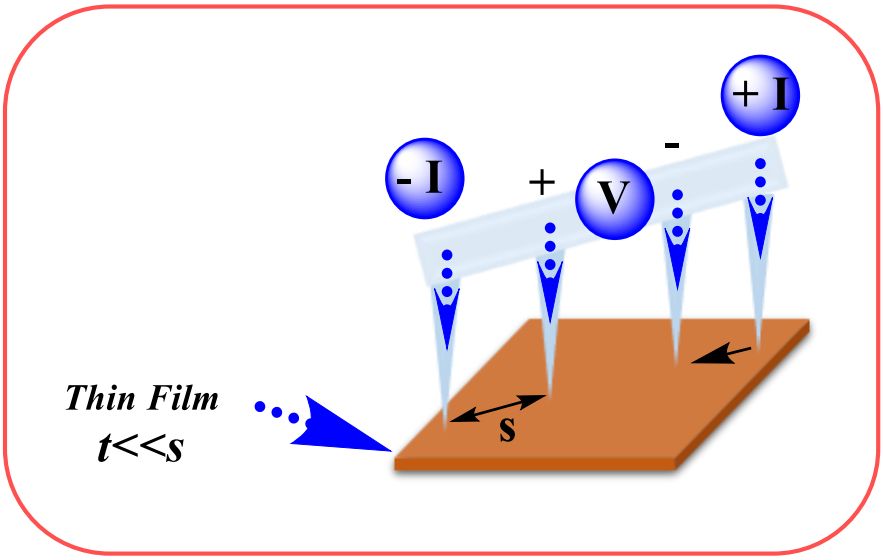

***Figure* (II.17):** *Schematic of four point method.*

(The four-point method measured was performed at the Laboratory of Semiconductor and Metallic Materials, University of Biskra).

II. 6. Fourier Transform Infrared Spectroscopy (FTIR)

An infrared spectrometer of (*type Perkinelmer Spectrum Two)* was used in the frequency range of 400–4000 cm^{-1} at room temperature to study the chemical bonding properties of the prepared films. (*This was performed at the Laboratory in Biskra*).

Figure* (II.18)*: *PERKINELMER Spectrum Two.*

II. 6. 1. Principle :

Fourier transform infrared spectroscopy (FTIR) is one of the most flexible analytical methods for the non-destructive chemical characterisation of samples. It may yield basic information on the molecular structure of both organic and inorganic components.

The FTIR technique's fundamental working principle is linked to changes in quantized vibrational energy levels. In FTIR analysis, an IR photon stimulates a molecule to a higher energy state by transferring to the molecule. This process is known as the absorption of IR radiation.

In the infrared area of the light spectrum, the excited states cause molecular bond vibrations, including stretching, bending, twisting, rocking, wagging, and out-of-plane deformation, to occur at different wave numbers (or frequencies). Each IR absorbance peak's wavenumber is defined by the matching molecule's inherent physicochemical characteristics [23].

In the infrared spectrum, band intensities can be expressed as transmittance (T) or absorption (A). The characteristic functional groups and bonds found in a chemical compound are represented by a variety of bands in the infrared spectrum, which can be used as a fingerprint to identify the molecule [24].

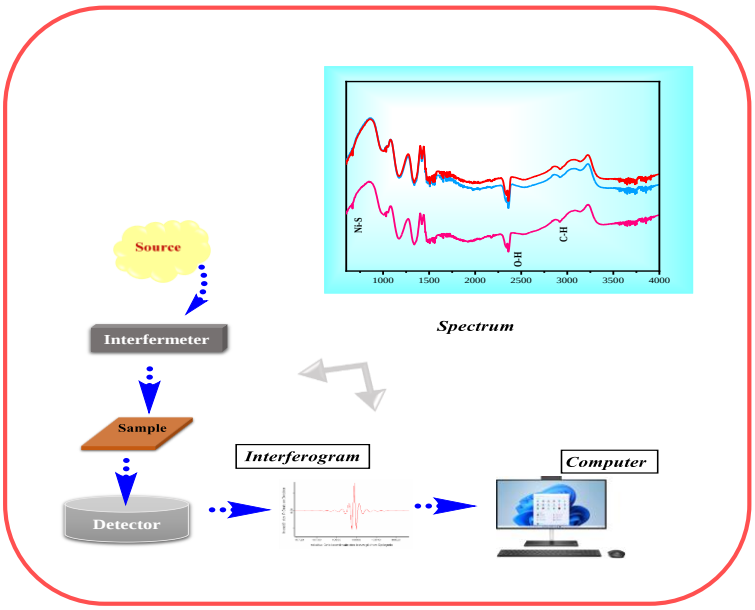

Figure* (II.19)*: *Schematic diagram of FTIR Spectrophotometer.*

II. 7. Conclusion

In this chapter, we have studied the spray peunematic method for deposition of undoped and Mg doped NiS thin films, which also we describe the steps of preparation of NiS solutions and thin films. The final thin films were characterized by various methods such as: XRD, The UV-VIS spectroscopy and electrical characterizations (the four point technique).

REFERENCES

[1] Perednis D, Gauckler LJ. Thin film deposition using spray pyrolysis. J Electroceramics 2005;14:103–11. https://doi.org/10.1007/s10832-005-0870-x.

[2] Prasada Rao T, Santhosh Kumar MC. Physical properties of Ga-doped ZnO thin films by spray pyrolysis. J Alloys Compd 2010;506:788–93. https://doi.org/10.1016/j.jallcom.2010.07.071.

[3] Filipovic L, Selberherr S, Mutinati GC, Brunet E, Steinhauer S, Köck A, et al. Methods of simulating thin film deposition using spray pyrolysis techniques. Microelectron Eng 2014;117:57–66. https://doi.org/10.1016/j.mee.2013.12.025.

[4] Nie P, Xu G, Jiang J, Dou H, Wu Y, Zhang Y, et al. Aerosol-Spray Pyrolysis toward Preparation of Nanostructured Materials for Batteries and Supercapacitors. Small Methods 2018;2:1–24. https://doi.org/10.1002/smtd.201700272.

[5] Pedanekar RS, Shaikh SK, Rajpure KY. Thin film photocatalysis for environmental remediation : A status review Thin fi lm photocatalysis for environmental remediation : A status review. Curr Appl Phys 2020;20:931–52. https://doi.org/10.1016/j.cap.2020.04.006.

[6] Youcef B. Elaboration and characterization of thin layers of zinc oxide (ZnO) deposited by ultrasonic spray for photovoltaic and optoelectronic applications. University Mohamed Khider of Biskra, 2019.

[7] Madler.L. Liquid-fed Aerosol Reactors for One-step Synthesis of Nano-structured Particles † 2004;22:107–20.

[8] Gauckler DB· AD· ARS· LJ. Spray pyrolysis of La0.6Sr0.4Co0.2Fe0.8O3-δ thin film cathodes 2006;16. https://doi.org/10.1007/s10832-006-6971-3.

[9] Hamedani HA. Iinvestigation of deposition parameters in ultrasonic spray pyrolysis for fabrication of solid oxide fuel cell cathode. Georgia Institute of Technology, 2008.

[10] Chafia K. Tin dioxide SnO 2 thin films deposited by ultrasonic spray technique: Properties and Applications. University of Med Khider Biskra, 2018.

[11] Perednis D. Thin Film Deposition by Spray Pyrolysis and the Application in Solid Oxide Fuel Cells. Eidgenossische Technische Hochschule (ETH) Zurich, 2003.

[12] Siefert W. Properties of thin In2O3 and SnO2 films prepared by corona spray pyrolysis, and a discussion of the spray pyrolysis process. Thin Solid Films 1984;120:275–82. https://doi.org/10.1016/0040-6090(84)90242-6.

[13] Vigui JC, Spitz J. C h e m i c a l V a p o r Deposition a t Low T e m p e r a t u r e s. J Electrochem Soc SOLID-STATE Sci Technol 1975;268:2–5.

[14] Migue, Pinto, Neves N. Al-doped ZnO ceramic sputtering targets based on nanocrystalline powders produced by emulsion detonation synthesis – deposition and application as a transparent conductive oxide material. Nova Liboa University, 2015.

[15] Srinivasulu T, Saritha K, Reddy KTR. Synthesis and characterization of Fe-doped ZnO thin films deposited by chemical spray pyrolysis. Mod Electron Mater 2017;3:76–85. https://doi.org/10.1016/j.moem.2017.07.001.

[16] Cheng H, Zhai X, Ouyang J, Zheng L, Luo N, Liu J, et al. Achieving a high energy storage density in Ag(Nb,Ta)O3 antiferroelectric films via nanograin engineering. J Adv Ceram 2023;12:196–206. https://doi.org/10.26599/JAC.2023.9220678.

[17] GHOUGALI M. Elaboration and characterization of nanostructuring NiO thin films for gas sensing applications. University of Mohamed Khider, BISKRA, 2019.

[18] N. Khedmi, M. Ben Rabeh MK. Structural Morphological and Optical Properties of SnSb2S4 Thin Films Grown by Vacuum Evaporation Method. Thin Solid Films 2019;669:633–40. https://doi.org/10.1016/j.tsf.2018.11.048.

[19] Patil VP, Pawar S, Chougule M, Godse P, Sakhare R, Sen S, et al. Effect of Annealing on Structural, Morphological, Electrical and Optical Studies of Nickel Oxide Thin Films. J Surf Eng Mater Adv Technol 2011;01:35–41. https://doi.org/10.4236/jsemat.2011.12006.

[20] Anouar Y. Optimization of indium oxide thin films properties prepared by sol gel spin coating process for optoelectronic applications. University Mohamed Khider of Biskra, 2020.

[21] Zaouche C, Aoun Y, Benramache S, Gahtar A. Synthesis and Characterization of Deposited NiO Thin Films by Spray Pyrolysis Technique. Sci Bull Valahia Univ - Mater Mech 2019;17:27–32. https://doi.org/10.2478/bsmm-2019-0015.

[22] Benramache S, Benhaoua B. Influence of substrate temperature and Cobalt concentration on structural and optical properties of ZnO thin films prepared by Ultrasonic spray technique. Superlattices Microstruct 2012;52:807–15. https://doi.org/10.1016/j.spmi.2012.06.005.

[23] Chen Y, Zou C, Mastalerz M, Hu S, Gasaway C. Applications of Micro-Fourier Transform Infrared Spectroscopy (FTIR) in the Geological Sciences — A Review. Int J Mol Sci 2015:30223–50. https://doi.org/10.3390/ijms161226227.

[24] Said B. Elaboration et caractérisation des couches minces de ZnO dopées cobalt et indium. University Mohamed Khider of Biskra, 2012.

CHAPTER THREE :

Investigation of High Electrical Conductivity in Superconducting NiS Thin Films

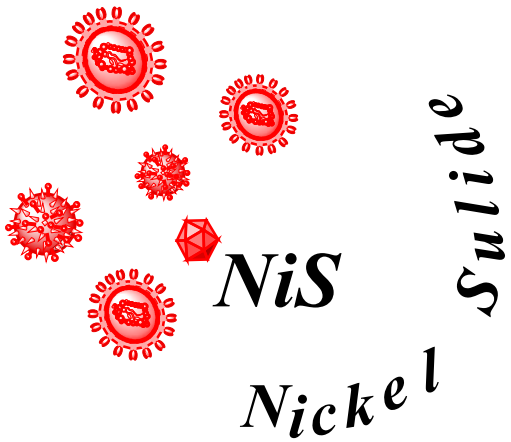

This chapter describes the spray pyrolysis process used to create NiS thin films on heated substrates. Investigations have been conducted into the effects of different precursor concentrations on the structural, optical, and electrical characterizations of NiS thin films

III.1. Introduction

To gain deeper insight into how the concentrations of precursor solutions affect the physical characteristics of NiS thin films, we conducted a study. NiS nanostructured thin films were fabricated and analyzed. These films were deposited onto glass substrates at 523 K using the spray pyrolysis method. We employed varying concentrations of precursors from Ni and S solution sources for this investigation, using nickel nitrate hexahydrate and thiourea, while keeping the other experimental conditions constant. Structural characterization was investigated through the results of x-ray diffraction analysis and confirmed by FTIR analysis. In addition, UV-visible spectroscopy was used to study the band gap energy. Finally, the sheet resistance (Rsh) was measured using the four-point probe method.

III. 2. Experimental Part

III. 2. 1. Nickel Sulfide thin films Preparation:

We prepared a spray solution containing nickel nitrate hexahydrate (Ni(NO3)2.6H2O = X) and thiourea ($CS(NH_2)_2$ = Y) as sources of nickel (Ni) and sulfur (S), respectively. This solution, with a molar concentration of X% [Ni] and Y% [S] (total concentration 0.15 M), was used in the spray pyrolysis process to deposit nickel sulfide thin films. After dissolving in 50 ml of distilled water, a clear, green solution was formed by shaking the mixture for an hour at 50°C. The deposition process was conducted at a temperature of T = 523 K. see figure (III.1) and table (III.1).

***Table*(III.1)** : *Experimental Conditions.*

Condition	*Values*
Sample 1	30% [X].70% [Y]

Sample 2	33% [X].67% [Y]
Sample 3	37% [X].63% [Y]
Glass Substrate temperature	T=523 K
Volume	V=50ml
Deposition time	10min
Distance	d=23cm
The spray rate	0.002 l/min
The glass substrates	(CAT.NO.7101) microscope glass slide

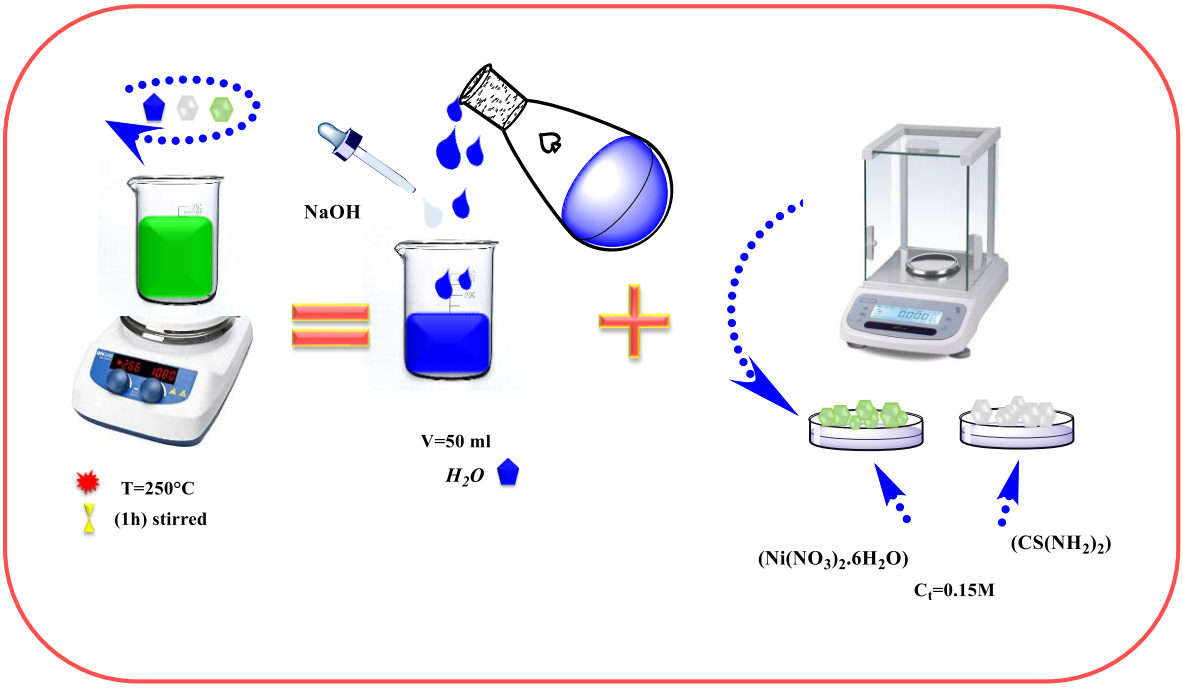

***Figure* (III.1):** *Steps to prepare a spray solution.*

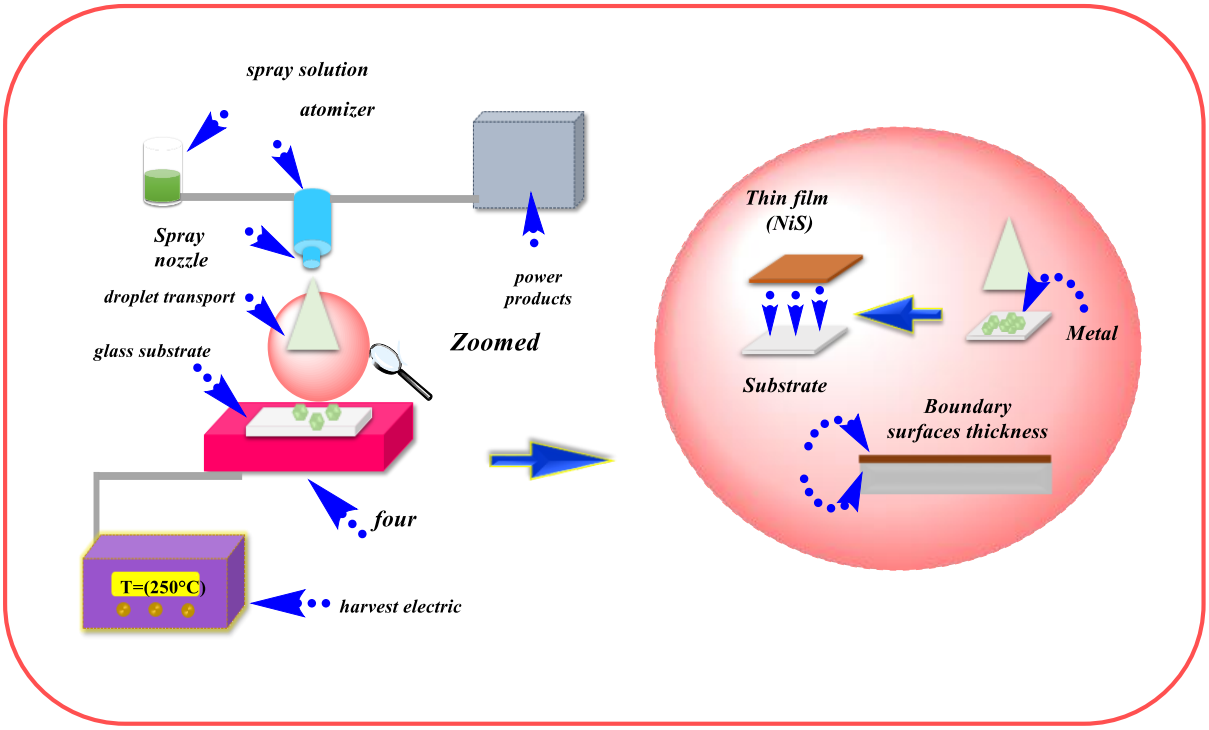

***Figure* (III.2):** *A diagram illustrating of nickel sulfide thin films deposition.*

III. 2. 1. Cracterization techniques:

An XRD (*Malvern Pnm analytical Empyrean- CRAPC-LAGHOUAT*) system operating in the radiation range of 20°–80° produced the X-ray diffraction diffractogram. Studying the structural characteristics of NiS thin films was the purpose of this. To examine the chemical bonding characteristics of the produced films, an infrared spectrometer of the (*Perkinelmer Spectrum Two - Photonics and Multifunctional Nanomaterials Physics Laboratory PMNPL, BISKRA*) type was employed in the 400–4000 cm^{-1} frequency range. As for the optical properties, they were measured using a UV-VIS spectrophotometer (*PERKINELMER Lambda 35 - Photonics and Multifunctional Nanomaterials Physics Laboratory PMNPL, BISKRA*) in a wavelength range of 200–1200 nm. The electrical properties were measured using the four-point approach.

To determine the thickness of the film, we employed the weighing technique, as described by the equation **[1]**:

$$t = \frac{\Delta m}{\rho \times s} \qquad \text{N° (III.1)}$$

Where:

- ***t*** is the film thickness
- ***m*** the mass deposited onto a substrate
- ***S*** the area of the film
- ***ρ*** is the density of NiS (5.50 g/cm^3) ~774 nm.

III.3 Results and Discussion

III. 3.1. The structural properties:

The structural characteristics of NiS thin films were examined through X-ray diffraction patterns. Figure (III.3) displays the XRD diffractogram for NiS thin films applied to a glass substrate using the spray pyrolysis technique at a temperature of 523 K. The figure reveals that all films are polycrystalline with a hexagonal structure, belonging to the P63/mmc space group, and exhibit a preferred orientation of (010) (ICSD 98-060-2488). Additionally, diffraction peaks with orientations of (010), (011), (012), (110), and (022) were observed, in accordance with the ICSD data card.

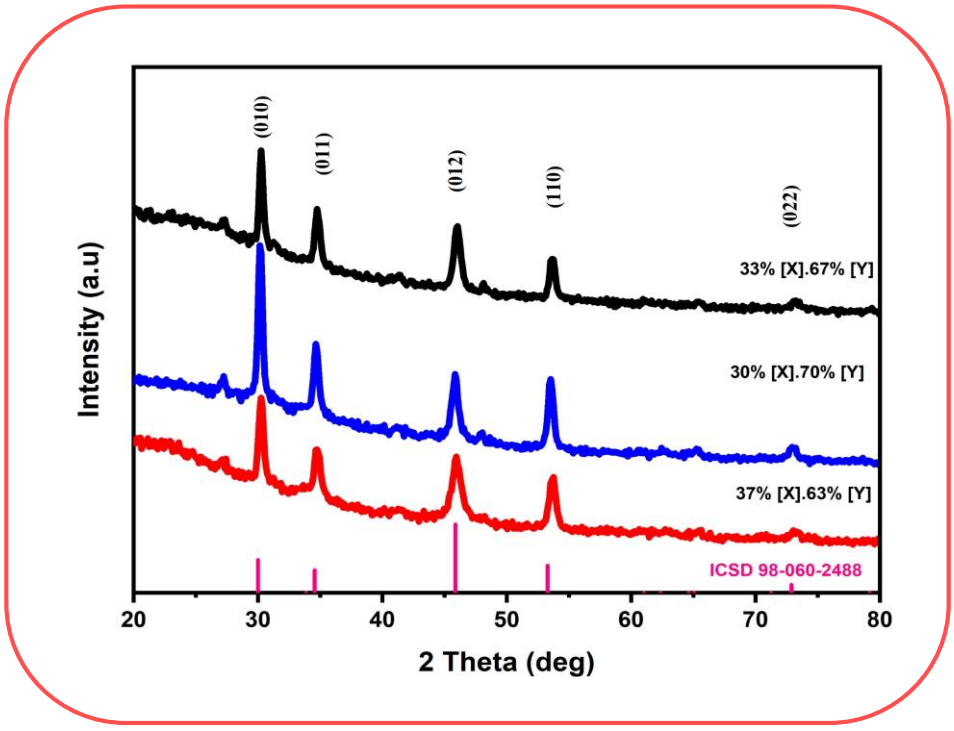

***Figure* (III.3):** *XRD diffractogram of nickel sulfide thin films.*

These diffractograms enable the determination of various physical parameters, such as crystallite size, dislocation density, and micro-strain. The Bragg angle 2θ, corresponding to the preferred orientation, is also noted and is determined as presented in table (III.2) below:

***Table* (III.2)** : 2 *Theta (deg) Variation per (hkl).*

	2 Theta (deg)		
(hkl)	***Sample 3***	***Sample 1***	***Sample 2***
(010)	30.252	30.187	30.251
(011)	34.757	34.679	34.770
(012)	45.939	45.853	46.021
(110)	53.710	53.546	53.674

The interplanar spacing $d_{(hkl)}$, which is determined by *Bragg's law* [2]:

$$2d_{hkl}\sin\theta = n\lambda \qquad \text{N° (III.2)}$$

***Table* (III.3)**: *Variation of d- spacing (Å) d(hkl) of NiS thin flms.*

Precursor concentration	***Sample 3***	***Sample 2***	***Sample 1***
$\boldsymbol{d_{(010)}}$**(Å)**	2.9534	2.9597	2.9534
$\boldsymbol{d_{(011)}}$**(Å)**	2.5802	2.5858	2.5793
$\boldsymbol{d_{(012)}}$**(Å)**	1.9748	1.9783	1.9715
$\boldsymbol{d_{(110)}}$**(Å)**	1.7060	1.7108	1.7070

According to formula N° (III.3), we can obtain the hexagonal lattice parameters (a and c) of the NiS thin film [3]:

$$\frac{1}{d^2{}_{hkl}} = \frac{4}{3}\left(\frac{h^2+k^2+hk}{a^2}\right) + \frac{l^2}{c^2} \qquad \text{N° (III.3)}$$

Table (III.4) : *The lattice parameters (a, c) compared to the values found in the ICSD 98-060-2488 database.*

Precursor concentration	*ICSD card*			*This work*		
	a = b (Å)	**c (Å)**	**c/a (Å)**	**a = b (Å)**	**c (Å)**	**c/a (Å)**
Sample 3	3.4200	5.300	1.55	3,41029	5,3027	1.55
Sample 1				3,41757	5,3148	1.56
Sample 2				3,41029	5,2949	1.55

The unit cell v is determined by applying Law N°(III.4) as follows [2]:

$$V = a.b.c.\sin(60°) \qquad \text{N° (III.4)}$$

Table (III.5) : *Variation of the unit cell volume V.*

Precursor concentration	**Semple 3**	**Semple 1**	**Semple 2**
***The unit cell v*(Å^3)**	53.39	53.74	53.31

The crystallite size was determined using the *Debye-Scherrer* relation [4] :

$$D_{hkl} = \frac{k\lambda}{\beta \cos\theta} \qquad \text{N° (III.5)}$$

Where:

- β(rad) is full width at half-maximum FWHM
- λ is the wavelength (1.5406 A°)
- k is a constant (k =0.89).

Table (III.6) : *The crystallites size $D_{(hkl)}$ (nm) of NiS films.*

Precursor concentration	*Sample 3*	*Sample 1*	*Sample 2*
$\boldsymbol{D_{(010)}}$	17.067	22.148	18.648
$\boldsymbol{D_{(011)}}$	12.152	15.052	13.179

$D_{(012)}$	9.915	12.858	11.467
$D_{(110)}$	15.901	18.625	14.101

In comparison to films {33% [X].67% [Y]} and {37% [X].63% [Y]}, a rise in the crystallites size was noted in the {30% [X].70% [Y]} film. These findings provide an explanation for the rise in the size of average crystallites. This is because throughout the crystallization process, the dislocations gather more energy and exhibit higher mobility, whereas the small crystallites are consumed. As the film crystallizes, these activated dislocations split in the direction of the grain boundaries and become neutral [5].

The dislocation density, denoted as $\delta_{(hkl)}$ is computed using the relation N° (III.6) that follows [6]:

$$\delta_{(hkl)} = \frac{1}{D^2} \qquad \text{N° (III.6)}$$

Table (III.7) : *The dislocation density* $\delta_{hkl}(10^{15} lines/m^2)$ *of NiS films.*

Precursor concentration	*Sample 3*	*Sample 1*	*Sample 2*
$\delta_{(010)}$	3.432	2.038	2.875
$\delta_{(011)}$	6.771	4.413	5.757
$\delta_{(012)}$	10.170	6.047	7.604
$\delta_{(110)}$	3.954	2.882	5.029

The Stokes-Wilson formula is used to determine the Micro-Strain $\varepsilon_{(hkl)}$ [7] :

$$\varepsilon_{(hkl)} = \frac{\beta}{4 \tan \theta} \qquad \text{N° (III.7)}$$

Table (III.8) : *Micro-stress* $\varepsilon_{(hkl)}$ *of NiS films.*

Precursor concentration	*Sample 3*	*Sample 1*	*Sample 2*
$\varepsilon_{(010)} \times 10^{-3}$	7.786	6.013	6.642

$\varepsilon_{(011)} \times 10^{-3}$	9.554	7.730	8.021
$\varepsilon_{(012)} \times 10^{-3}$	8.962	6.923	6.555
$\varepsilon_{(110)} \times 10^{-3}$	4.827	4.133	4.338

As demonstrated in the accompanying table (III.9) & Figure (III.4), a decrease in lattice defects correlates with an increase in crystallite size, which in turn causes a drop in internal stress and dislocation intensity [8].

***Table* (III.9)** : *Variations of $D_{(010)}$, $\varepsilon_{(010)}$ and $\delta_{(010)}$ of NiS films.*

Precursor concentration	***Sample 3***	***Sample 1***	***Sample 2***
$D_{(010)}$	17.067	22.148	18.648
$\delta_{(010)}$	3.432	2.038	2.875
$\varepsilon_{(010)} \times 10^{-3}$	7.786	6.013	6.642

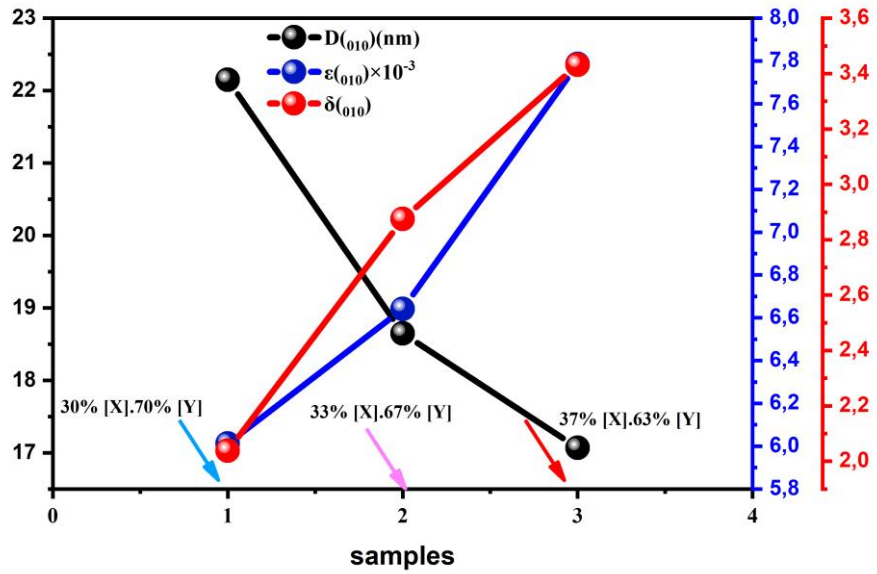

***Figure* (III.4):** *Variations of $D_{(010)}$, $\varepsilon_{(010)}$ and $\delta_{(010)}$ of NiS films as function of precursor concentration.*

III. 3. 2. Chemical composition

The results of FTIR spectroscopy for NiS thin films are detailed. thin films were synthesized using varying the precursor concentrations of sulfur S and nickel Ni by the spray pyrolysis technique, as depicted in figure (III.5). The FTIR analysis involved scanning the samples over a wavelength range from (400 to 4000 cm^{-1}). This analysis was used to ascertain the presence of types of chemical bonds by identifying the specific vibrations corresponding to each bond within the infrared spectrum. A summary of these findings is provided in table (III.10).

***Table* (III.10)** : *FTIR peaks and The band of NiS film.*

Vibrations	*The band*	*Reference*
626 cm^{-1}	Ni-S	[9], [10]
1092 cm^{-1}	C-S	[9], [11]
1483 cm^{-1}	C-H	[9], [12]
3275 cm^{-1}	O-H	[13]
2375 cm^{-1}	C=O=O	[14]

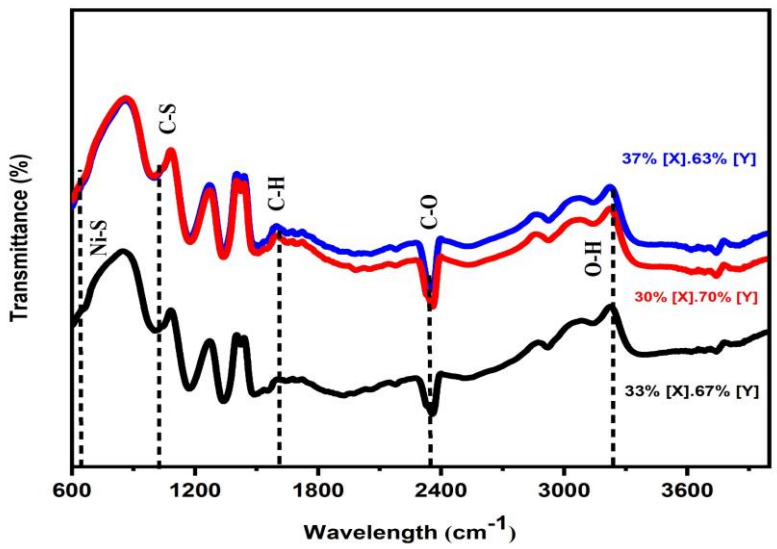

***Figure* (III.5)**: *FTIR spectrum of NiS films prepared at different Precursor concentration.*

III. 3. 3. Optical properties

The absorption spectra of NiS thin films produced by spray pyrolysis technique at a T= 523 K are shown by the curve in figure (III.6). The optical absorption edge of all NiS films is observed at the UV region 280 to 380. The absorbance decreases with increasing wavelength. In comparison to film placed at {30% [X].70% [Y]}, the thin films deposited in {33% [X].67% [Y]}&{37% [X].63% [Y]} exhibit the highest optical absorption ratio.The variations in the shape and crystalline structure of the produced films may account for this.

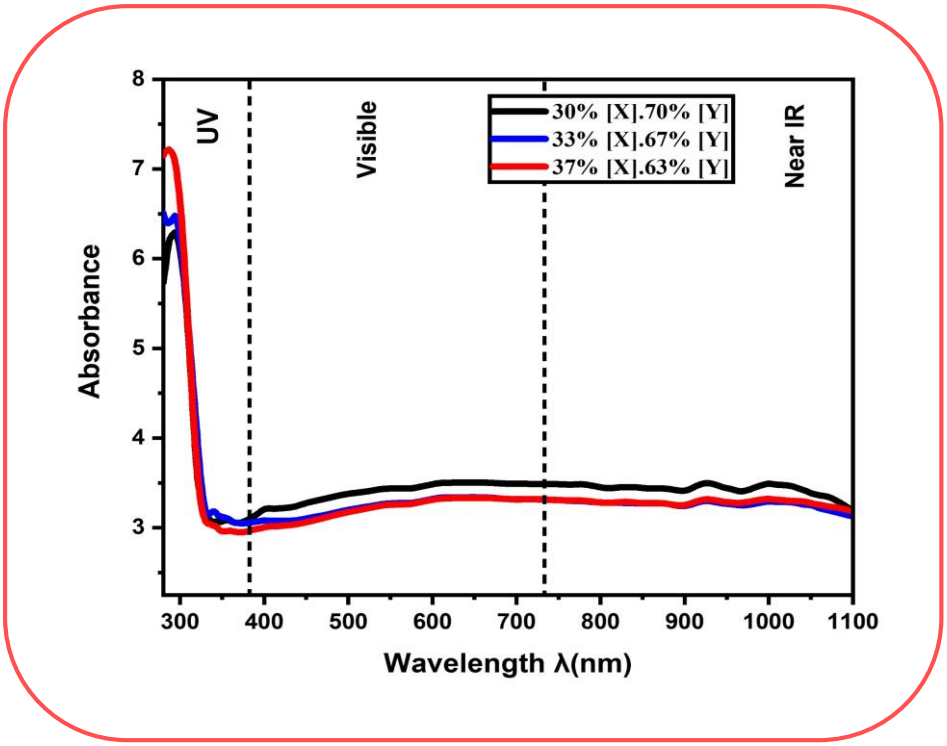

***Figure* (III.6)**: *Optical absorbance spectra of the NiS thin films.*

The point at which the straight line intersects with the photon energy (hv)A = 0 correlates with the optical band gap Eg of NiS thin films formed at T= 523 K, as illustrated in figure (III.7). The relationships labeled III.8 and III.9 are relevant in this context.**[15]**, were used to extract the optical band gap energy Eg of NiS thin films from the transmission spectra, as shown in table (III.10).

$$A = \alpha d = -\ln(T) \qquad \text{N° (III.8)}$$

$$(Ahv)^2 = B(hv - Eg)/A = \alpha d \qquad \text{N° (III.9)}$$

Where:

- A is the absorbance
- d is the film thickness (t)
- T is the transmittance spectra
- α is the absorption coefficient values
- B is a constant
- hv is the photon energy.

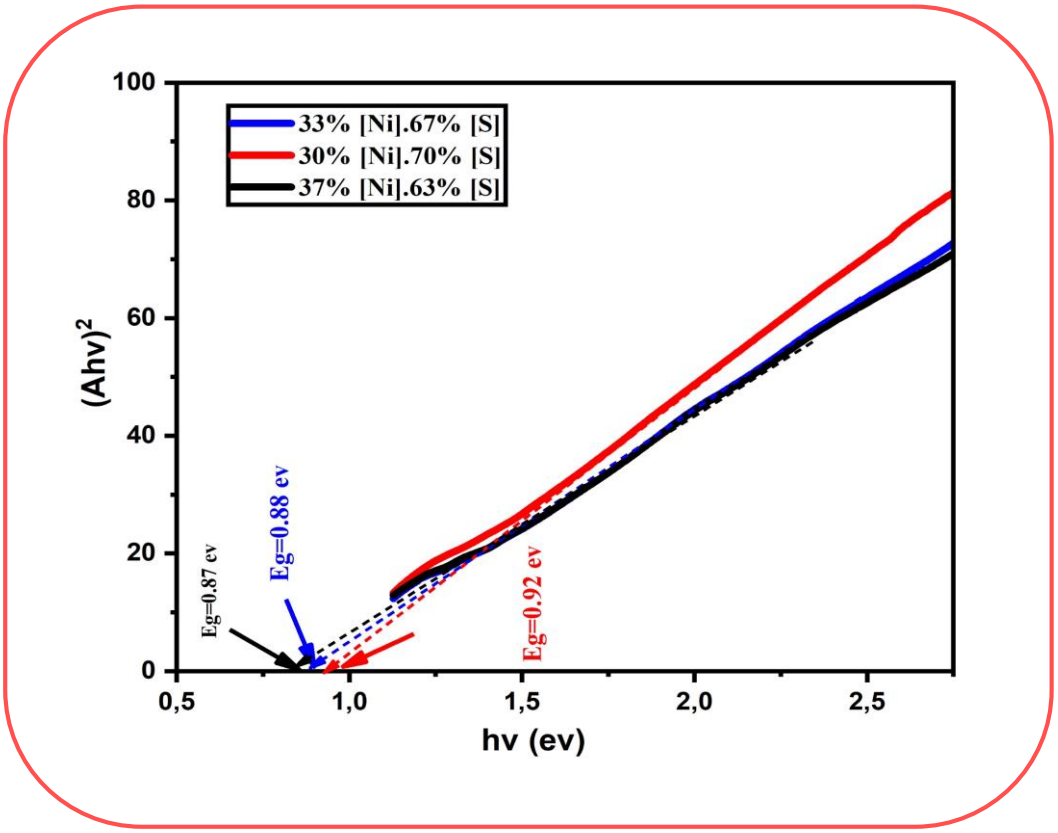

***Figure* (III.7)**: *The graph of (Ahv)* ^{2} *vs hv plots for NiS films.*

However, the Urbach energy can be calculated using the following equation: [16]:

$$A = A_0 exp\left(\frac{hv}{Eu}\right) \qquad \text{N° (III.9)}$$

Where:

- A_0 is a constant
- Eu is the Urbach Energy by plotting $Ln(A)$ in terms of hv we can ascertain the value of Eu as the reciprocal of the linear tangent that intersects the photon energy at x=0.

The energy values of the gaps for thin films {30% [X].70% [Y]}, {33% [X].67% [Y]}, & {37% [X].63% [Y]} differ from 0.92ev, 0.88ev and 0.87ev.This is caused, in turn, by a variation in the ratio of nickel to sulfur, which modifies the density of states for the conduction and valence bands as well as the energy of the gaps [17].

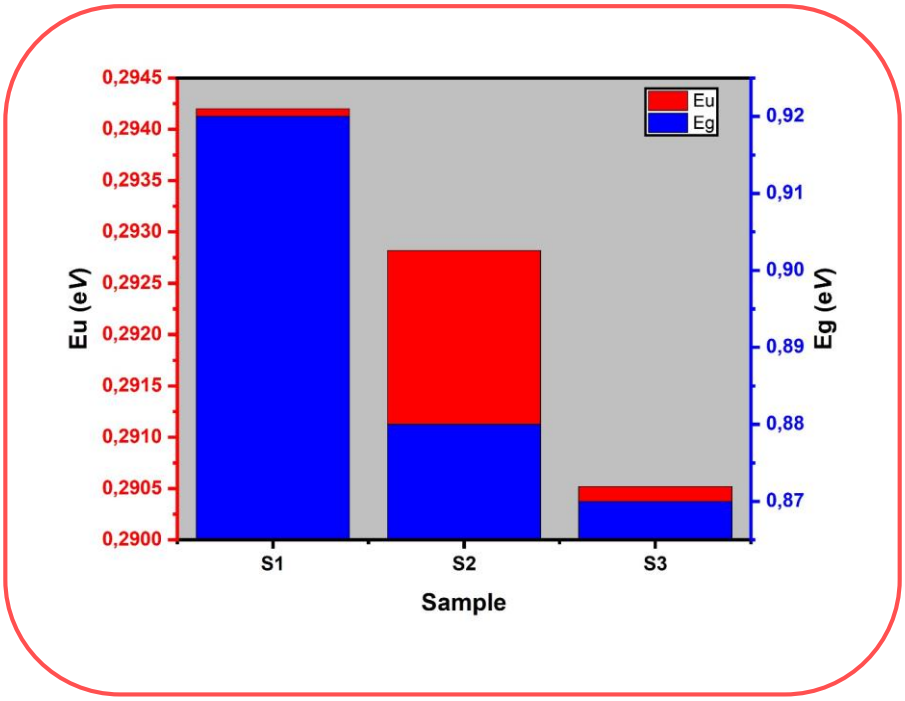

***Figure* (III. 8)** : *The variation of the optical band gap energy and Urbach energy as a function of precursor concentration.*

***Table* (III.11)** : *Band gap energy & Urbach energy of NiS thin film.*

Samples	$Ts(°C)$	$Eg(ev)$	$Eu(mev)$
Sample 1	250°C	0.92	294.20
Sample 2	250°C	0.88	292.82
Sample 3	250°C	0.87	290.52

III. 3. 4. Electrical characteristics

The electrical characteristics of NiS thin films were analyzed using the four-point method at room temperature. Figure (III.9) illustrates how voltage varies with current, demonstrating the electrical resistivity changes in these films. Notably, voltage increased

linearly with current in the range of 0 – 80 mA. A higher voltage value was observed for the sample with lower sulfur concentration ({30% [X].70% [Y]}) compared to the samples with {33% [X].67% [Y]} and {37% [X].63% [Y]} compositions thin films {30% [X].70% [Y]} exhibited the best resistance, measured at 5.304 Ω, indicating superior electrical conductivity of 2.43×10^{3} $(\Omega.cm)^{-1}$ when compared to the other two samples. The electrical conductivity σ of the NiS thin films was calculated as per equation N°(III.11) [18] and the results, including variations in sheet resistance, resistivity and electrical conductivity of thin films, are summarized in table (III.11).

$$R_{Sh} = \frac{\pi}{Ln(2)} \times \frac{V}{I} \,\&\, \sigma = \frac{1}{\rho} = \frac{1}{e \times R_{Sh}} \qquad \text{N° (III.11)}$$

Where:

- ρ is the electrical resistivity
- e is the film thickness
- I is the applied current
- V is the Measurement voltage.

Table (III.12) : *Values of V, I, Rsh, ρ and σ of NiS thin film.*

Samples	I(mA)	V(mV)	Sheet resistance Rsh(Ω)	Electrical resistivity ρ (Ω.cm)	Electrical Conductivity σ$(\Omega.cm)^{-1}$
Sample 1	50.5	59.13	5.304	$4.11\ 10^{-4}$	$2.43\ 10^{3}$
Sample 2		69.46	6.230	$4.82\ 10^{-4}$	$2.07\ 10^{3}$
Sample 3		64.00	5.741	$4.44\ 10^{-4}$	$2.25\ 10^{3}$

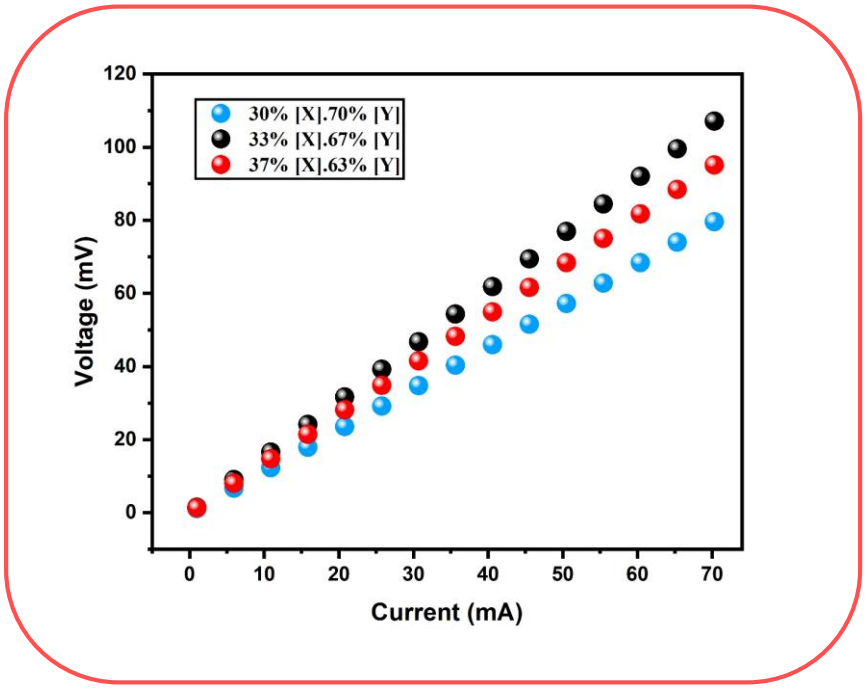

***Figure* (III.9)**: *Voltage changes in terms of current intensity of NiS thin films.*

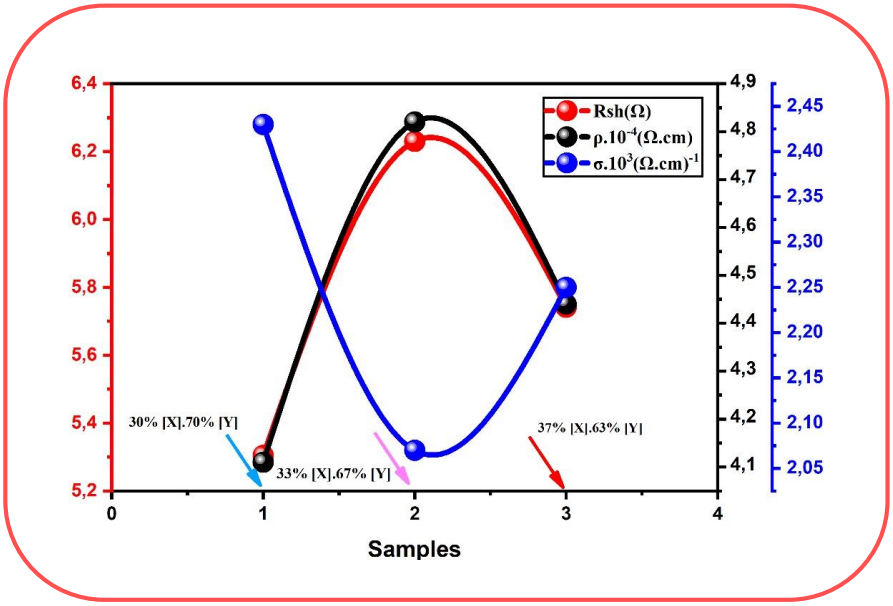

***Figure* (III.10)**: *Variation of Sheet resistance, Electrical resistivity & Electrical Conductivity of NiS thin films.*

III. 4. Conclusion

In this research, we successfully deposited NiS thin films on glass substrates at 523 K using the spray pyrolysis technique. We investigated the impact of varying nickel sulfide precursor concentrations on the structural, optical, and electrical properties thin films, focusing on the specific concentrations of {30% [X].70% [Y]}, {33% [X].76% [Y]}, and {36% [X].73% [Y]}. X-ray diffraction analysis confirmed that all films are polycrystalline with a hexagonal structure, predominantly oriented in the (010) direction. The maximum crystallite size calculated at 22.148 nm, was observed in the films with a {30% [X].70% [Y]} ratio. FTIR Spectroscopy analysis corroborated the presence of Ni-S bonds, indicated by the frequency at 626 cm^{-1}, which aligns with the XRD findings. Optical band gap values for all films were determined to be 0.92, 0.86, and 0.88 eV, respectively. Furthermore, the sheet resistance values were found to be 5.304, 6.230, and 5.741 Ω for the respective samples. This work demonstrates that NiS thin films exhibit excellent crystallinity and high conductivity, which encourages further exploration of their potential applications.

REFERENCES

[1] Patil VP, Pawar S, Chougule M, Godse P, Sakhare R, Sen S, et al. Effect of Annealing on Structural, Morphological, Electrical and Optical Studies of Nickel Oxide Thin Films. J Surf Eng Mater Adv Technol 2011;01:35–41. https://doi.org/10.4236/jsemat.2011.12006.

[2] Gahtar A, Benramache S, Zaouche C, Boukacham A, Sayah A. Effect of Temperature on the Properties of Nickel Sulfide Films Performed by Spray Pyrolysis Technique. Adv Mater Sci 2020;20:36–51. https://doi.org/10.2478/adms-2020-0015.

[3] Srinivasulu T, Saritha K, Reddy KTR. Synthesis and characterization of Fe-doped ZnO thin films deposited by chemical spray pyrolysis. Mod Electron Mater 2017;3:76–85. https://doi.org/10.1016/j.moem.2017.07.001.

[4] Cheng H, Zhai X, Ouyang J, Zheng L, Luo N, Liu J, et al. Achieving a high energy storage density in Ag(Nb,Ta)O3 antiferroelectric films via nanograin engineering. J Adv Ceram 2023;12:196–206. https://doi.org/10.26599/JAC.2023.9220678.

[5] Gahtar A, Benramache S, Ammari A, Boukhachem A, Ziouche A. Effect of molar concentration on the physical properties of NiS thin film prepared by spray pyrolysis method for supercapacitors. Inorg Nano-Metal Chem 2022;52:112–21. https://doi.org/10.1080/24701556.2020.1862225.

[6] Kumar V, Sharma DK, Sharma K, Dwivedi DK. Investigation on physical properties of polycrystalline nickel sulphide films grown by simple & economical screen-printing method. Optik (Stuttg) 2018;156:43–8. https://doi.org/10.1016/j.ijleo.2017.10.169.

[7] Rao KS, Kumar BVN, Rajeev YN, Venkatarao K, Cole S. Structural, morphological and photoluminescence properties of Eu3+ doped Cd2Sr(PO4)2 nanopowder. J Mol Struct 2023;1284:135406. https://doi.org/10.1016/j.molstruc.2023.135406.

[8] Muswareen, SK K, Venkatarao K, Cole S. Comparative Study of Crystallite Size from XRD and TEM Results for Pure and V2O5 Doped CdO-FePO4 Composite Nanopowders. Phys Chem Res 2023. https://doi.org/10.22036/PCR.2022.337333.2077.

[9] Nandhini S, Christina AJ, Muralidharan G. Facile microwave-hydrothermal synthesis of NiS nanostructures for supercapacitor applications. Appl Surf Sci 2018:1–7. https://doi.org/10.1016/j.apsusc.2018.01.024.

[10] Umm-e F, Ahmad KS, Hussain Z, Majid S. Synthesis, characterization and PVD assisted thin film fabrication of the nano-structured bimetallic Ni3S2/MnS2 composite. Surfaces and Interfaces 2018;12:190–5. https://doi.org/10.1016/j.surfin.2018.06.003.

[11] Ofeliya O B, Azizov AA, Muradov MB, Maharramov AM, M Goncha E, Alosmanov

RM, et al. β-NiS and Ni3S4 nanostructures: fabrication and characterization. Mater Res Bull 2015. https://doi.org/10.1016/j.materresbull.2015.11.037.

[12] Buchmaier C, Glänzer M, Torvisco A, Poelt P, Wewerka K, Kunert B, et al. Nickel sulfide thin films and nanocrystals synthesized from nickel xanthate precursors. J Mater Sci 2017;52:10898–914. https://doi.org/10.1007/s10853-017-1265-5.

[13] Kristl M, Dojer B, Gyergyek S, Kristl J. Synthesis of nickel and cobalt sulfide nanoparticles using a low cost sonochemical method. Heliyon 2017;3:1–19. https://doi.org/10.1016/j.heliyon.2017.e00273.

[14] Ghezelbash A, Sigman MB, Korgel BA. Solventless Synthesis of Nickel Sulfide Nanorods and Triangular Nanoprisms. Nano Lett 2004.

[15] Benramache S, Benhaoua B. Influence of annealing temperature on structural and optical properties of ZnO : In thin films prepared by ultrasonic spray technique. Superlattices Microstruct 2012;52:1062–70. https://doi.org/10.1016/j.spmi.2012.08.006.

[16] Zaouche C, Aoun Y, Benramache S, Gahtar A. Synthesis and Characterization of Deposited NiO Thin Films by Spray Pyrolysis Technique. Sci Bull Valahia Univ - Mater Mech 2019;17:27–32. https://doi.org/10.2478/bsmm-2019-0015.

[17] Gedi S, Minnam Reddy VR, Park C, Chan-Wook J, Ramakrishna RR. Comprehensive optical studies on SnS layers synthesized by chemical bath deposition. Opt Mater (Amst) 2015;42:468–75. https://doi.org/10.1016/j.optmat.2015.01.043.

[18] Abdelouahab G, Zaouche C, Ammari A, Dahbi L. Growth and characterization of bimetallic (Ni , Co) sulfide thin films deposited by spray pyrolysis Growth and characterization of bimetallic (Ni , Co) sulfide thin films deposited by spray pyrolysis. Chalcogenide Lett 2023. https://doi.org/10.15251/CL.2023.205.377.

CHAPTER FOUR :

The Influence of Mg Doping on Electrical, Optical and Structural Properties of NiS Thin Films Supercapacitors

In this work, we have studied the effect of doping levels of Mg on structural, optical and electrical properties of NiS thin films. The Mg doped NiS thin films were deposited at different ratios (0, 2, 4, 6 and 8%) on glass substrate at 250 °C using a spray pneumatic technique.

IV. 1. Introduction

The spray pneumatic technique (SPT) was used to deposit thin films of pure nickel sulfide (NiS) and doping with magnesium Mg at different ratios (2, 4, 6 and 8%) at a substrate temperature of 250°C. The structural properties of Mg doped NiS thin films were performed by an X-ray diffraction (XRD), using Fourier transform infrared spectroscopy FTIR at room temperature. The Optical properties were studied using UV absorption spectra to determine the optical band gap energy and Urbach energy. Finally, the variation of electrical resistance as a function of magnesium concentrations was measured using the four-point method.

IV. 2. Experimental Part

IV. 2. 1. Synthesis Protocol :

In the beginning, we prepared a pure spray solution of nickel sulfide by dissolving an amount of nickel nitrate hexahydrate ($Ni(NO_3)_2.6H_2O$) and thiourea ($CS(NH_2)_2$) as a source of nickel Ni and sulfur S, respectively in distilled water. The mixture was stirred continuously at 50 °C for hour on a magnetic stirrer leading to the formation of a clear green and homogeneous solution. To prepare the magnesium Mg doping solution; we kept the same conditions and used magnesium nitrate hexahydrate ($Mg(NO_3)_2$, $6H_2O$) as the precursor Mg molar ratio chosen $x=[Mg^{+2}] / [Ni^{+2}]$; it was 0, 2, 4, 6 and 8%.

IV.2.2 Synthesis Mg doped NiS thin films

The resulting of NiS and NiS:Mg solutions were placed to prepare the Mg doped NiS thin films using the spray pneumatic method. Mg doped NiS thin films were sprayed on microscopic glass slide as a substrate. The Figure (IV.2) presents the experimentally steps; this glass has been tested to withstand temperatures of up to 620 °C. The NiS:Mg solution was transformed into a stream formed with uniform and fine droplets of 30 µm average diameters by studding several Mg concentrations are 0, 0.1, 2, 4, 6 and 8 %, The Mg doped

NiS thin films were deposited at 250 °C by spraying 20 ml with a deposition time approaching 10 min as shows in table (IV.1).

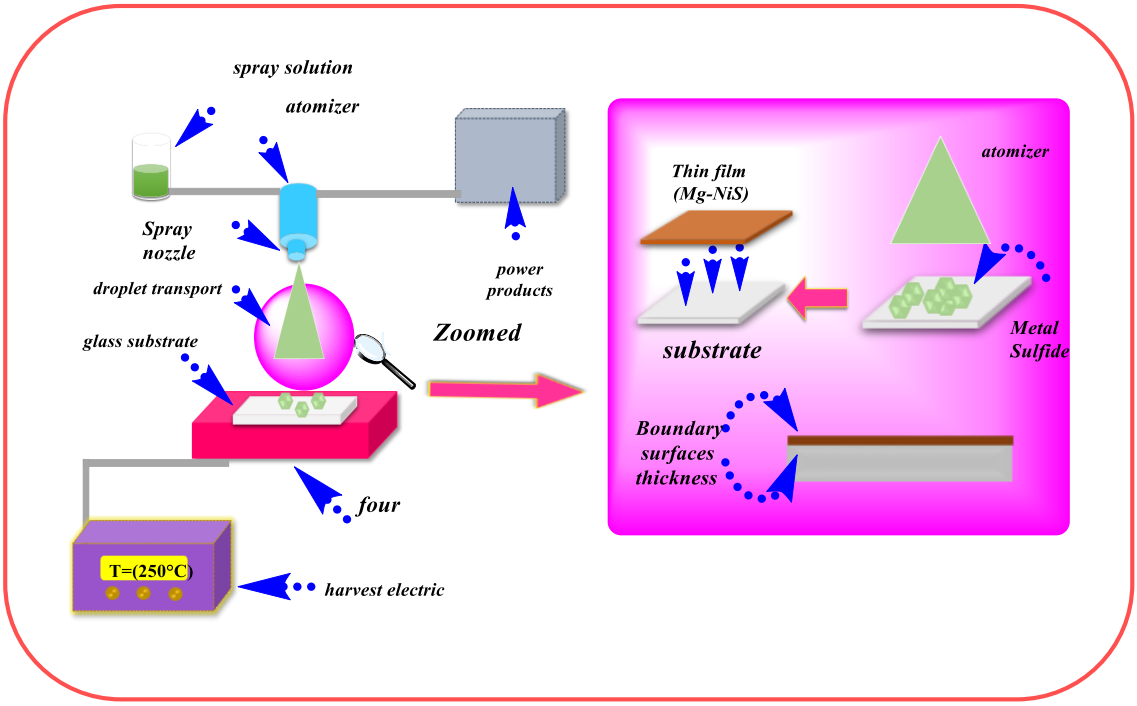

***Figure* (IV.1):** *The deposition steps of undoped and Mg doped NiS films doped using a spray pneumatic technique.*

***Table* (IV.1):** *Optimized deposit conditions for Mg:NiS thin films.*

Condition	*Values*
Dopant	Mg
Mg levels (%)	0%, 2%, 4%, 6% & 8%
Spray mode	spray pneumatic technique
Precursor Concentration (mol/l)	0.15 mol/l
Deposition temperature (C°)	T=250°C
Volume	V=20ml
Deposition time	10min
Distance nozzle – substrate	d=23cm
Flow rate of solution	0.002 l/min
The glass substrats	(CAT.NO.7101) microscope glass slide

IV. 2. 3. Characterization techniques :

Thin films were characterized using various analytical techniques, The X-Ray diffraction diffractogram was obtained by a (*XRD Malvern Pnm analytical Empyrean - CRAPC-LAGHOUAT)* system with Cu-Ka radiation source of wavelength 0.15406 nm in the range of (30–80°) this is in order to study the structural properties of nickel sulfide thin films Infra-Red Spectrometer, type (*Perkinelmer Spectrum Two Photonics and Multifunctional Nanomaterials Physics Laboratory PMNPL- BISKRA)* was used in the frequency range of 400-4000cm^{-1} to study the chemical bonding properties of the prepared films. As for the optical properties of undoped and Mg-doped NiS, were taken by UV-Visible spectrophotometer (*PERKINELMER Lambda 35- Photonics and Multifunctional Nanomaterials Physics Laboratory PMNPL- BISKRA)* at room temperature in a wavelength range (200-1200nm), the electrical properties measurements of the prepared thin films were measured using a four-point method (*Laboratory SMML -BISKRA)*.

IV. 3. Results and discussion

IV. 3. 1. XRD analysis :

Figure (IV.2) represents the X-ray diffraction patterns of the prepared undoped and Mg-doped NiS thin films at various Mg concentrations. We can clearly see that Mg-doped NiS thin films have a four observed peaks are (010), (011), (012), (110) and (022), indicating that the films are polycrystalline nature with a hexagonal phase and P63/mmc space group according to the (ICSD 98-060-2488) card, it has a preferential orientation along to (010) direction. As can be seen, we have not observed any another phase for nickel sulfide, also we have not observed any related phase of NiO or MgO in the XRD diffractogram.

In figures (IV.3), we notice samples with concentrations of Mg (2, 4, 6 and 8%) have a change in the peak positions of (010), (011), (012) and (110) shift towards a higher angle as shows table(IV.2), this behavior can be explained by a difference in the ionic radius between Mg^{+2} (72 pm) and Ni^{+2} (69 pm) **[1]**. As shown by the XRD patterns, the intensity of all peaks decreases with increasing Mg levels, indicating a decrease in the crystallite size of Mg doped NiS thin films.

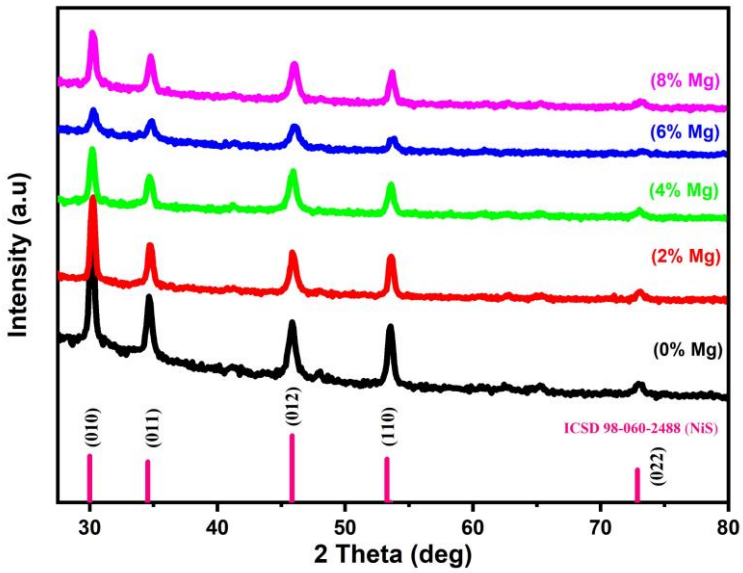

***Figure* (IV.2):** *X-ray patterns of undoped and Mg-doped NiS thin films at various Mg levels (%).*

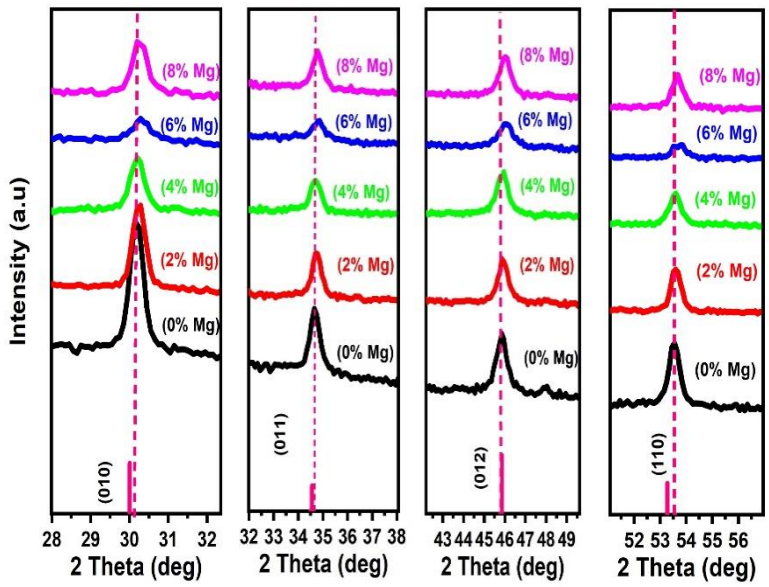

***Figure* (IV.3):** *an emphasis of the (010), (011), (012) and (110) peaks showing a shift towards higher angles for the doped thin films.*

***Table* (IV.2):** *2 Theta (deg) Variation per (hkl) for Mg-NiS thin films.*

(hkl) / 2 theta (deg)	0% Mg	2%Mg	4% Mg	6% Mg	8% Mg
(010)	30.187	30.243	30.196	30.315	30.274
(011)	34.679	34.749	34.695	34.851	34.788
(012)	45.853	45.937	45.968	46.118	46.028
(110)	53.546	53.588	53.595	53.716	53.624

Figure (IV.4) depicts the crystal composition of the nickel sulfide (NiS) compound, where blue spheres represent nickel atoms, and red spheres indicate sulfur atoms. This structure suggests a hexagonal arrangement, as evidenced by the presence of sulfur atoms coordinating in a trigonal prismatic manner with nickel atoms. This means that each sulfur atom is surrounded by six nickel atoms at the vertices of a trigonal prism.

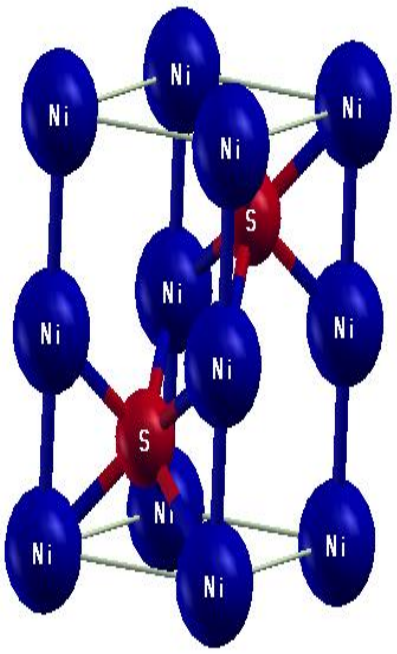

***Figure* (IV.4):** *structures of hexagonal NiS thin films. Red and bleu balls represent Sulfur and nickel atoms, respectively.*

$$\frac{1}{3}\ Hexahonal \begin{cases} \mathrm{Ni}(1): (0\ 0\ 0) \\ \mathrm{Ni}(2): (0\ 0\ \frac{1}{2}) \\ \mathrm{S}(1): (\frac{1}{3}\ \frac{2}{3}\ \frac{3}{4}) \\ \mathrm{S}(2): (\frac{2}{3}\ \frac{1}{3}\ \frac{3}{4}) \end{cases}$$

Figure (IV.5) depicts a model of the crystal structure of magnesium doped nickel sulfide, with violet spheres representing magnesium (Mg) atoms, blue spheres representing nickel (Ni) atoms, and red spheres for sulfur (S) atoms, respectively. In this structure, magnesium replaces some of the nickel atoms at various doping ratios of 2, 4, 6, and 8%.

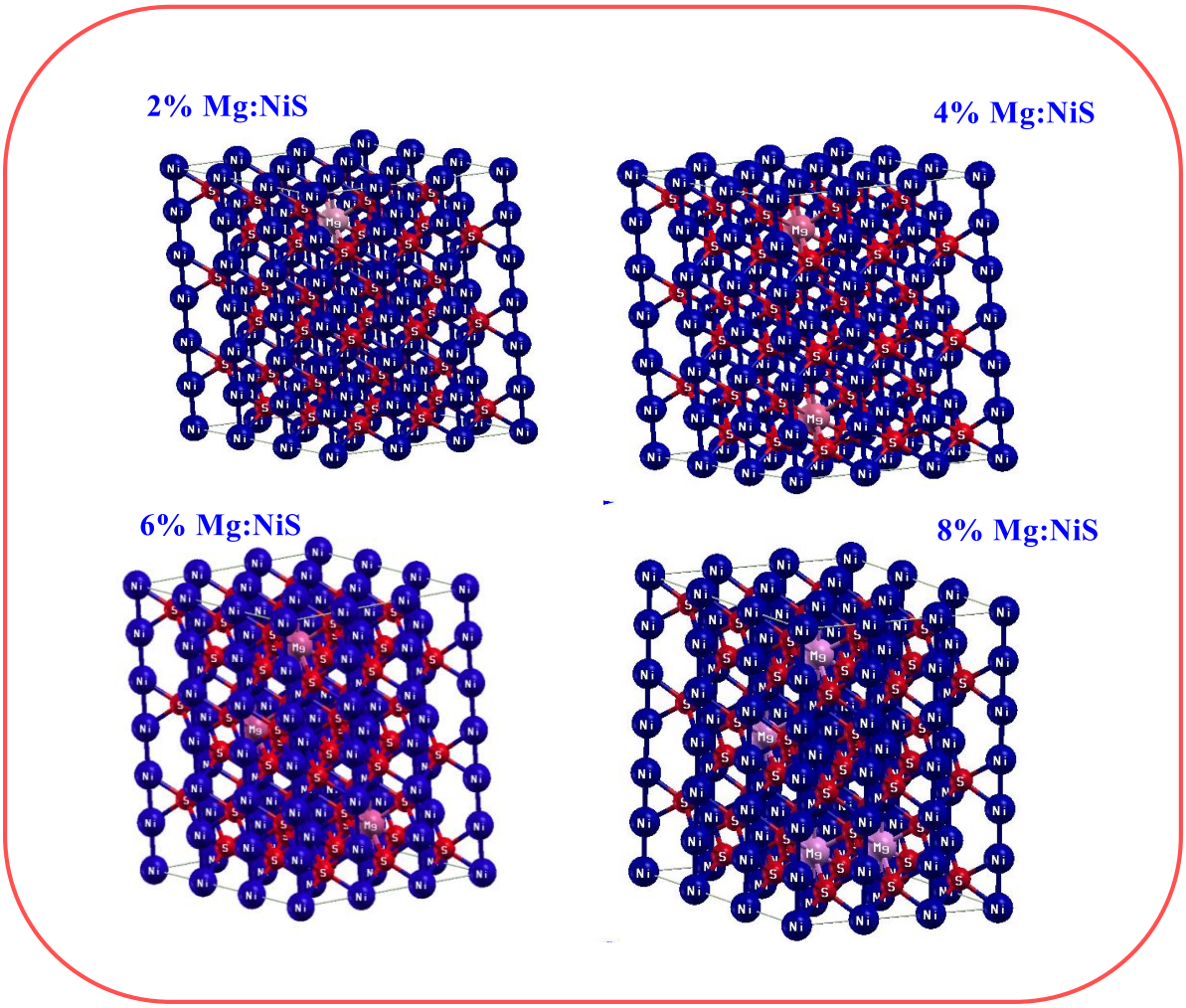

***Figure* (IV.5):** *structures of hexagonal Mg-doped NiS thin films. Red, bleu and purple balls represent Sulfur, nickel and magnesium atoms, respectively.*

IV.3.1.1. Lattice parameters and d-spacing :

The inter planer d_{hkl} of Mg doped NiS can be calculated from the position 2θ of (010), (011), (012) and (110) peaks using the *Bragg's Law* [2] :

$$2d_{hkl}\sin\theta = n\lambda \qquad \text{N° (IV.1)}$$

So:

$$d_{hkl} = \frac{n\lambda}{2\ sin\,\theta} \qquad \text{N° (IV.2)}$$

Where:

- d_{hkl} is the inter planer
- (hkl) are Miller indices
- θ is the half diffraction angle of the centroid of the peak
- λ is the wavelength of X-ray diffraction (λ = 1.5406 A°)
- n is the diffraction order ($n=1$ is first order).

The lattice parameters a and c of Mg doped NiS hexagonal structure can be determined by using the following formula [3]:

$$\frac{1}{d^2_{hkl}} = \frac{4}{3}\left(\frac{h^2+k^2+hk}{a^2}\right) + \frac{l^2}{c^2} \qquad \text{N°(IV.3)}$$

Thus:

$$d_{hkl} = \frac{a}{\sqrt{\frac{4}{3}\left(h^2+k^2+hk\right)+l^2\frac{a^2}{c^2}}} \qquad \text{N° (IV.4)}$$

Where:

- a and c are the lattice parameters

***Table* (IV.3):** *Inter-planar distance* (*d*) *per* (*hkl*) *for Mg-NiS thin films.*

(hkl) / d-spacing (Å)	0% Mg	2%Mg	4% Mg	6% Mg	8% Mg
(010)	2.959	2.954	2.958	2.947	2.951
(011)	2.585	2.580	2.584	2.573	2.578
(012)	1.978	1.974	1.973	1.967	1.971
(110)	1.710	1.709	1.709	1.705	1.708

***Table* (IV.4):** *Lattice parameters (a, b, & c) of Mg :NiS thin films prepared compared to those values of the ICSD card* (98-060-2488).

Mg levels (%)	*ICSD card*			*This work*			
	a = b (Å)	**c (Å)**	**c/a (Å)**	**a = b (Å)**	**c (Å)**	**c/a (Å)**	*V* (Å^3)
0	3.4200	5.300	1.55	3.416	5.314	1.555	62.045
2				3.409	5.302	1.554	61.688
4				3.416	5.310	1.554	61.962
6				3.403	5.279	1.551	61.132
8				3.407	5.295	1.554	61.462

IV.3. 1. 2. The Texture Coefficient & The Crystallite Size :

The texture coefficient $TC(hkl)$ of Mg doped NiS can be measured from the X–ray data for the highest intensity peaks of the (010), (011), (012) and (110) planes using the following equation [4]:

$$TC(hkl) = \frac{I_{hkl} / I_{0hkl}}{N^{-1}\sum_{n} I_{hkl} / I_{0hkl}} \qquad \text{N° (IV.5)}$$

Where:

- I_{hkl} is the relative intensity of the peaks (hkl),
- I_{0hkl} is the standard intensity of the plane (hkl), it was taken from the ICSD data,
- N is the reflection number
- n is the number of diffraction peaks detected.

The variation of $TC(hkl)$ values for the major four peaks of (010), (011), (012) and (110) are presented in Figure (IV.6). As can be observed, the texture coefficient of the (010) peak is the highest one. This finding indicates that all films prefer an a-axis orientation along the (010) plane.

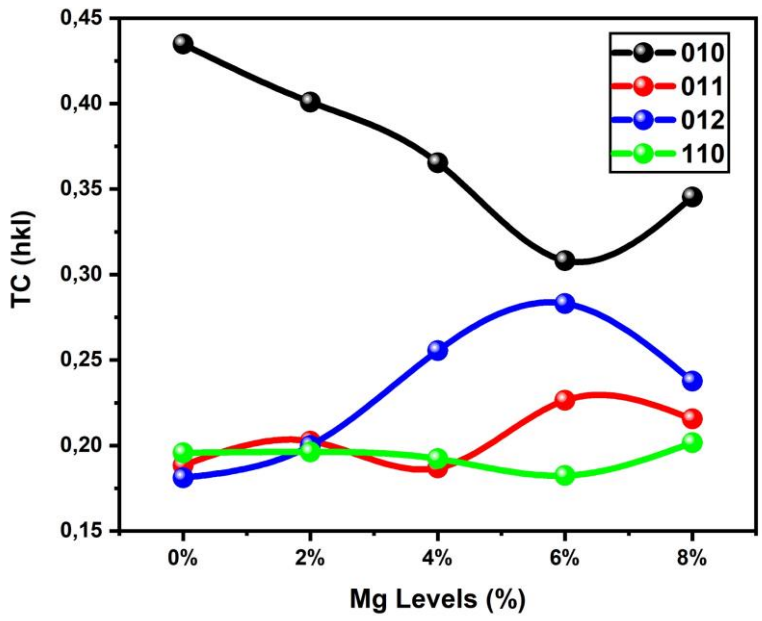

***Figure* (IV.6):** *Variation of the texture coefficient for the (010), (011), (012) and (110) peaks at various Mg levels (%).*

The crystallite size D_{hkl} of undoped and Mg-doped NiS thin films was calculated using the Debye–Scherrer's equation [5]:

$$D_{hkl} = \frac{k\lambda}{\beta \cos\theta} \qquad \text{N° (IV.6)}$$

Where:

- β is full width at half-maximum (FWHM)
- k is a constant (k =0.89).

Figure (IV.7) & Table (IV.5) show the variations of the crystallite size D_{hkl} of Mg doped NiS thin films, it were presented for major four peaks of (010), (011), (012) and (110). When increased in the Mg levels from 0 to 8% the crystallite sizes decreased, they can be indicated by the increase in grain boundaries, also can improve the electrical properties of Mg doped NiS thin films.

***Table* (IV.5)**: *Values of the crystallite size D for the (hkl) plane of NiS thin films as a function Mg levels(%).*

$D_{hkl}(nm)$ / Mg levels (%)	0% Mg	2% Mg	4% Mg	6% Mg	8% Mg
$D_{(010)}$	20.326	20.881	18.017	19.016	17.630
$D_{(011)}$	19.637	18.983	15.895	15.958	17.701
$D_{(012)}$	14.851	15.568	13.829	11.888	12.548
$D_{(110)}$	19.005	17.772	17.753	15.359	17.766

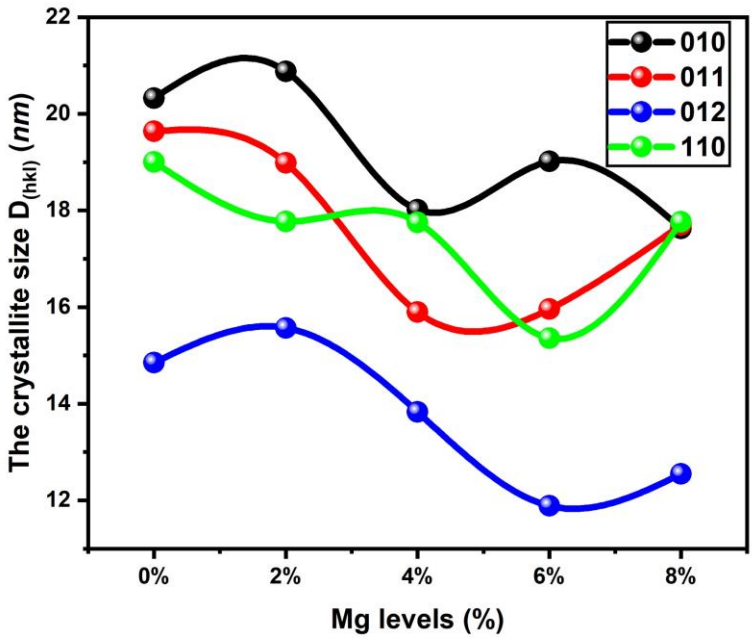

***Figure* (IV.7):** *Variation of the crystallite size for the (hkl) peaks at various Mg levels (%).*

IV.3. 1. 3. The dislocation densities & Micro-Strain:

The dislocation densities δ_{hkl} of Mg doped NiS thin films were determined by following equation [6]:

$$\delta_{hkl} = \frac{1}{D_{hkl}^2} \qquad \text{N° (IV.7)}$$

***Table* (IV.6)**: *Values of the dislocation densities for the (hkl) plane of NiS thin films as a function Mg levels (%).*

δ_{hkl})×10^{15} (Lines m^{-2}) / Mg levels (%)	0% Mg	2% Mg	4% Mg	6% Mg	8% Mg
δ_{010}	2.420	2.293	3.080	2.765	3.217
δ_{011}	2.593	2.775	3.958	3.926	3.191
δ_{012}	4.534	4.126	5.229	7.075	6.351
δ_{110}	2.767	3.166	3.172	4.239	3.168

The Micro-Strain ε_{hkl} was calculated using Stokes-Wilson relation [7]:

$$\varepsilon_{hkl} = \frac{\beta}{4\tan\theta} \qquad \text{N° (IV.8)}$$

***Table* (IV.7)**: *Values of the Micro-Strain for the (hkl) plane of NiS thin films as a function Mg levels(%)*

ε_{hkl} ×10^{-3} / Mg levels (%)	0% Mg	2% Mg	4% Mg	6% Mg	8% Mg
ε_{010}	6.55	6.36	7.38	6.97	7.53
ε_{011}	5.92	6.11	7.31	7.26	6.55
ε_{012}	5.99	5.71	6.43	7.45	7.07
ε_{110}	4.05	4.33	4.33	4.99	4.32

***Table* (IV.8)**: *Values of the crystallite size, The dislocation densities & the Micro-Strain for the (hkl) plane of NiS thin films as a function Mg levels(%).*

Mg levels(%)	*the crystallite size*	*The dislocation densities*	*Micro-Strain*
0% Mg	18.455	2.936	5.627
2% Mg	18.301	2.985	5.627
4% Mg	16.373	3.729	6.362
6% Mg	15.555	4.132	6.667
8% Mg	16.411	3.712	6.367

As shown from figure (IV.8) and table (IV.8) the crystallite size of Mg doped NiS decrease from 18.301 nm to 15.555 nm when the concentration of magnesium increases at

6%. The residual stress of NiS pure and Mg doped NiS thin films has been found to increases with Mg content as well as the dislocation density and Micro-Strain.

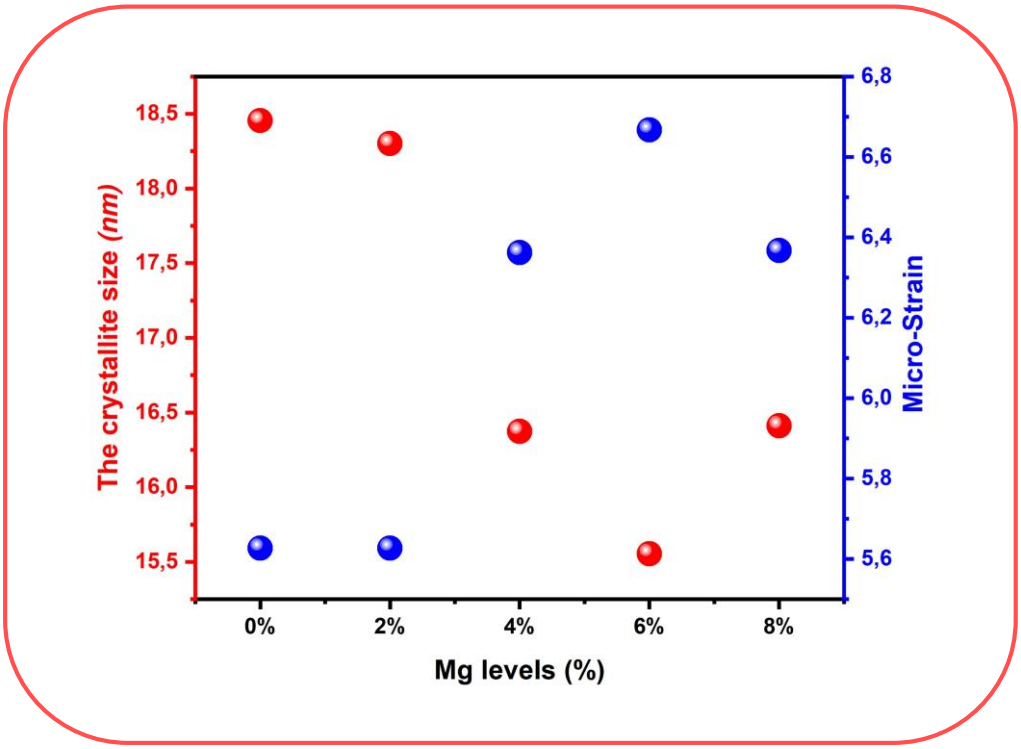

***Figure* (IV.8)**: *Crystallite size and strain NiS and Mg-doped NiS thin film as a function of Mg levels (%).*

IV.3.2. Chemical composition

FTIR spectra of the prepared of pure NiS and Mg doped NiS thin films deposited on glass substrate is shown in figure (IV.9). Broad 3275 cm^{-1} can be attributed to water (O-H) adsorbed to the surface of the film [8], we can see the strong peaks at 623 cm^{-1} which related to the bending and stretching vibration of pure (Ni-S bonds) [9],[10]. The peak observed at 1092 cm^{-1} is attributed of (C-S) bond arising out of the precursors [9], and the other is around 1483 cm^{-1}denotes the bending vibration of (C-H) [11]. Consequently, these results may confirm the successful adhesion of NiS thin films on a glass substrate, The band observed at 2375 cm^{-1} which are ascribed to the stretch in vibration of O=C=O bond, as the result, atmospheric molecules adsorbed on the surface of the aero-gels [12], [13].

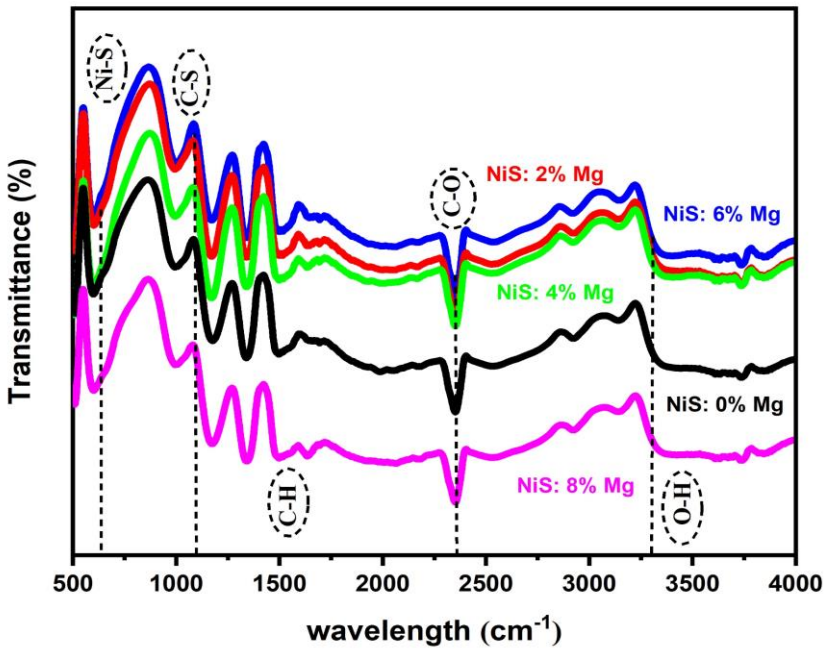

***Figure* (IV.9):** *FTIR spectra of NiS and Mg:NiS thin film.*

IV.3. 3. Optical study

IV.3. 3. 1. The transmission & The absorption:

The optical properties of sprayed undoped and Mg doped NiS thin films at various Mg concentrations are shown in figure (IV.10). Presents the transmission as can seen, when Mg level increased the transmission was increased, indicating to cooperate between the Ni and Mg. However, the absorption of Mg doped NiS thin films is indicted in figure (IV.11), it can be seen a decrease was observed in absorption edge of the thin films with increasing Mg doping concentration, the reduction in the absorption edge might be due to the Mg doping.

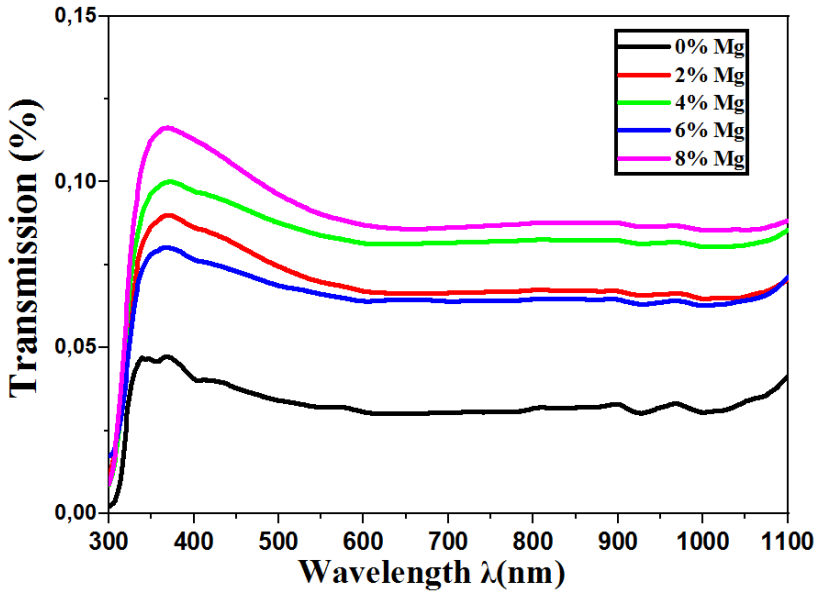

***Figure* (IV.10):** *Transmission of undoped and Mg:doped NiS thin films at various Mg levels (%).*

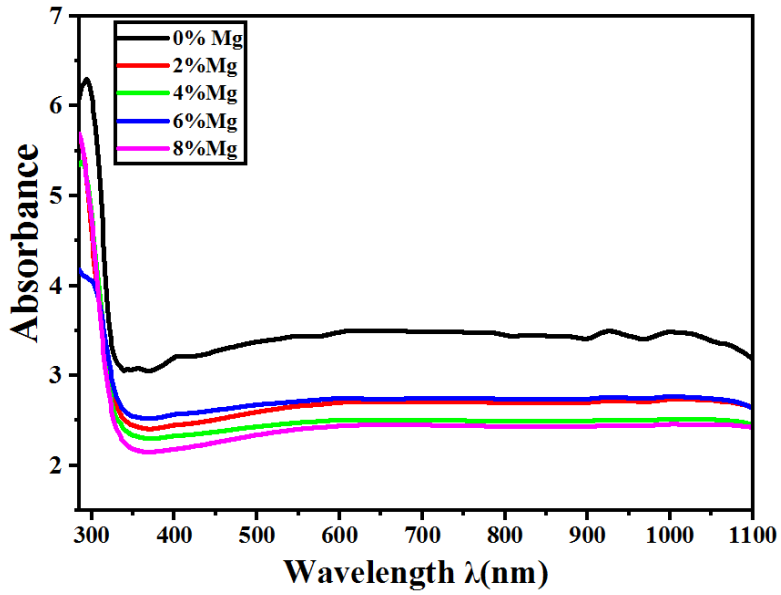

***Figure* (IV.11):** *Transmission of undoped and Mg:doped NiS thin films at various Mg levels (%).*

IV.3. 3. 2. The optical band gap & The Urbach energy:

The optical band gap (Eg) of undoped and Mg-doped NiS films deposited at 250 °C is associated with the point of intersection of the linear line with the photon energy (hv)A = 0 as shown in figure (IV. 12). Moreover, the optical band gap energy of the synthesized films was calculated using the formula (N° IV.9 & N° IV.10), was obtained from the transmission spectra is calculated according to the following equations [14]:

$$A = \alpha d = -\ln(T) \qquad \text{N° (IV.9)}$$

$$(Ahv)^2 = B(hv - Eg)/A = \alpha d \qquad \text{N° (IV.10)}$$

However, the Urbach energy was measured by means of the slope of the rectum between the two turning points as shows in figure (IV.13). The relationships between the optical transmission and absorption can be realized to determine the optical band gap energy and Urbach energy E_u with the variation of photo energy ($h\upsilon$) are given by the following formulas [15]:

$$A = A_0 \exp\left(\frac{h\upsilon}{E_u}\right) \qquad \text{N° (IV.11)}$$

Where:

- α is the absorption coefficient
- A is absorbance values
- A_0 and C are constants
- d is a constant thickness of the films
- E_g is the optical gap
- E_u is Urbach energy of the Mg doped NiS thin films.

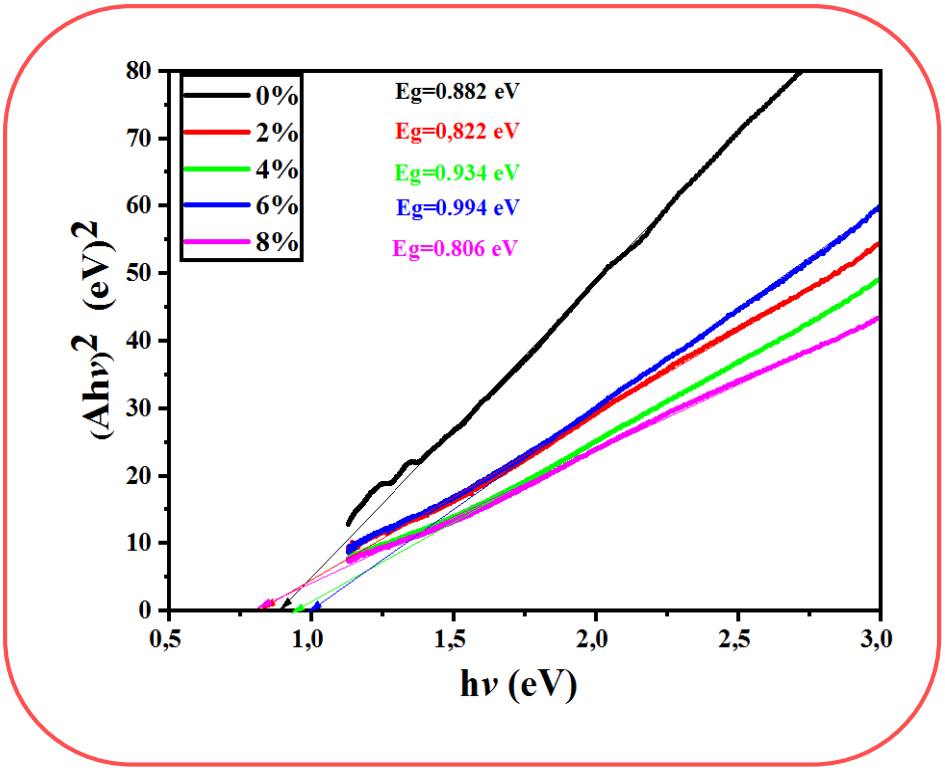

***Figure* (IV. 12):** *The plot of $(Ahv)^2$ versus hv for the optical band gap energy.*

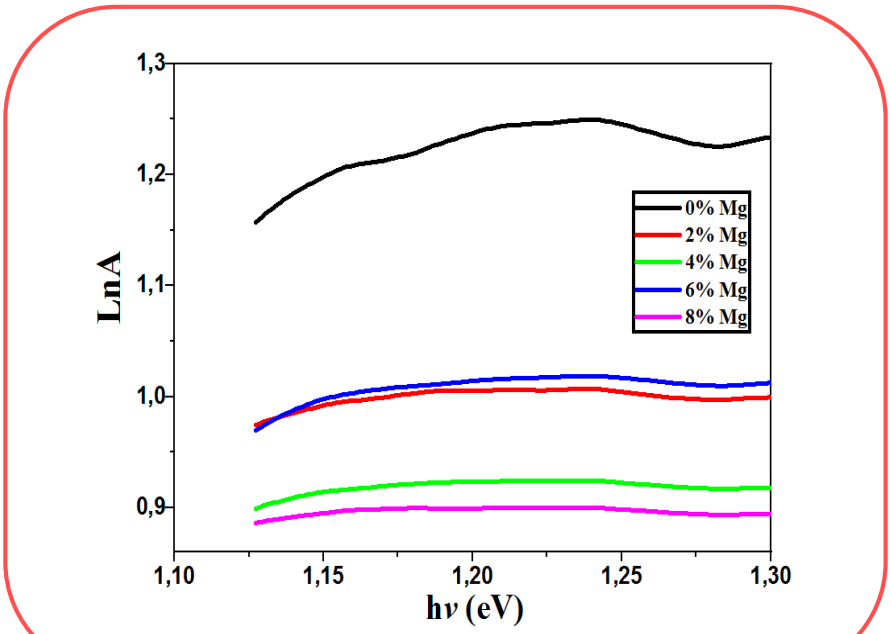

***Figure* (IV.13):** *The plot of LnA versus hv for the Urbach energy.*

The variations of optical band gap energy and Urbach energy of Mg doped NiS thin films are presented in figure (IV.14). The first observation is that the change in one is inversely proportional to the change in the other. The optical band gap of the Mg doped NiS thin films increased after doping with Mg and then decreased to a minimum value for 8 % Mg, this can be related to the decrease in the crystallite size. However, because of the increase in transparency, the sprayed Mg doped NiS thin film with 6% Mg achieved the lowest Urbach energy.

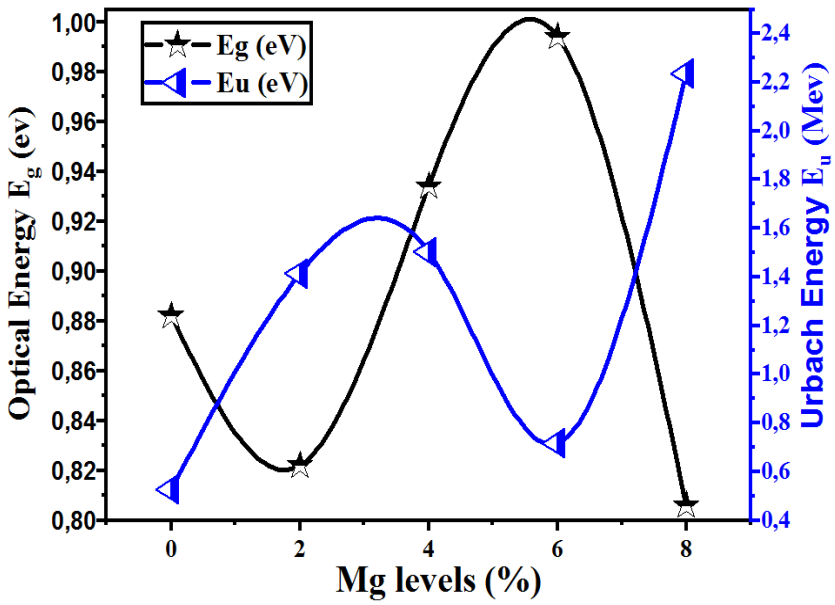

***Figure* (IV.14):** *the variation of the optical band gap energy and Urbach energy as a function of Mg levels (%).*

IV.3.4. Electrical study

The electrical properties of the Mg doped NiS thin films representing the calculation of electrical resistance; it is measured by the four-points method, when varying an applied current I to find the voltage values V using the following equations [16]:

$$R_{sh} = \frac{\pi}{Ln2}\frac{V}{I} \qquad \text{N° (IV.12)}$$

Figure (IV.15) & figure (IV.16) present the electrical properties of the Mg doped NiS thin films, figure (IV.15) show the variation of voltage-current (V-I) characteristics when observed that the Mg doped NiS have a good measurements due to the applying current and measurements voltage in order to mA and mV, respectively. The insert show the capacity of each sample, we find for example, the Mg doped NiS thin film sprayed with 6%Mg has the best current and good tension. However, figure (IV.15) presents the sheet resistance as a function of Mg concentration, as can be seen. The variation in electrical conductivity corresponds well to the fluctuation in thin film Urbach energy see figure (IV.13). It was increased with Mg concentration and decreased up to the minimum value of 5,569 Ω see table (IV.9) found for sprayed thin film with 6%Mg. However, the decrease in the sheet resistance is explained by decreasing the potential barriers, which relate to the introduced atoms and are segregated into the grain boundaries see figure (IV.7).

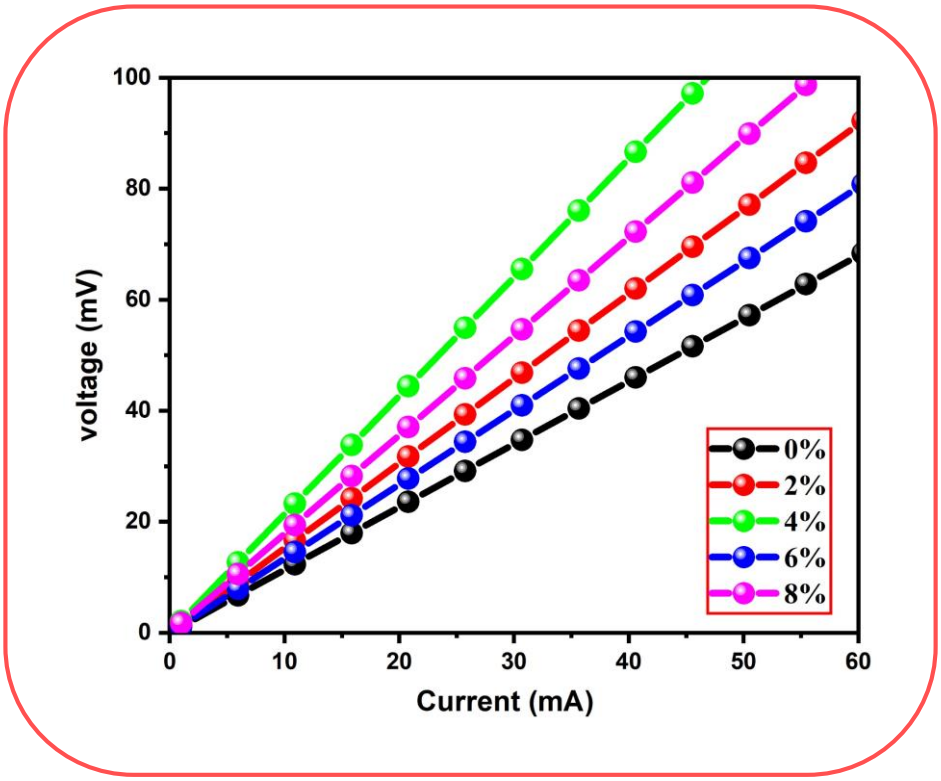

***Figure* (IV.15):** *Voltage versus Current characteristics of Mg:NiS thin films.*

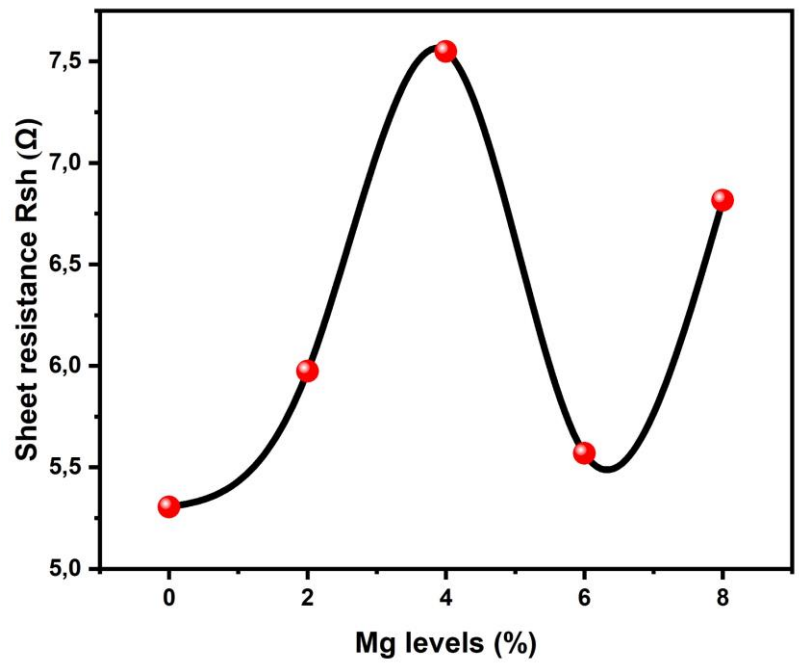

***Figure* (IV.16):** *Variation of Sheet resistance R_{sh} as a function to the Mg levels (%).*

***Table* (IV.9):** *Variation of Sheet resistance Rsh of of Mg:NiS thin films.*

Mg levels (%)	**0%**	**2%**	**4%**	**6%**	**8%**
Sheet resistance R_{sh} (Ω)	5.304	5.974	7.549	5.569	6.816

IV.4. Conclusion

In the conclusion, the structural, optical and electrical properties of Mg doped NiS thin films were investigated. The high quality Mg doped NiS thin films were created on glass substrates at 250 °C via the chemical spray pneumatic technique with various Mg concentrations. The following conclusions summarize the above research work: The Mg doped NiS thin films' XRD patterns reveal that they are polycrystalline with a hexagonal structure (wurtzite) and a strong (010) preferred orientation. The structure of thin films was in good after Mg doping due to improve of the crystallite size. Mg doped NiS thin films have

good absorption in the visible, when Mg concentration increased from 0 to 6%Mg, the band gap shrinkage of up to 0.1 eV was observed; it narrowed from 0.882 to 0.994 eV. It is also shown that the Mg doped NiS thin film deposited 6%Mg has the minimum Urbach energy of 0.717 eV. The electrical sheet resistance decreased after Mg doping up to the minimum value of 5,569 Ω 6%Mg, it was explained by decreasing the potential barriers, which relate to the introduced atoms and are segregated into the grain boundaries. Finally, suitable Mg doped NiS thin films can be used for the supercapacitors because of their lowest sheet resistance.

REFERENCES

[1] Amor M Ben, Boukhachem A, Boubaker K, Amlouk M. Materials Science in Semiconductor Processing Structural , optical and electrical studies on Mg-doped NiO thin films for sensitivity applications. Mater Sci Semicond Process 2014;27:994–1006. https://doi.org/10.1016/j.mssp.2014.08.008.

[2] Abdel Rafea M, Eid A, Mustapha N. The effect of annealing on the structure, morphology, and optical properties of Co3O4 thin films prepared using a modified dip coating technique. Mater Sci Eng B 2023;290:116294. https://doi.org/10.1016/j.mseb.2023.116294.

[3] Mahdi R, Jarrah A, Muslem E, Adel K, Alkhayatt HO. Annealing and operating temperatures effect on spray - deposited nanocrystalline ZnO thin - film gas sensor. Appl Phys A 2022;128:1–11. https://doi.org/10.1007/s00339-022-05659-x.

[4] Boughalmi R, Rahmani R, Boukhachem A, Amrani B, Amlouk M. Metallic behavior of NiS thin film under the structural , optical , electrical and ab initio investigation frameworks. Mater Chem Phys 2015;163:99–106. https://doi.org/10.1016/j.matchemphys.2015.07.019.

[5] Bouachibaa Y, ABDELOUADOUD M, Abderrahmane B, Oualid R, Saber S, Adel T, et al. Optoelectronic and Birefringence Properties of Weakly Mg Doped ZnO Thin Films Prepared by Spray Pyrolysis. Res Sq 2022:1–17. https://doi.org/https://doi.org/10.21203/rs.3.rs-1021475/v3.

[6] Rouchdi M, Salmani E, Fares B, Hassanain N, Mzerd A. Synthesis and characteristics of Mg doped ZnO thin films : Experimental and ab-initio study. Results Phys 2017;7:620–7. https://doi.org/10.1016/j.rinp.2017.01.023.

[7] Abed C, Ben M, Addad A, Elhouichet H. Growth , structural and optical properties of ZnO-ZnMgO-MgO nanocomposites and their photocatalytic activity under sunlight irradiation. Mater Res Bull 2019;110:230–8. https://doi.org/10.1016/j.materresbull.2018.10.041.

[8] Buchmaier C, Glänzer M, Torvisco A, Poelt P, Wewerka K, Kunert B, et al. Nickel sulfide thin films and nanocrystals synthesized from nickel xanthate precursors. J Mater Sci 2017;52:10898–914. https://doi.org/10.1007/s10853-017-1265-5.

[9] Nandhini S, Christina AJ, Muralidharan G. Facile microwave-hydrothermal synthesis of NiS nanostructures for supercapacitor applications. Appl Surf Sci 2018:1–7. https://doi.org/10.1016/j.apsusc.2018.01.024.

[10] Moulahi A. Cu Doped NiS / ZnS Nanocomposites for Photodegradation of Methyl Green , Methylene Blue and Congo Red Pollutants. J Inorg Organomet Polym Mater 2023. https://doi.org /10.1007/s10904-023-02702-z.

[11] Gahtar A, Benramache S, Ammari A, Boukhachem A, Ziouche A. Effect of molar concentration on the physical properties of NiS thin film prepared by spray pyrolysis

method for supercapacitors. Inorg Nano-Metal Chem 2022;52:112–21. https://doi.org/10.1080/24701556.2020.1862225.

[12] Ghezelbash A, Sigman MB, Korgel BA. Solventless Synthesis of Nickel Sulfide Nanorods and Triangular Nanoprisms. Nano Lett 2004.

[13] Majid S, Ahmad KS. Optik Analysis of dopant concentration effect on optical and morphological properties of PVD coated Cu-doped Ni 3 S 2 thin films. Opt - Int J Light Electron Opt 2019;187:152–63. https://doi.org/10.1016/j.ijleo.2019.05.025.

[14] Benramache S, Benhaoua B. Influence of substrate temperature and Cobalt concentration on structural and optical properties of ZnO thin films prepared by Ultrasonic spray technique. Superlattices Microstruct 2012;52:807–15. https://doi.org/10.1016/j.spmi.2012.06.005.

[15] Zaouche C, Aoun Y, Benramache S, Gahtar A. Synthesis and Characterization of Deposited NiO Thin Films by Spray Pyrolysis Techniqu. Sci Bull VALAHIA Univ - Mater Mech 2019;17. https://doi.org/10.2478/bsmm-2019-0015.

[16] Abdelouahab G, Zaouche C, Ammari A, Dahbi L. Growth and characterization of bimetallic (Ni , Co) sulfide thin films deposited by spray pyrolysis Growth and characterization of bimetallic (Ni , Co) sulfide thin films deposited by spray pyrolysis. Chalcogenide Lett 2023. https://doi.org/10.15251/CL.2023.205.377.

CHAPTER FIVE :

Effects of oxygen annealing atmosphere on Mg :NiS thin films.

This chapter presents the effects of an oxygen annealing atmosphere on the physical properties of thin films of undoped nickel sulfide and magnesium-doped nickel sulfide, as prepared and discussed in Chapter Four. Structural, optical and electrical characterizations of these films are provided.

V.1. Introduction

The term 'oxygen annealing atmosphere' refers to a specific environment used in the annealing process, a heat treatment technique. In this context, annealing occurs in an oxygen-rich atmosphere. This environment can significantly affect the properties of the material being annealed. The goal of annealing is to change a material's physical and occasionally chemical characteristics. This process typically involves heating the material to a specified temperature, maintaining that temperature for a set period, and then allowing it to cool. The Benefits of this process include reducing internal stresses, facilitating diffusion, and altering the material's microstructure. When performed in an oxygen-rich atmosphere, annealing can influence the oxidation states, electrical properties, and structural characteristics of the material. In our case, oxygen annealing can impact thin films, affecting aspects like crystal structure, defect densities, and electrical conductivity. This is particularly crucial in semiconductor and nanotechnology applications. *Chuangye Y et al.* **[1]** Conducted a study on Co_3O_4 thin films and found that annealing in various atmospheres, including oxygen, significantly affects their resistive switching. The research highlighted that the annealing atmosphere influences the distribution of oxygen vacancies, which, in turn, alters the electrical properties of the films.

V. 2. Experimental procedure

V. 2. 1. Annealed thin films preparation:

Herein, an annealing process is reported, aimed at improving the superconducting properties of nickel sulfide. The annealing was performed in the presence of oxygen at a temperature of 300°C and 350°C for 3h30min and 3h, respectively.This process involved a comparison between annealing at low temperature for an extended period and at high

temperature for a shorter duration. Figure (V.1) presents a schematic diagram illustrating the preparation process of annealed films from nickel sulfide.

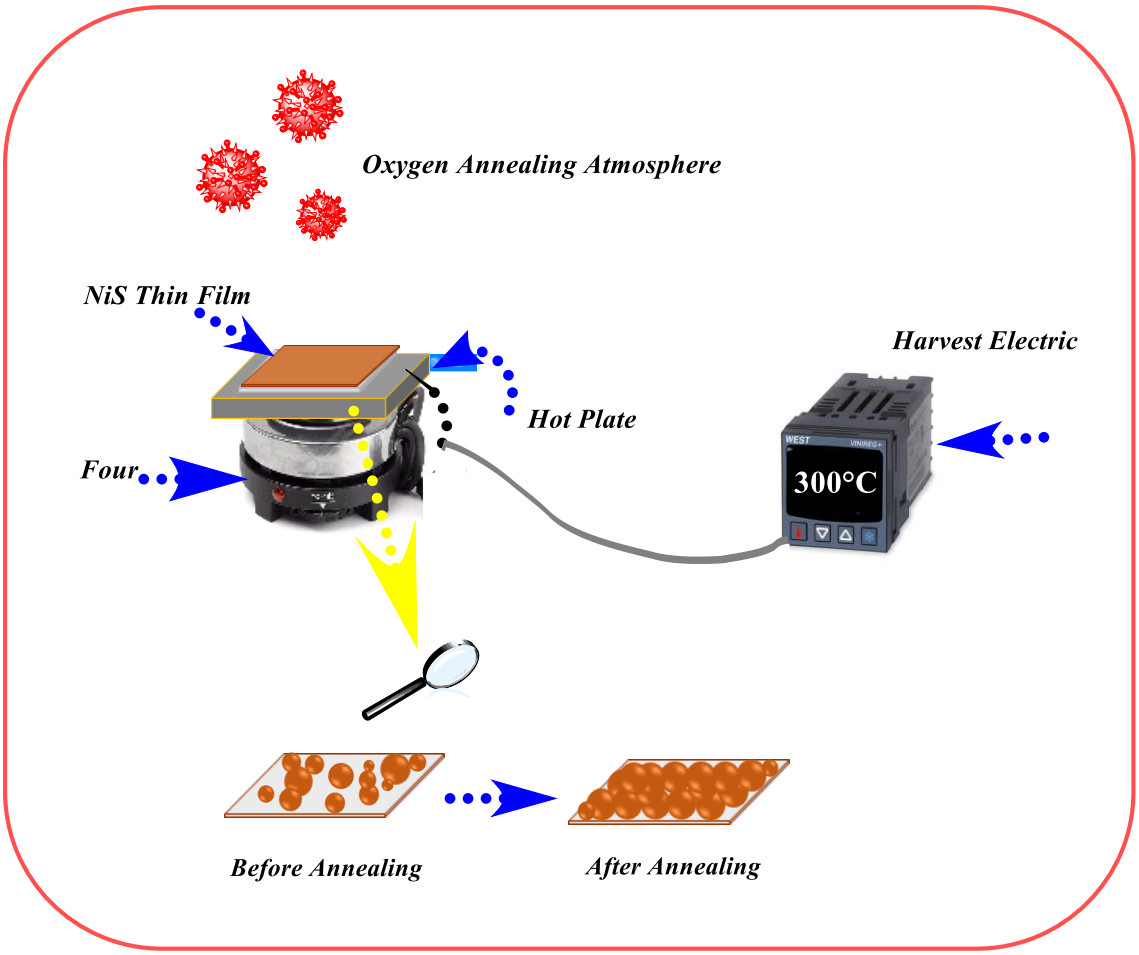

Figure* (V.1) :A schematic diagram illustrating the preparation process of annealed films.*

V. 2 .2. Thin Film characterization:

X-ray diffraction analysis was performed in the angular range 2θ = 20°-80° using a device (*Materials Preparation and Manufacturing MEMP, CONSTANTINE*). The radiation was produced by a CuKα source with a wavelength of λ=1.541838 Å at room temperature. For the infrared spectroscopy analysis, the (Perkinelmer Spectrum Two instrument, located at the *Photonics and Multifunctional Nanomaterials Physics Laboratory (PMNPL) in Biskra*), was utilized. This instrument was specifically used to scan frequencies ranging from 400 to 4000 cm^{-1}.The absorbance spectra of the annealed thin films were measured using a

spectrophotometer (*PERKINELMER Lambda 35-Photonics and Multifunctional Nanomaterials Physics Laboratory PMNPL, BISKRA*) in the wavelength range from 200 to 1100 nm at room temperature. Finally, the electrical properties were measured using the four-point method.

V. 3. Results and discussion

V. 3. 1. XRD analysis:

Figure V.2 (0, 2, 4, and 6) displays the X-ray diffraction patterns of nickel sulfide thin films annealed in oxygen atmospheres. We observed strong crystallization in all films, with the NiS phase peaks present in each, at both 300°C for 3h30min and 350°C for 3h, indicating polycrystalline behavior. Moreover, thin films annealed in oxygen revealed the formation of secondary phases. Using the ICSD 98-060-2488 data card, we were able to identify the hexagonal structure of all films, characterized by a preferred growth direction along (010) at 2theta ~ 30° and a P63/mmc space group. The intensity of this peak is significantly higher compared to others. Notably, distinct peaks with strong intensities were observed at (011), (012), (110), (013), (020), (021), and (220). Additionally, as per the JCPDS No.04–0835 card, other secondary peaks at (111) and (200) in 2theta ~ 37.5° and 43.3°, respectively, suggest the cubic (FCC) phase of NiO [2]. However, we can conclude that annealing in an oxygen atmosphere can significantly impact the structural properties of thin films. This includes changes in oxidation states, which may alter the crystal structure and promote the growth of certain crystalline phases while inhibiting others.

***Table* (V.1)** : *The crystal structure corresponding to each (hkl) plane.*

2θ(°)	*(hkl)*	*Crystal Structure*	*References*
30.006	**(010)**	Hexagonal NiS	98-060-2488
34.556	**(011)**	Hexagonal NiS	98-060-2488
37.998	**(111)**	cubic NiO	No.04–0835
43.296	**(200)**	cubic NiO	No.04–0835
45.865	**(012)**	Hexagonal NiS	98-060-2488
53.278	**(110)**	Hexagonal NiS	98-060-2488
61.033	**(013)**	Hexagonal NiS	98-060-2488

62.361	**(020)**	Hexagonal NiS	98-060-2488
65.071	**(021)**	Hexagonal NiS	98-060-2488
72.886	**(220)**	Hexagonal NiS	98-060-2488

***Table* (V.2)** : *2Theta values corresponding to (hkl) planes of the annealed films.*

(hkl) / Mg levels (%)	$2\theta(°); O_2 in\ 300°C$	$2\theta(°); O_2 in\ 350°C$	$2\theta(°); O_2 in\ 300°C$	$2\theta(°); O_2 in\ 350°C$
	0% Mg		**2% Mg**	
(010)	**30.1966**	**30.2062**	**30.1950**	**30.1850**
(011)	**34.6894**	**34.7280**	**34.6789**	**34.6685**
(111)	**37.1800**	**37.3328**	**37.3661**	**37.3660**
(200)	**43.3443**	**43.2790**	**43.3661**	**43.4364**
(012)	**45.8867**	**45.8794**	**45.8290**	**45.7890**
(110)	**53.5493**	**53.5703**	**53.5195**	**53.4939**
(013)	/	/	**60.7366**	**60.7672**
(020)	**62.7269**	**63.0165**	**62.5640**	**62.6239**
(021)	**65.2939**	**65.2497**	**65.2823**	**65.2315**
(220)	**73.1381**	**73.1127**	**72.9922**	**72.8653**
	4% Mg		**6% Mg**	
(010)	**30.2244**	**30.1484**	**30.1894**	**30.2746**
(011)	**34.7278**	**34.6966**	**34.6885**	**34.8204**
(111)	**37.2928**	/	/	/
(200)	**43.2719**	**43.2747**	**43.3842**	**43.4078**
(012)	**45.9185**	**45.8391**	**45.8386**	**46.0118**
(110)	**53.6146**	**53.4954**	**53.4891**	**53.6243**
(013)	**60.9307**	**60.7735**	**60.8168**	**61.0934**
(020)	**62.7363**	**62.6997**	**62.7772**	**62.7741**
(021)	**65.3844**	**65.2855**	/	**65.4530**
(220)	**73.7882**	**73.114**	**72.8512**	**73.2410**

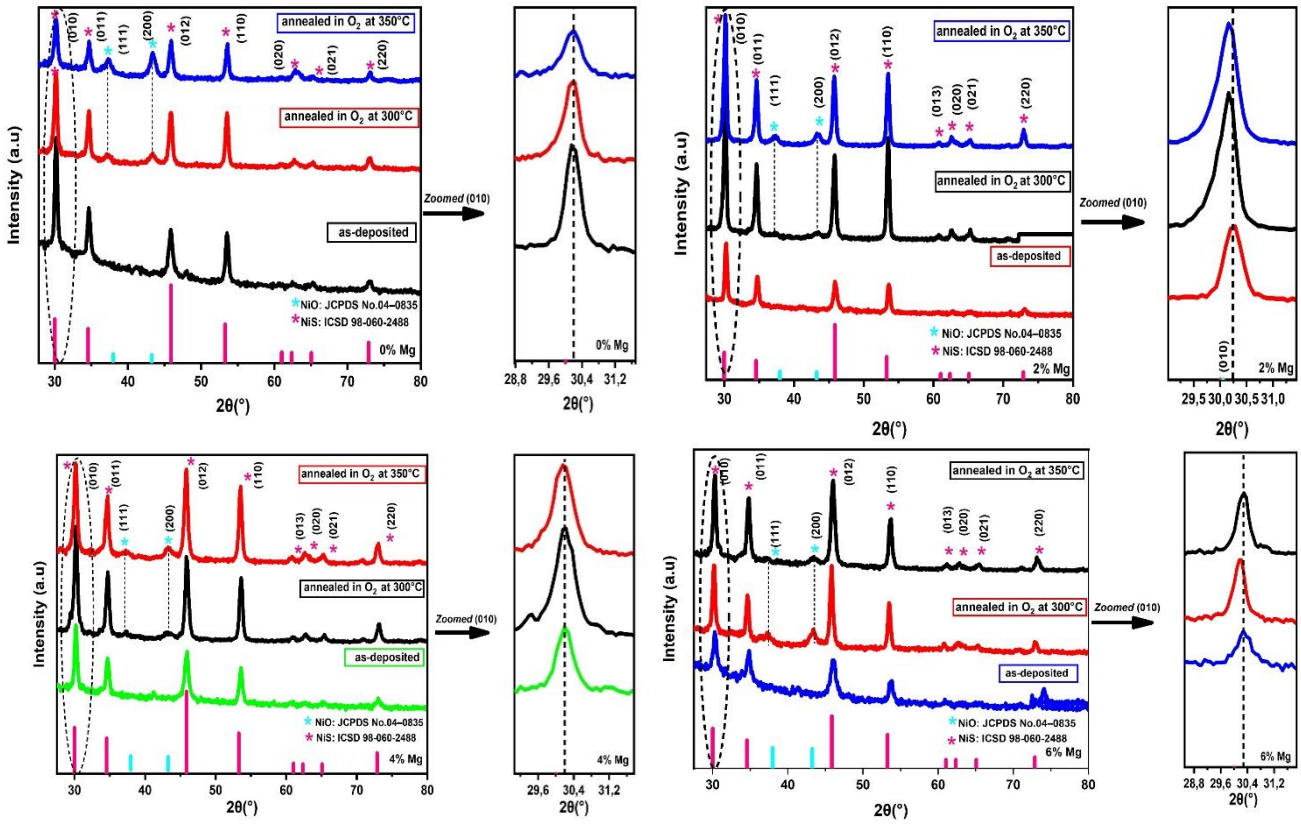

***Figure* (V.2) :** *XRD patterns of the annealed Mg :NiS thin film.*

V. 3. 1 .2. The Crystallite Size & Micro-Strain:

The crystallite size (D_{hkl}) of Mg-doped NiS films, annealed in O_2 atmospheres at 300°C for 3h30min and 350°C for 3h, was calculated using Debye–Scherrer's equation [3]:

$$D_{hkl} = \frac{k\lambda}{\beta \cos\theta} \qquad \text{N° (V.1)}$$

Where:

- β is full width at half-maximum (FWHM)
- k is a constant.

This formula is used to calculate the Micro-Strain (ε_{hkl}) [4]:

$$\varepsilon_{(hkl)} = \frac{\beta}{4 \tan\theta} \qquad \text{N° (V.2)}$$

***Table* (V.3) :** *The Crystallite size values for each of the annealed Mg :NiS films.*

(hkl) / Mg levels (%)	$D_{hkl}; O_2 in\ 300°C$	$D_{hkl}; O_2 in\ 350°C$	$D_{hkl}; O_2 in\ 300°C$	$D_{hkl}; O_2 in\ 350°C$
		0% Mg		2% Mg
(010)	20.48	19.68	22.33	20.45
(011)	20.39	18.66	20.20	20.02
(012)	17.53	16.30	19.58	18.44
(110)	21.00	19.87	22.85	22.42
		4% Mg		6% Mg
(010)	19.16	18.03	21.93	20.51
(011)	17.65	17.49	20.18	19.17
(012)	16.65	16.52	16.29	15.56
(110)	19.25	18.96	18.29	18.39

***Table* (V.4) :** *Micro-Strain values for each of the annealed Mg :NiS films.*

(hkl) / Mg levels (%)	$\varepsilon_{hkl}10^{-3}; O_2 in\ 300°C$	$\varepsilon_{hkl}10^{-3}; O_2 in\ 350°C$	$\varepsilon_{hkl}10^{-3}; O_2 in\ 300°C$	$\varepsilon_{hkl}10^{-3}; O_2 in\ 350°C$
		0% Mg		2% Mg
(010)	6.50	6.76	5.96	6.51
(011)	5.70	6.23	5.76	5.81
(012)	5.07	5.46	4.55	4.83
(110)	3.66	3.87	3.37	3.44
		4% Mg		6% Mg
(010)	6.92	7.39	6.09	6.47
(011)	6.95	6.65	5.76	6.04
(012)	5.35	5.39	5.46	5.70
(110)	4.00	4.06	4.19	4.18

According to the results in Table (V.5), a clear change in crystallite size average is observed for Mg doped NiS films annealed in O_2 atmospheres at 300°C for 3h30min and at 350°C for 3h, especially when compared to the as-deposited films. (Figure V.3) illustrates

these changes in average crystallite size as a function of magnesium content in the nickel sulfide thin films. Notably, there was a significant increase in crystallite size with annealing at 300°C for 3h30min, compared to annealing at 350°C for 3h. This suggests that annealing in O_2 atmospheres at 300°C is more effective than at 350°C, despite the shorter duration. However, We can conclude that annealing in an oxygen atmosphere can lead to an increase in the crystallite size of films, corresponding to reduced microstrain. This is supported by *Senthilkumar et al.* **[5]** Research on the effects of annealing on indium oxide (In_2O_3), where improved crystallinity was noted in their investigations. Moreover, their findings also indicated a reduction in microstrain and dislocation density.

***Table* (V.5) :** *The Crystallite size and Micro-Strain average values for each of Mg :NiS annealed films and (as-deposited).*

(hkl) / Mg levels (%)	*D*;as-deposited	*D*;O_2 in 300°C	*D*; O_2 in 350°C	$\varepsilon\ 10^{-3}$;as deposited	$\varepsilon\ 10^{-3}$;O_2 in 300°C	$\varepsilon\ 10^{-3}$;O_2 in 350°C
0%	18.45	19.85	18.63	5.63	5.23	5.58
2%	18.30	21.24	20.30	5.63	4.91	5.15
4%	16.73	18.18	17.75	6.36	5.81	5.87
6%	15.55	19.17	18.40	6.66	5.38	5.60

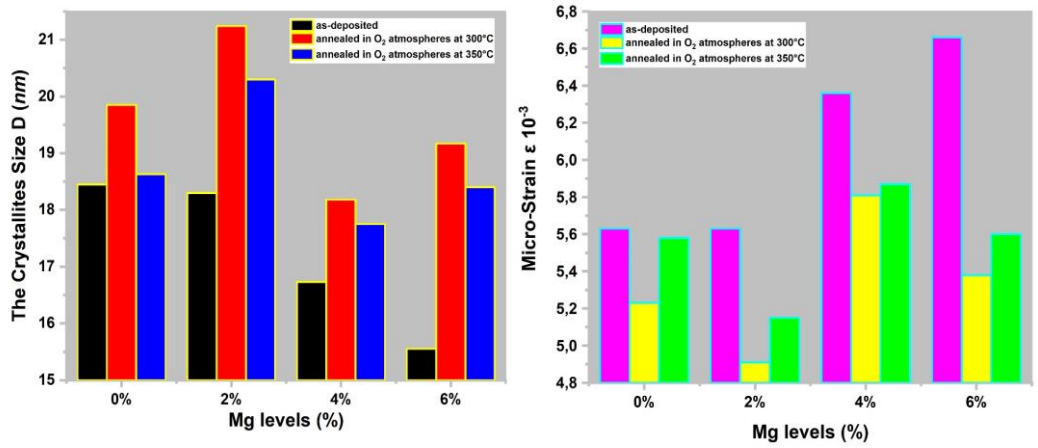

***Figure* (V.3) :** *Variation of D and ε average of the annealed films.*

V. 3. 2. Chemical composition of Mg: NiS annealed films

Figure (V.4) shows that FTIR spectroscopy provides information on the presence of various functional groups in the Mg-doped NiS films annealed in O_2 atmospheres at 300 and 350°C for 3h30min and 3h, respectively. The significant bands observed at 626 and 618 cm^{-1} are attributed to the Ni–S stretching vibration modes [6]. Notably, this investigation reveals a decrease in the intensity of the Ni–S bands with oxygen annealing at 350°C, indicating enhanced oxygen diffusion. The bands at 1175 and 1158 cm^{-1} depict the presence of C–S vibrations in all annealed films [7]. In contrast, the stretching and bending vibrations of O–H are noticeable at the peak of 3349 cm^{-1} for the 4% Mg-doped NiS film annealed in O2 at 350°C for 3h [8],[9], which are absent in all other annealed films. However, peaks at 2355 cm^{-1} [10], corresponding to the stretching vibration of O=C bonds, are present in all samples, suggesting the adsorption of atmospheric molecules on the aerogel surface.

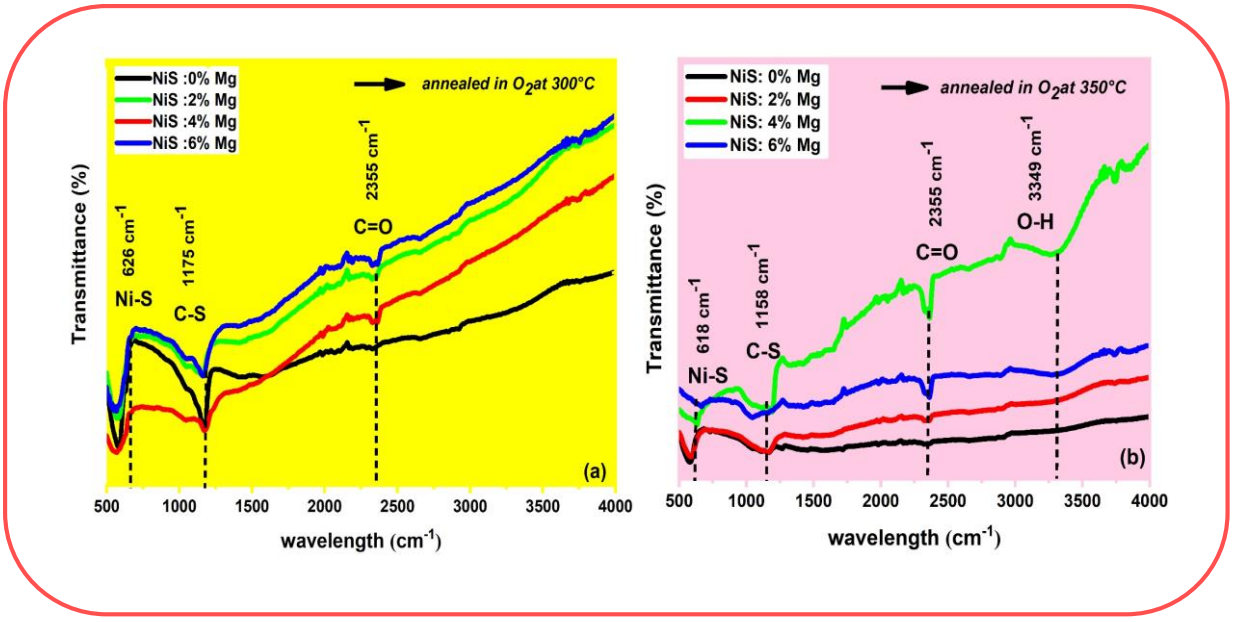

***Figure* (V.4) :** *FTIR spectra of Mg :NiS films annealed.*

V. 3. 3. The optical properties of Mg: NiS annealed films

V. 3. 3. 1. UV–vis absorbance:

Figure (V.5) displays the optical absorption spectra of NiS and Mg-doped NiS annealed thin films, covering the range from 200 to 1100 nm. It's evident that the absorption edge for

all films is situated in the UV region of 280 to 380nm. Initially, a decrease in absorbance was observed in thin films annealed in O_2 atmospheres at 300 and 350°C for 3h30min and 3h, respectively, indicating an increase in transmittance. Additionally, an increase in absorbance is observable in the visible region 380 to 740 nm and to some extent in the near-infrared region 740 to 900 nm, approximately by 4 to 6 units, with annealing in O_2 atmospheres at both 300°C and 350°C, compared to the as-deposited films. This increase in absorbance with respect to annealing is consistently observed.

V. 3. 3. 2. The band gap energy:

The band gap energy (Eg) of NiS and Mg-doped NiS thin films can be evaluated from the absorbance data presented in Figure (V.5), using Relation N°(V.4) for this purpose [11]:

$$A = \alpha d = -\ln(T) \qquad \text{N° (V.3)}$$

So :

$$(Ahv)^2 = B(hv - Eg)/A = \alpha d \qquad \text{N° (V.4)}$$

Where:

- A is the absorbance
- d is the film thickness
- T is the transmittance spectra of thin films
- α is the absorption coefficient values
- B is a constant
- hv is the photon energy
- Eg is the band gap energy.

In Figure (V.6) extrapolating the curves of $(Ahv)^2$ to zero allows for the determination of the optical band gap energy. The values obtained range from 0.822 to 1.182 eV for the as-deposited and annealed films in oxygen atmospheres at 300°C and 350°C for 3h30min and 3h. Respectively, The band gap energy differences can be attributed to the in-plane compressive strain relaxation during thermal annealing, which refers to the changes in the band gap energy of a material being attributed to the relaxation of compressive strain within the plane of the material during the process of thermal annealing [12].

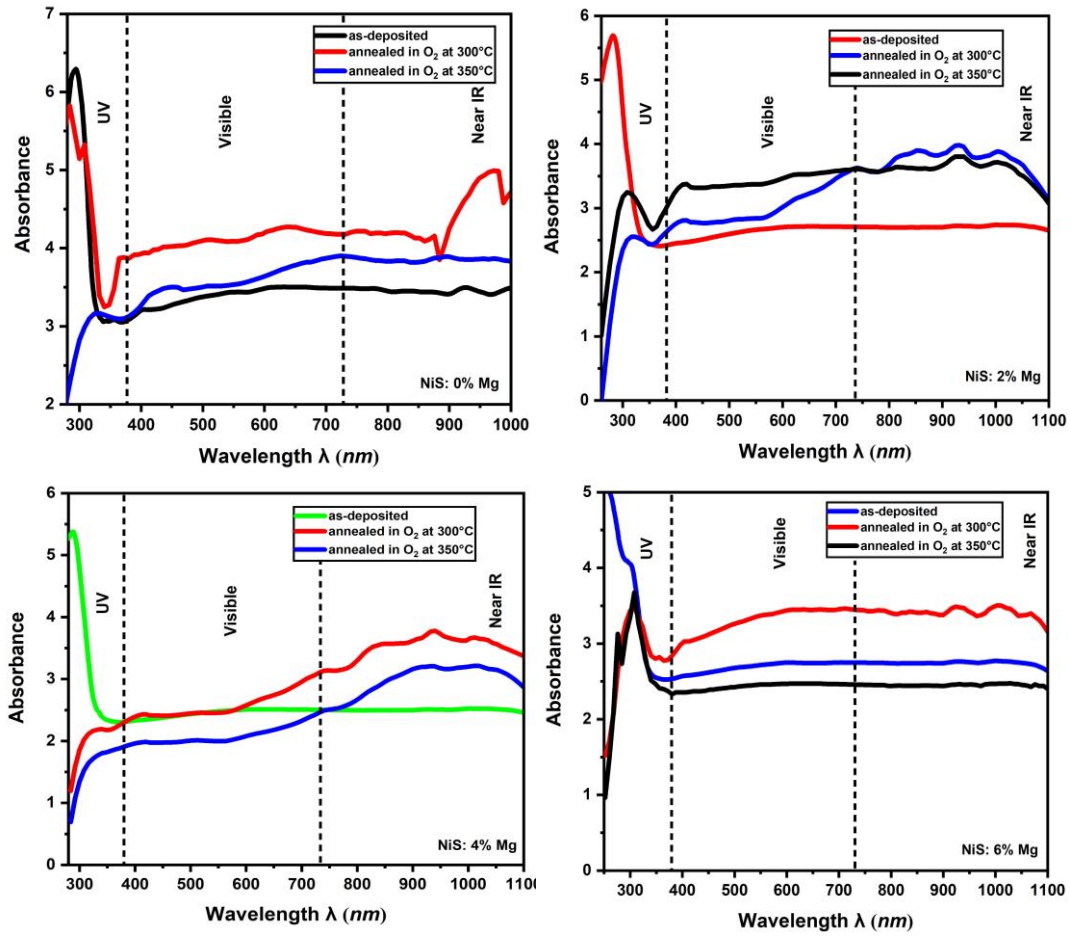

***Figure* (V.5) :** *Optical absorbance spectra of Mg :NiS annealed films.*

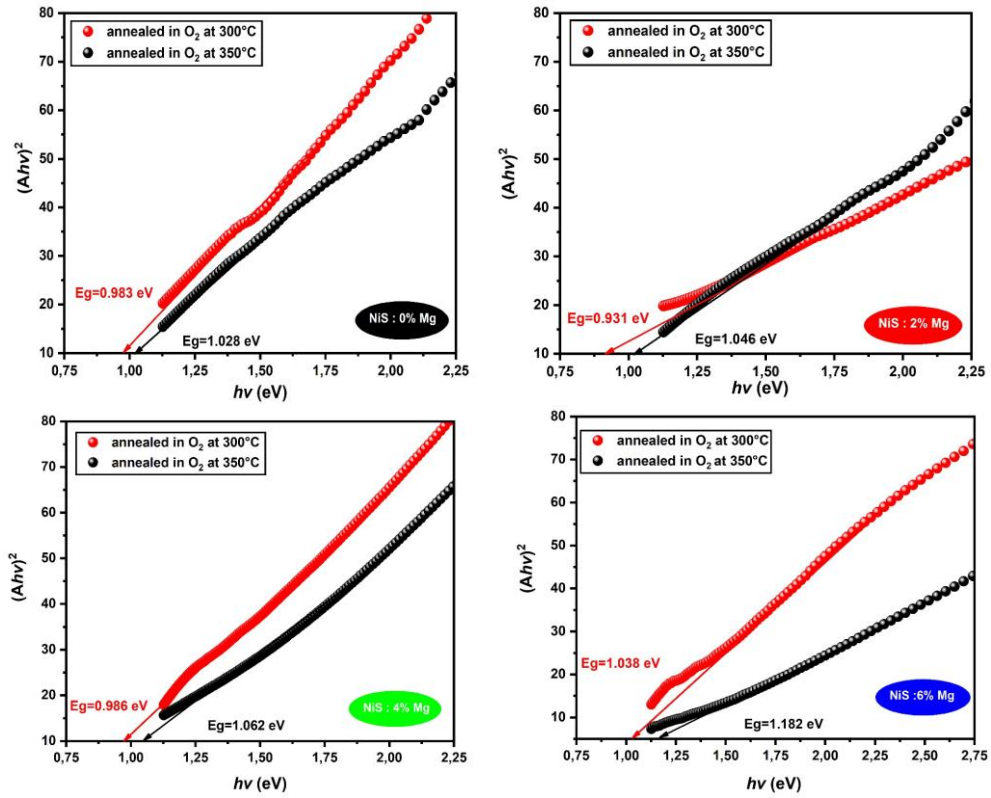

***Figure* (V.6) :** *The variation of $(Ahv)^2$ with the hv of Mg :NiS annealed films.*

From the data in the table (V.6) and figure (V.7), we notice an increase in energy for the annealed films. This increase in optical band gap energy after annealing in an oxygen atmosphere can be attributed to changes in the crystal structure and a reduction in defects and impurities. Specifically, the annealing process facilitates the relaxation of the crystal lattice, altering the electronic structure of the material and affecting its optical properties.

***Table* (V.6) :** *The optical band gap energy values of Mg :NiS annealed films.*

(hkl) / Mg levels (%)	Eg; as deposited	Eg; O_2 in 300°C	Eg; O_2 in 350°C
0%	0.882	0.983	1.028
2%	0.822	0.931	1.046
4%	0.934	0.986	1.062

6%	0.994	1.038	1.182

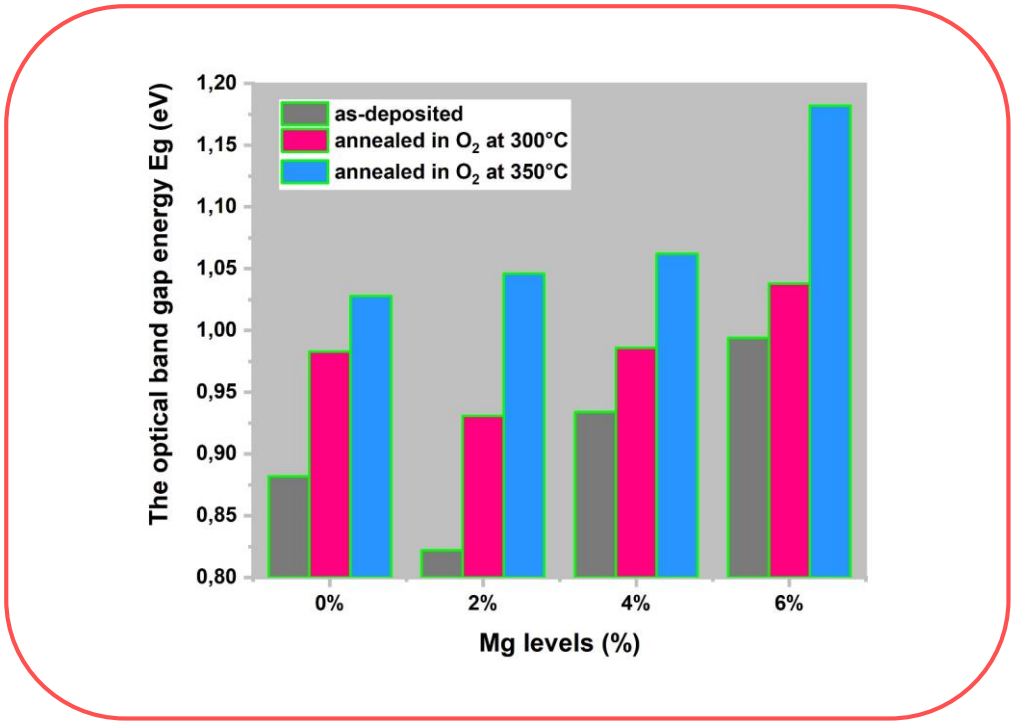

***Figure* (V.7) :** *The variation of Eg of Mg :NiS annealed films.*

V. 3. 4. Electrical study of annealed films

V. 3. 4. 1. Sheet resistance of Mg: NiS annealed films:

Figure (V.8) displays the voltage-current characteristics of Mg-doped NiS annealed films within the 0-100 mA range. The linear increase in voltage with increasing current is evident, suggesting the reliability of the measurements. The electrical sheet resistance of the Mg:NiS thin films annealed in O_2 atmospheres at 300°C for 3h30min and at 350°C for 3h, was determined using the four-point method at room temperature. Figure (V.9) and table (V.7) illustrate the variation of sheet resistance (Rsh) with the Mg content for both deposited and annealed films. It was observed that the sheet resistance decreases with increasing oxygen annealing atmosphere at both temperatures, with Rsh values ranging from 1.87 to 8.30 (Ω/Sheet). Consequently, the increase in crystalline sizes of NiS annealed films at 300°C and 350°C leads to a decrease in trapping states at the grain boundaries. This indicates that the free charge carriers become more mobilized **[13]**, resulting in reduced resistance. It is

possible to interpret these results to suggest that annealing may enhance the sheet resistance (Rsh). Therefore, these results suggest that annealing potentially improves the electrical conductivity of Mg:NiS thin films.

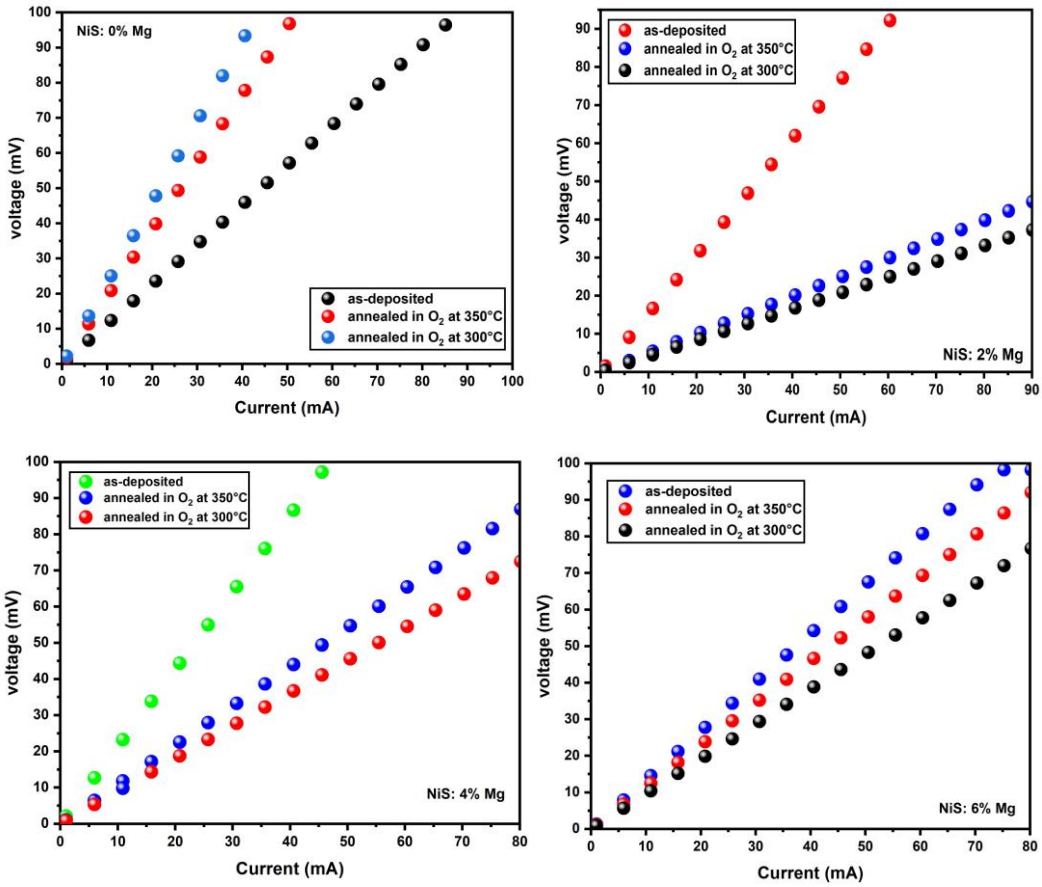

***Figure* (V.8) :** *Voltage changes as a function of current intensity of Mg :NiS annealed films.*

***Table* (V.7) :** *The sheet resistance values of Mg :NiS annealed films.*

	As-deposited	O_2 at 300°C	O_2 at 350°C
0%	5.304	8.3	6.92
2%	5.974	1.87	2.25
4%	7.549	3.95	4.74
6%	5.569	4.83	5.097

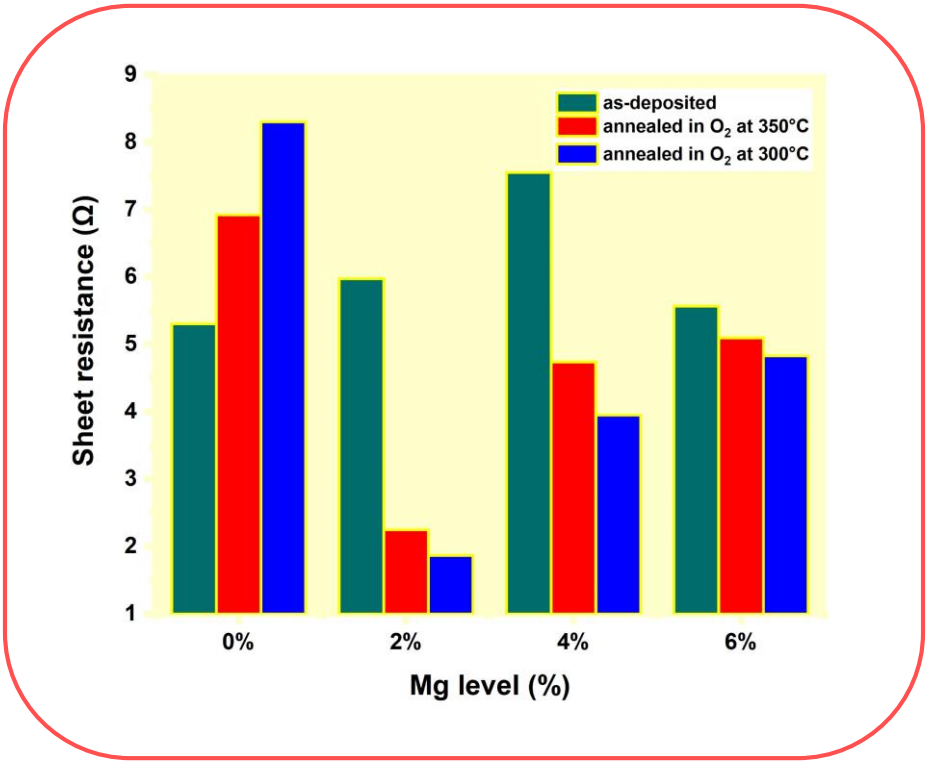

***Figure* (V.9) :** *The variation of Rsh of Mg :NiS annealed films.*

V. 3. 4. 2. The Electrical Conductivity of NiS annealed films :

As previously highlighted, nickel sulfide is categorized as a p-type semiconductor and is widely recognized for its electrochemical activity, primarily due to its broad range of applications, including use in supercapacitors. In the findings presented in the third chapter, we examined the electrical conductivity of pure nickel sulfide thin films and We will examine films annealed in an O_2 atmosphere at temperatures of 300°C for 3h30min 350°C for 3h, respectively. This examination utilized the following formula **[14]**:

$$\sigma = \frac{1}{\rho} = \frac{1}{e \times R_{Sh}} \qquad \text{N° (V.5)}$$

The results of annealing nickel sulfide thin films at 300°C and 350°C in an oxygen atmosphere are detailed in figure (V.10) and table (V.8). As shown, an increase in resistance and a corresponding decrease in conductivity are observed. The decrease in electrical conductivity during annealing in an oxygen atmosphere may be attributed to the oxidation of nickel sulfide. This oxidation process can lead to the formation of nickel oxide on the

surface or within the film, which typically exhibits lower electrical conductivity compared to nickel sulfide.

Table (V.8) : *The Rsh, ρ and σ values of NiS annealed films.*

	As-deposited	annealed in O_2 300°C	annealed in O_2 350°C
Rsh(Ω)	5.304	8.30	6.92
ρ (Ω.cm)	$4.11\ 10^{-4}$	$6.43\ 10^{-4}$	$5.36\ 10^{-4}$
σ(Ω.cm)$^{-1}$	$2.430\ 10^{3}$	$1.560\ 10^{3}$	$1.870\ 10^{3}$

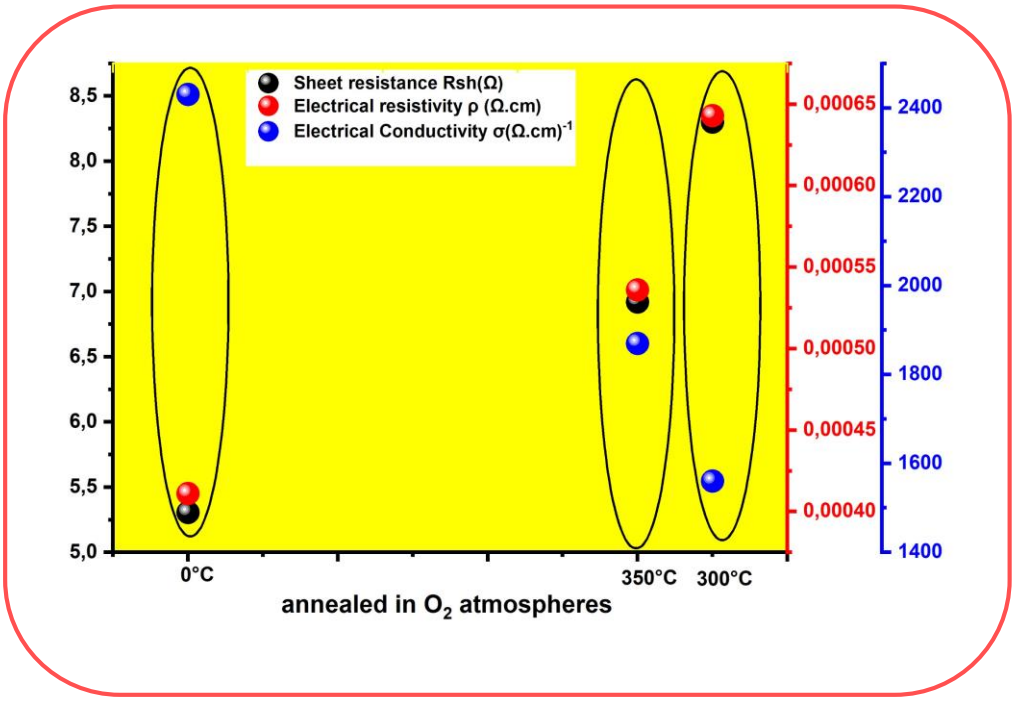

***Figure* (V.9) :** *The variation of Rsh, ρ and σ of NiS annealed films.*

V. 4. Conclusion

Mg-doped NiS thin films were prepared in an oxygen annealing atmosphere at 300°C for 3 hours and 30 minutes, and at 350°C for 3 hours. The results demonstrated that the films are primarily composed of a NiS structure with a secondary NiO phase. It was also observed that there is an increase in the crystallite size, particularly noticeable when annealing at 300°C for 3 hours and 30 minutes. This suggests an enhancement in the crystalline structure, and the annealed films exhibit a good optical band gap. The annealed films exhibited

favorable sheet resistance, ranging between 1.87 and 8.30 (Ω/Sheet). In conclusion, the optimal annealing condition for these thin films appears to be 300°C for 3 hours and 30 minutes used in supercapacitor applications.

References

[1] Yao C, Ismail M, Hao A, Thatikonda SK, Huang W, Qin N, et al. Annealing atmosphere effect on the resistive switching and magnetic properties of spinel Co3O4 thin films prepared by a sol-gel technique. RSC Adv 2019;9:12615–25. https://doi.org/10.1039/c9ra01121h.

[2] Dastan D, shan K, Jafari A, Marszalek T, Mohammed MKA, Tao L, et al. Influence of heat treatment on H2S gas sensing features of NiO thin films deposited via thermal evaporation technique. Mater Sci Semicond Process 2023;154:107232. https://doi.org/10.1016/j.mssp.2022.107232.

[3] Chfii H, Bouich A, Soucase BM, Abd-Lefdil M. Structural and physical properties of Mg-doped CuCoO 2 delafossite thin films. Mater Chem Phys 2023;306. https://doi.org/10.1016/j.matchemphys.2023.128006.

[4] Boughalmi R, Rahmani R, Boukhachem A, Amrani B, Driss-Khodja K, Amlouk M. Metallic behavior of NiS thin film under the structural, optical, electrical and ab initio investigation frameworks. Mater Chem Phys 2015;163:99–106. https://doi.org/10.1016/j.matchemphys.2015.07.019.

[5] Senthilkumar V, Vickraman P. Annealing temperature dependent on structural, optical and electrical properties of indium oxide thin films deposited by electron beam evaporation method. Curr Appl Phys 2010;10:880–5. https://doi.org/10.1016/j.cap.2009.10.014.

[6] Nandhini S, Christina AJ, Muralidharan G. Facile microwave-hydrothermal synthesis of NiS nanostructures for supercapacitor applications. Appl Surf Sci 2018:1–7. https://doi.org/10.1016/j.apsusc.2018.01.024.

[7] Gahtar A, Benramache S, Ammari A, Boukhachem A, Ziouche A. Effect of molar concentration on the physical properties of NiS thin film prepared by spray pyrolysis method for supercapacitors. Inorg Nano-Metal Chem 2022;52:112–21. https://doi.org/10.1080/24701556.2020.1862225.

[8] Abo-Bakr AM, Salman HM, Ismael EM, Ebnalwaled AA. Thiocarbohydrazide as a Sulfur Source for the Preparation of Nickel Sulfide Nanoparticles. J Pharm Appl Chem 2020;6 (2):41–5. https://doi.org/10.18576/jpac/060201.

[9] Balayeva OO, Azizov AA, Muradov MB, Maharramov AM, M Goncha E, Alosmanov RM, et al. β-NiS and Ni3S4 nanostructures: fabrication and characterization. Mater Res Bull 2015. https://doi.org/10.1016/j.materresbull.2015.11.037.

[10] Majid S, Ahmad KS. Optik Analysis of dopant concentration effect on optical and morphological properties of PVD coated Cu-doped Ni 3 S 2 thin films. Opt - Int J Light Electron Opt 2019;187:152–63. https://doi.org/10.1016/j.ijleo.2019.05.025.

[11] Sbaihi A, Benramache S, Benbrika C. Synthesis of High Electrical Conductivity of

Superconductor NiS Thin Films. J Nano- Electron Phys 2024;16:01022-1-01022–6. https://doi.org/10.21272/jnep.16(1).01022.

[12] Feng Z, Huang L, Feng Q, Li X, Zhang H, Tang W, et al. Influence of annealing atmosphere on the performance of a β-Ga 2 O 3 thin film and photodetector . Opt Mater Express 2018;8:2229. https://doi.org/10.1364/ome.8.002229.

[13] Anitha N, Anitha M, Raj Mohamed J, Valanarasu S, Amalraj L. Influence of tin precursor concentration on physical properties of nebulized spray deposited tin disulfide thin films. J Asian Ceram Soc 2018;6:121–31. https://doi.org/10.1080/21870764.2018.1450026.

[14] Gahtar A, Benramache S, Ammari A, Boukhachem A. Study of the Structural, Optical, Electrical and Morphological Properties of Nickel Sulfide Thin Films Used in Supercapacitors. Ann West Univ Timisoara - Phys 2021;63:1–13. https://doi.org/10.2478/awutp-2021-0001.

GENERAL CONCLUSION

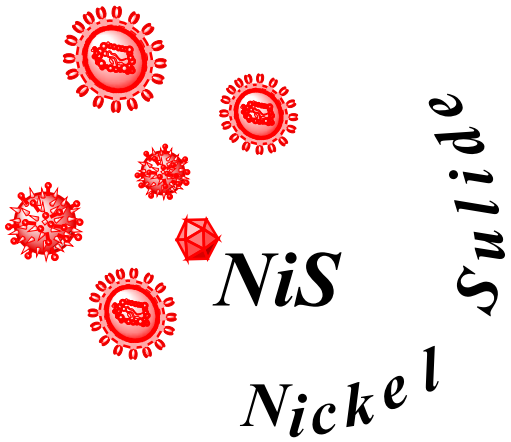

General Conclusion

This thesis attempts to study the factors affecting the physical properties of nickel sulfide superconductors through magnesium doping and the use of annealing oxygen atmosphere. Notably, these factors were studied on thin films prepared using the spray pyrolysis technique, with a constant deposition temperature of 250°C for all experiments. Initially, the research focused on the physical properties of pure NiS films. X-ray diffraction analysis revealed that all NiS thin films possessed a fundamental hexagonal structure with a preferred orientation of (010). The optimal crystal size was estimated at 22.148 nm. FTIR analysis corroborated these findings, particularly through the identification of the Ni-S chemical bond at 626 cm^{-1}, indicating successful film formation. Furthermore, optical measurement results showed band gap energy values ranging between 0.87 and 0.92 eV. Lastly, the electrical conductivity results were promising, suggesting that pure nickel sulfide thin films have potential applications in Supercapacitors (SCs).

Subsequently, we deposited thin films of nickel sulfide doped with magnesium (Mg) in various percentages (2%, 4%, 6%, and 8%). The most notable results were observed at 6% Mg doping. The X-ray diffraction (XRD) results for the magnesium-doped NiS thin films revealed a polycrystalline, hexagonal structure with a preferred peak orientation of (010). As the level of magnesium doping increased, the crystallite size of these films decreased, reaching a minimum of 14.015 nm at a doping concentration of 6%. Using FTIR at room temperature, we confirmed the presence of NiS doped with Mg, as evidenced by the Ni-S chemical bond appearing at 632 cm^{-1}. This result indicates the successful formation of the films. We also investigated the optical properties using UV absorption spectra to determine the optical band gap energy and Urbach energy. The band gap energy was found to range from 0.882 to 0.994 eV. Finally, we measured the variation in electrical resistance relative to the magnesium levels using the four-point method. It was observed that the minimum electrical resistance, 5.569 ohms, occurred at 6% Mg concentration

Mg-doped NiS thin films were prepared in an oxygen annealing atmosphere, treated at 300°C for 3 hours and 30 minutes, and at 350°C for 3 hours. The results indicated that the films primarily consist of a NiS structure with a secondary phase of NiO. Notably, there was

an increase in crystallite size, especially pronounced for films annealed at 300°C for 3 hours and 30 minutes. This suggests an enhancement in the crystalline structure. Furthermore, the annealed films demonstrated good optical band gap properties. The sheet resistance of these films was favorable, ranging between 1.87 and 8.30 Ω/sheet. In conclusion, the optimal annealing condition for these thin films, particularly for supercapacitor applications, appears to be at 300°C for 3 hours and 30 minutes.

Future Work

Based on this study, work can continue on:

Performing further characterizations, such as Hall effect measurements.

Exploring the alloy effect in magnesium nickel sulfide (MgNiS) thin films.

Investigating the effects of doping additional substances into thin films of nickel sulfide.

Studying the magnetic properties of nickel sulfide thin films.

ANNEXES

Name and formula

Reference code:	98-060-2488
Compound name:	Nickel Sulfide
Common name:	Nickel Sulfide
Chemical formula:	Ni_1S_1

Crystallographic parameters

Crystal system:	Hexagonal
Space group:	P 63/m m c
Space group number:	194
a (Å):	3,4360
b (Å):	3,4360
c (Å):	5,2900
Alpha (°):	90,0000
Beta (°):	90,0000
Gamma (°):	120,0000
Calculated density (g/cm^3):	5,57
Volume of cell (10^6 pm^3):	54,09
Z:	2,00
RIR:	4,80

Subfiles and quality

Subfiles:	User Inorganic
Quality:	User From Structure (=)

Comments

Creation Date:	01/08/2008
Modification Date:	30/12/1899
Original ICSD space group:	P63/MMC. At least one temperature factor missing in the paper.. No R value given in the paper.. X-ray diffraction (powder) N
Structure type:	NiAs
Pressure in MPa:	2800
Metals Sdata Record:	INT= film; RAD= Mo; APP= Debye-Scherrer
Metals formula record:	Ni S (z = 2) P63/MMC
Structure type:	NiAs
Recording date:	8/1/2008
ANX formula:	NO
Z:	2
Calculated density:	5.57
Pearson code:	hP4
Wyckoff code:	c a

Publication title: Equation of state and high pressure phase transition of Ni S in the Ni As structure
ICSD collection code: 602488
Structure: NiAs
Chemical Name: Nickel Sulfide
Second Chemical Formula: Ni S

References

Structure: Heinz, D.L.;Campbell, A.J., *Journal of Physics and Chemistry of*

Peak list

No.	h	k	l	d [A]	2Theta[deg]	I [%]
1	0	1	0	2,97566	30,006	52,6
2	0	0	2	2,64500	33,863	4,1
3	0	1	1	2,59351	34,556	38,8
4	0	1	2	1,97691	45,865	100,0
5	1	1	0	1,71800	53,278	45,2
6	0	1	3	1,51699	61,033	6,0
7	0	2	0	1,48783	62,361	4,9
8	1	1	2	1,44076	64,640	2,6
9	0	2	1	1,43226	65,071	4,9
10	0	0	4	1,32250	71,247	5,4
11	0	2	2	1,29675	72,886	19,5
12	0	1	4	1,20852	79,195	3,7
13	0	2	3	1,13713	85,283	2,3
14	1	2	0	1,12470	86,455	2,7
15	1	2	1	1,10011	88,887	4,1

Structure

No.	Name	Elem.	X	Y	Z	Biso	sof	Wyck.
1	S1	S	0,33333	0,66667	0,25000	0,5000	1,0000	2c
2	NI1	Ni	0,00000	0,00000	0,00000	0,5000	1,0000	2a

Stick Pattern

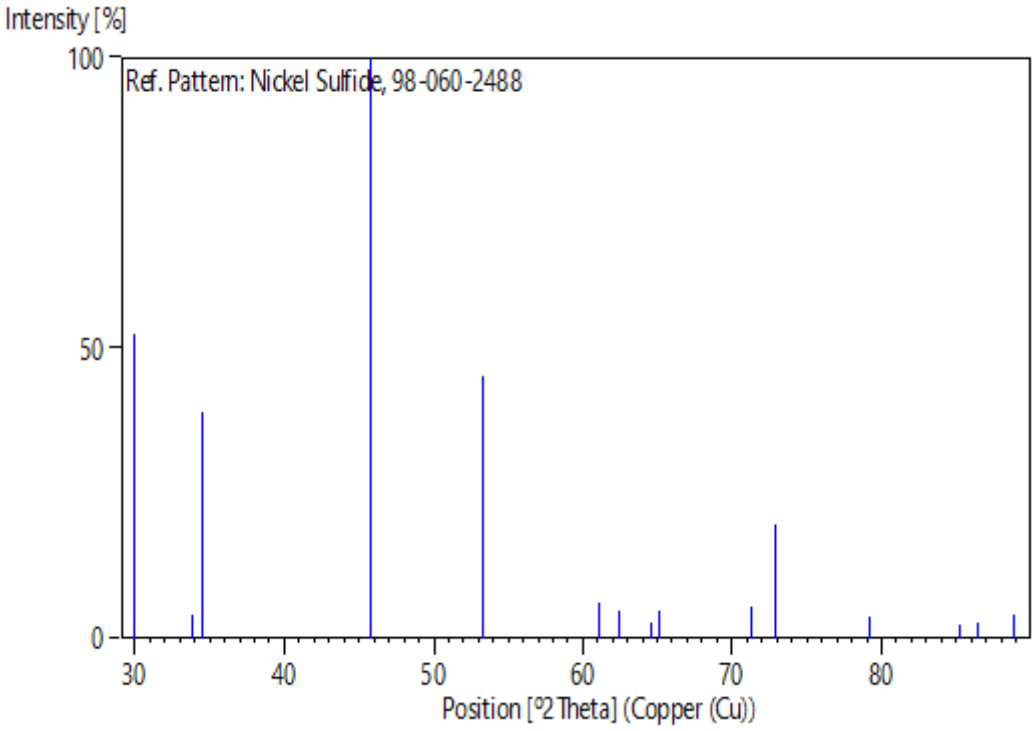

LIST OF PUBLICATIONS

[1] *Synthesis of High Electrical Conductivity of Superconductor NiS Thin Films*

AMIRA Sbaihi, SAID Benramache, CHAIMA Benbrika

https://doi.org/10.21272/jnep.16(1).01022.

[2] *Enhanced phtocatalytic degradation of rhodamine B using Fe/Ba-doped $Bi_4Ti_3O_{12}$ nanostructures : Mechanism and performance evalution*

CHAIMA Benbrika, HAYET Menasra, ANKUSH Kularkar, LAKHDER Smaili, **AMIRA Sbaihi**

https://doi.org/10.1016/jpcs.2020.111702

[3] *Synthesis by Organic Solar Cells SnO_2 Thin Films for Gas Sensing*

Y. Aoun, S. Benramache, B. Maaoui, **A. Sbaihi**

https://doi.org/10.21272/jnep.16(1).01023

[4] *Synthesis of High transparency of F doped NiO moncrystalline thin films by spray deposition*

Mounira Mammi, SAID Benramache, Yacine Aoun, **AMIRA Sbaihi**